USING SELF-ASSEMBLED BLOCK COPOLYMER MACROSTRUCTURES FOR CREATING A MODEL SYSTEM FOR CELL MIMICRY

A Dissertation

by

JEFFERY SIMON GASPARD

Submitted to the Office of Graduate Studies of
Texas A&M University
in partial fulfillment of the requirements for the degree of

DOCTOR OF PHILOSOPHY

December 2009

Major Subject: Chemical Engineering

USING SELF-ASSEMBLED BLOCK COPOLYMER MACROSTRUCTURES FOR CREATING A MODEL SYSTEM FOR CELL MIMICRY

A Dissertation

by

JEFFERY SIMON GASPARD

Submitted to the Office of Graduate Studies of
Texas A&M University
in partial fulfillment of the requirements for the degree of

DOCTOR OF PHILOSOPHY

Approved by:

Chair of Committee,	Mariah Hahn
Committee Members,	Melissa Grunlan
	Michael Pishko
	Zhengdong Cheng
Head of Department,	Michael Pishko

December 2009

Major Subject: Chemical Engineering

ABSTRACT

Using Self-Assembled Block Copolymer Macrostructures for Creating a Model System for Cell Mimicry.

(December 2009)

Jeffery Simon Gaspard, B.S., Texas A&M University;

M.S., Texas A&M University

Chair of Advisory Committee: Dr. Mariah Hahn

The objective of this research is to investigate three classes of block copolymers, the vesicle structures they form, their response to stimuli in solution and their capabilities for use in biomimicry. The self-assembled structures of all classes of polymers will be used as a basis for templating hydrogel materials, in the interior of the vesicles, and the resulting particles will be designed to show the structural and mechanical properties similar to living cells.

The synthetic block copolymers are a poly(ethylene glycol) and poly(butadiene) (PEO-*b*-PBd) copolymer, a poly(ethylene glycol) and a poly(dimethyl siloxane) (PEO-*b*-PDMS) copolymer and the polypeptide block copolymer is a lysine and glycine (K-*b*-G) copolymer. Investigation using the synthetic block copolymers will focus on whether the polymer can form vesicles, size limitations of vesicle structures, and the formation of internal polymer networks. Subsequent investigations will look at the needed steps for biomimicry.

The PDMS copolymer is a novel entrant into amphiphilic block copolymers. Although characterization of the copolymer solution behavior is known, the mechanical

properties of the polymer are not known. PDMS was investigated along with the PBd polymer due to the similar chemical structure and nature.

The lysine-glycine copolymers are a new system of materials that form fluid vesicle structures. Therefore, characterization of how K-*b*-G assembly behavior and investigations of how K-*b*-G responds to solution conditions are needed before incorporating this copolymer into a cellular mimic. The size and mechanical behavior of the lysine-glycine vesicles are measured to compare and contrast to the synthetic systems.

The goals in creating a biomimic are a hollow sphere structure with a fluid bilayer, a vesicle that has controllable mechanical properties, and with a controllable surface chemistry and density. Overall, these experiments were successful; the various properties are easily controllable: the size of vesicles created, the material properties of the vesicle interior and shell, as well as the surface chemistry of the vesicles.

Investigations into the novel block copolymers were conducted, and the polypeptide block copolymer showed the ability to create vesicles that are responsive to changing salt and pH concentrations. The PDMS block copolymer system offers a new material system that will perform as well as the PBd system, but without some of the inherent drawbacks.

ACKNOWLEDGEMENTS

I would like to thank both Dr. James Silas and Dr. Mariah Hahn for their support and guidance through all the research and experimentation. They are both great educators and great professors to work for. Also, I would like to thank the members of my committee: Dr. Melissa Grunlan, Dr. Zhengdong Cheng and Dr. Michael Pishko. These professors have provided invaluable guidance, insights, and suggestions that have enabled me to finish this work and experimentation in a timely fashion.

I would like to thank the members of my research group: Karym Kinnibrugh, Clemente Contreas, and Winnie Chang. Additionally, I would also like to thank members of other research groups that helped me throughout my research: Shannon Eichmann of Dr. Michael Bevan's group, Dr. Allen Bulick and Dany Munoz of Dr. Mariah Hahn's group and Dr. Jan Jeng Shiung of Dr. Dan Shantz's group. Without these individuals, this research would have moved at a much slower pace.

I would like to thank the Material Characterization Facility for their support and guidance on their confocal microscopes as well as the use of their facilities. I would also like to thank Dr. Bergbreiter and Hai Fu for the use of their goniometer.

I would like to thank the staff of the Chemical Engineering department, specifically Louis Muniz and Randy Marek. Louis ensured our labs were always in working order and Randy for his help in fabrication of many items around our lab.

And finally, I would also like to thank my family, Mom, Dad, Lee Anne and Thorston, for their continued support throughout my education through the years. They have helped me with the tough times and celebrated with me during the fun times.

TABLE OF CONTENTS

Page

Page

LIST OF FIGURES

Page

Page

LIST OF TABLES

Page

1. INTRODUCTION

1.1 Overview

Block copolymers bridge several research areas including chemistry, colloids, self-assembled materials and polymer physics. Amphiphilic di-block copolymers, copolymers, with one hydrophobic and one hydrophilic block, are designed to form self-assembled multi-ordered length scale structures in water, from vesicles to micelles[1-7]. The use of self-assembled materials spans many different fields of scientific research, but our primary motivation for their use in this research is biomimicry.

The constituent blocks of amphiphilic block copolymers can be made from either amino acids or synthetic components. Since the investigation into creating vesicles using synthetic block copolymers is well established, these polymers will be used as a basis for testing and experimentation of the attributes needed for a biomimic. One goal of this research will be to incorporate the use of polypeptide block copolymers to make vesicles for use in a biomimic, rather than relying on the synthetic block copolymers. Since the self-assembly properties of polypeptide block copolymers are not as well understood as the self-assembly properties of synthetic block copolymers, polypeptides warrant more detailed studies before they can be incorporated into biomimetic particles.

Several studies[2, 8-14] have been directed at using polypeptides as one or all of the blocks in a copolymer. Polypeptide synthesis has been fueled by the interest of making

---

This dissertation follows the style of *Science*.

a natural polymer that would have some ability to interact with biological systems, such as the human body[2, 5]. The two main categories of block copolymers utilizing polypeptides are synthetic-polypeptide copolymers and all polypeptide copolymers.

A novel polymer into the amphiphilic block copolymer area is a poly(dimethyl siloxane) (PDMS) polymer. PDMS polymers offer a high degree of flexibility, as well as high polymer stability with a low interfacial energy.

The primary attributes we wish to achieve in a cellular mimic are a hollow sphere, fluid bilayer, adjustable or controllable surface chemistry and density, responsive particles to solution conditions, and controllable mechanical properties. This dissertation will focus on particles responsive to solution conditions, controllable surface chemistry and controllable mechanical properties.

1.1.1 Biomimicry

There are a variety of reasons for wanting to create a biomimic. The first reason is a purely research goal: create an artificial membrane or membrane system to test biological functions. The second reason for developing a biomimic is for drug delivery or other medical therapies in which macromolecules or compounds of interest can not be solubilized easily in aqueous conditions[5, 6, 15, 16].

The basic traits of living cells sought in this work are a fluid bilayer membrane that encloses a spherical volume, an easily modifiable surface and controlled surface density, characteristic mechanical properties, and a responsive nature to surrounding

conditions. Ideally, these specific traits are may be pursued and developed independently. This allows specific control over one aspect without compromising another aspect. This also leads to a fail-safe designed system; the failure of one system or component does not destroy or cripple the entire system.

The first component of the biomimic is a synthetic membrane analogous to a natural cell membrane. Making a bilayer membrane is easily achieved with the use of amphiphilic block copolymers that create vesicles. These copolymers self-assemble into a lamellar phase vesicular macrostructure in aqueous conditions, and are discussed in more detail in the sections 3 thru 5.

The second component of the biomimic is an easily modifiable surface chemistry and controllable surface density. A vesicle with a tailored surface chemistry and surface density allows the biomimic to be a "smart" creation; interacting with the solution and conditions present in a designated way. If the vesicle contains an easily reacted group or retains the ability to add specific components after the vesicle has been formed, the biomimic can selectively interact with its surroundings through modifications of the reactive sites on the surface of the vesicle. This component is best achieved by making the terminal ends on some of the copolymer chains in the vesicle's bilayer reactive. Two methods are outlined in section 1.2.1.

A third component of the biomimic is controllable mechanical properties. Using synthetic monomer systems, encapsulation of various monomer solutions will be used to tailor material properties similar to natural systems, such as the cytoskeleton, the

cytoplasm and the actin network. Tailoring the specific material characteristics will depend on the type of internal network that will be modeled.

The remaining component of the biomimic is a responsive particle. This trait is incorporated into the novel polypeptide block copolymer investigated in these research experiments. The polymer is a polyelectrolyte, which will allow the polymer to change conformation due to salt or pH conditions. The polymer also possesses a hydrophobic section that does not contain any reactive sites nor does it change its conformation in solution due to changing conditions. This trait can be imparted on the other two polymer systems, but only after a reaction to convert the ends of some polymer chains to a more reactive specie.

The three general types of block copolymers investigated in this research are a synthetic block copolymer of poly(ethylene oxide)-block-poly(butadiene) (EO_mBd_n), a synthetic block copolymer of poly(ethylene oxide)-block-poly(dimethyl siloxane) (EO_mDMS_n) and a polypeptide block copolymer, made from poly(lysine)-block-poly(glycine) (K_mG_n), where *m* and *n* denote the number of units in each block. For the synthetic block copolymer, the hydrophobic section is butadiene or siloxane; while for the polypeptide block copolymer the hydrophobic section of polymer is Glycine. All hydrophobic blocks form random coils in solution. This feature allows both synthetic and polypeptide vesicles to maintain a fluid hydrophobic region, rather than a crystalline or glassy bilayer. Fluid bilayers are most responsive to changes in solution conditions and give rise to vesicles with a stable bilayer phase in dynamic equilibrium, rather than

kinetically trapped structures. Each of these copolymers will be discussed in sections 3 thru 5.

1.2 Synthetic Block Copolymers

Synthetic analogues of a natural membranes system is an area that has garnered much interest[1, 4-6, 17-21]. The result of others' research is a fluid bilayer sphere, similar to a cell membrane, called a vesicle. Whether from a small molecule lipid or a block copolymer, vesicles have been instrumental in understanding the chemistry and physics of the cell membrane. Block copolymer vesicles have the same advantages as lipid vesicles, but with greater stability and ease of use[1, 6, 19, 22]. These structures formed in solution fulfill the requirements for the first component of a biomimic. Studies[6, 17, 18, 23] show how chain length and chemistry of the block copolymers used for the bilayer will affect the bending modulus, the rigidity, the elasticity, the stability, and the ease of assembling in solution[6, 17, 18, 24-26]. Much of the vesicle formational procedures are adapted from Hammer et al and the lipid vesicle literature.

1.2.1 Surface Modification

The second component of the biomimic is surface modification for responsive particles. The ultimate goal of this research area would be to have a particle with many

different moieties incorporated onto the surface, similar to a real cell. Several studies[4, 6, 23, 27-30] have shown simple procedures in which the hydrophilic ends of the block copolymers can be modified or functionalized to include easily spliced leaving groups, such as tresyl chloride. Tresylated polymer can be incorporated into the bilayer and later reacted in order to have various functional groups on the surface of a vesicle. The drawback to this system is that the overall conversions of the reactions are low, whether it is the reaction of the end groups or the creation of the tresylated polymer. Also, the vesicle structures have to be formed before the reaction takes place. This can make it difficult to control surface density, as well as controlling solution conditions in order to maintain vesicle structures.

A newer approach to this problem is looked at by our research group by Karym Kinnibrugh. In our procedure, the hydroxyl ends of the polymer are converted into a carboxylic acid group, which allows for peptide linkage chemistry of any primary amine functional group. This procedure allows for higher yields, more control and more reaction options than the tresylated polymer. The block copolymers can undergo reaction in a monomeric state, alleviating the solution condition requirements.

1.2.2 Internal Structure

The third component of the biomimic is the formation of an internal structure. The purpose is to create an analogue to the cell's cytoskeleton within the sequestered volume of the block copolymer vesicle. By coupling the bilayer to an internal structure,

the vesicle becomes more robust, being able to withstand solution conditions that would mechanically rupture the vesicle bilayer alone. Also, an internal structure allows elements that can be attached that span the membrane and reach outward to the solution; a transmembrane element. If the bilayer coupling is achieved, the internal network, not the membrane, supports the stresses and shears of attachment, much like cell-surface attachments, and allows the biomimic to more accurately model cellular mechanics. Instead of relying on ligand-hydrophobic interactions, forces applied to the ligand or transmembrane element would be transferred down the extension and into the mass of polymer, similar to forces transferred to the cytoskeleton in cells. An example is shown in Figure 1-1 of an approach for creating an internal polymer network is that of templating.

Some examples of ligand-hydrophobic interactions are in cell adhesion system studies[23, 27, 28, 30]. These studies relied on the hydrophobic region to hold on to a block copolymer that was chemically linked to the ligand, instead of trying to have a trans-membrane member that can link with the ligand and act as an extension of the internal polymer network. Here the strength of the hydrophobic core is tested, not the adhesion energy of the various adhesion systems, due to the fact that hydrophobic interactions are not sufficient to maintain the copolymer-ligand strand in the membrane.

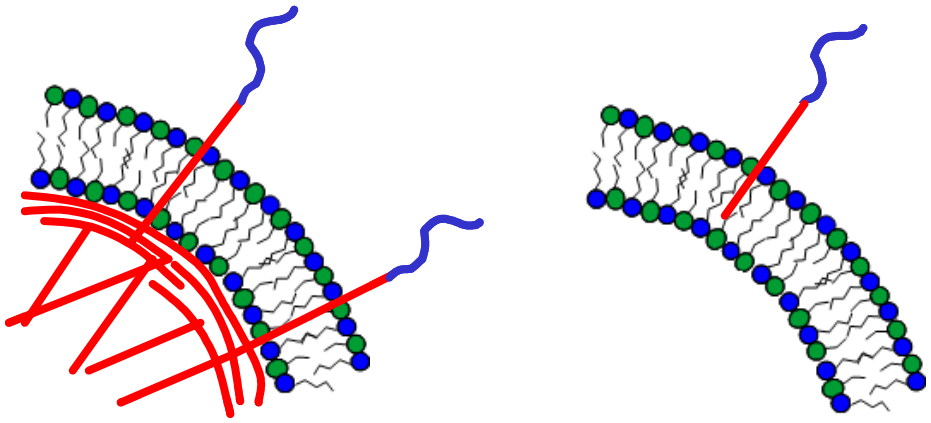

Figure 1-1: Ligands linked to extensions from an internal polymer network. The figure on the left is a representation of an extension of the interior polymer network and a functional group attached to the extension. If the ligand undergoes stresses, the force is transferred to the internal network and structure, not just the membrane. The figure on the right is how current methods attach functional groups to the membrane. The ligand is held in the hydrophobic section of the membrane. Stresses from the ligand are applied to the membrane and if enough force is applied, the vesicle membrane will rupture, causing the destruction of the vesicle.

1.2.2.1 Templating

Templating is a process that builds a temporary chemical structure so that the more permanent, desired chemical structure can be built with increased ease around the temporary structure. Much of the interest in the idea of templating builds off the ability to create new, more complex structures by first creating an organized structure in solution, then building off the structure. A biological example of this phenomenon is biomineralization of structures on the cellular level[31, 32]. Being able to produce an ordered structure from a previously self-assembled structure is of great interest in

material and catalyst research. By looking at the way the template is assembled in solution, better templates can be build, ones that can cross multiple length scales. Through better templates, more complex features can be incorporated into the structure that would then be transferred to the superstructure built off of the template, such as pores or internal supports.

The research in this dissertation focuses on building a better template, rather than the end structure. Much of the published work, discussed in the next three subsections, that has been done so far deals with creating a more complex template that leads to a more complex structure. For this dissertation, the template itself will be looked at, along with creating a simple structure inside the template.

Previous published work from which this research draws addresses three main areas: templating of structures for organized media, robust templates, and encapsulation.

The first area, templating of structures for organized media, looks at organized gels using a copolymer or surfactant.

1.2.2.1.1 Organized Media

As shown by Kaler[33] and others [6, 34-42], creating organized gels or structures from copolymers is easily done. Most of the techniques discussed in the papers describe using the surfactant or copolymer to solubilize a superstructure material. Upon polymerization of the superstructure material, the vesicles or template structures are destroyed, due to mechanical stresses. In some cases, solvent is added, removing the

copolymers or surfactants, leaving behind the superstructure. Experiments will be done to investigate creating particles of similar size and distribution with block copolymers.

1.2.2.1.2 Colloidal Interest

Templating using a copolymers or surfactants system for colloidal interests, in the form of small solid spheres of polymer, has been successful[42-46]. Colloidal interest experiments typically focus not on making a superstructure, but creating a uniform distribution and reproducible particle using surfactant/copolymer. The main area of interest is in latexes, from paints to biological interests. Gin [47] and Kaler [48] both report on using surfactants for microemulsions. Forming microemulsions differs from organized media experiments because the surfactant rearranges and stabilizes the particles as the polymerization takes place. These techniques result in particles less than 100 nm in size, whereas the organized media experiments create particles up to several microns in size.

1.2.2.1.3 Robust Template

For some copolymer or surfactant systems, such as lipid structures, a narrow range of operating temperatures, solution conditions and solvent concentrations exist. One approach to make a more robust template is a polymerized shell in which the

copolymer or surfactant is chemically linked to one another, making the current shape permanent. Polymerizing a shell can be achieved several different ways: having a double bond in the copolymer chain, introducing an agent that will bond with the hydrophobic section of the copolymer or surfactant system, or presenting an agent that will interact with the hydrophilic section of either the copolymer or surfactant system. The advantage of polymerizing the shell is the vesicle becomes impervious to mild or moderate changes in solutions or conditions.

In Discher [22], polymerized vesicles were subjugated to chloroform which, under normal circumstances, would redissolve the polymer monomerically and destroy the self-assembled structures. But having a polymerized shell, the bilayer could not rearrange or redissolve, thus keeping the vesicle intact. Shell polymerized vesicles were also subjugated to being removed from solution, air dried, and then placed back inside of solution[22]. The particles were able to maintain their shell and return to normal solution behavior once placed back into solution. Fluid vesicles cannot maintain their structure outside of solution nor withstand the pressure forces due to evaporation.

Using a surfactant system and swelling the hydrophobic region to create a vesicle shell was done by both Jung[49] and Meier[50]. These two similar systems create vesicles with a surfactant, and then dissolve a hydrophobic monomer, either heptadiene or a methacrylate, into the solution, forcing the monomer to reside inside the hydrophobic layer. The monomer is then polymerized, and the surfactant removed. The resulting shell is stable and considered a two dimensional polymer network.

Another motivation to create particles that can withstand air drying is to resuspending the sample in another solvent. Kaler[51, 52] provides two examples of creating vesicles with polymerized shells and drying out the solution. One application for this approach is creating ordered hard material from vesicle structures. Creating hard, ordered materials, such as silica synthesis, require solvents and conditions in which the vesicles would be redissolved or mechanically destroyed. Creating vesicles in an aqueous environment and then being able to put them into another solution is desirable due to maximizing material selection and operating environments.

1.2.3 Encapsulation

Encapsulating chemicals by creating vesicles is important because vesicles contain a separate aqueous center that is only accessible through the vesicle membrane. The separate aqueous volume allows the vesicles to sequester a compound of interest, such as a monomer. Encapsulating a monomer inside a vesicle is the pathway in which we will attempt to tailor the mechanical properties for the biomimic. By encapsulating monomer inside a vesicle, a microgel can be created which will provide the mechanical strength for the biomimic. The internal structure for the biomimic can also be utilized for other goals, such as being a nanoreactor, a temperature dependent particle or a drug eluting delivery vehicle.

1.2.3.1 Nanoreactors

Graff[53] presents a complex nanoreactor system; a vesicle structure with a large protein built into the bilayer. By swelling the bilayer with a methacrylate and then polymerizing the hydrophobic section, the vesicle still maintains some of the mobility the shell possessed before being polymerized. Proteins incorporated into the shell of the vesicle selectively allow the passage of small molecules, in particular ampicillin. The protein in the bilayer allows ampicillin to enter the vesicle, wherein it is attacked by an encapsulated enzyme, and then the product is expelled. The rate of enzymatic activity is monitored by an iodine stain, easily revealing the kinetics of the system.

Keller and Li[4] discuss various different reactive polymers for use in a nanoreactor setting. Instead of incorporating a protein or a channel in the bilayer, charged polymer chains are used. As the charge is placated, the chains will open up, allowing the sequestered interior and the bulk exterior to mix.

Another idea from Keller is to use either divalent crosslinkers, such as Ca^{2+}, to link chains together. With this approach, the use of salt or acid concentration can used to control vesicle or pore openings. An advantage of this method is that the system will respond much faster than a temperature or cleaving agent system. This is due to the inherently faster kinetics. One main drawback is that most of the structures mentioned are not fluid bilayers, but actually sol or gel structures in solution. These structures are not in dynamic equilibrium; they are kinetically trapped structures.

Other researchers have ideas for nanoreactors: Nardin et al[54], Meier et al[6, 55], Khomane et al[56], and Kita-Tokarczyk et al[6]. These nanoreactors follow the general idea of using vesicles as bioreactors; either with proteins on the surface or converting organic matter.

1.2.3.2 Temperature Dependent Particles

Another encapsulation system of research interest is making a temperature dependent particle, similar to Jesorka[57]. They create giant unilamellar vesicles (GUVs) and then inject into the GUV various solutions of N-isopropyl-acrylamide (NIPAM) into the interior of the vesicles. Using light microscopy, they observe the changes in the vesicle as they raise and lower the temperature above the lower critical solution temperature (LCST), for NIPAM, approximately 32^{o}C. The vesicle undergoes a phase change, having the NIPAM precipitate out of solution as the temperature rises, and then having the NIPAM come back into solution as the temperature cools. With this property, a vesicle or particle could destroy itself by going through a temperature dependent phase transition.

1.2.3.3 Drug Eluting Devices

A drug eluting device would be a structure in solution that elutes a drug of interest, at a certain rate, for a certain period of time[58-65]. From the initial work done by Lim and Wichterle[63], the idea is to have a gel or compound that will readily absorb another compound or macromolecule of interest and release the compound of interest when it is favorable. Some of the initial work was done with glycol monomethacrylates, but later expanded into poly(vinyl alcohol) (PVOH), poly(ethylene oxide) (PEO or PEG) and poly(N-vinyl pyrrolidone) (PNVP)[58, 59, 64, 65]. All the polymers are hydrophilic polymers; they have been used extensively for creating and testing drug release models.

Integrating drug elution into a biomimic presents some challenges. An artificial cell needs to have non-deteriorating components for the lifetime of the experiment; drug delivery capsules generally deteriorate during the delivery of the drugs. A biomimic should be able to move and interact with the surrounding. The drug delivery device is usually placed in an area and does not need to move. The only desired interaction with the surroundings is the elution of drugs.

But instead of focusing on the biomimic nature as an artificial cell, the focus is on using the biomimic as a delivery system to present the drug eluting device to a target area. In this sense, the biomimic is more of a "smart" particle. By combining the aspects of drug elution, surface modification, internal structure, self-organized media

and a responsive particle to area conditions, the "smart" particle can operate fairly unhindered and without assistance.

By integrating a combination of these cited techniques and ideas, achievement of one aspect of this research goal is reached by creating a complex particle that is capable of biomimicry.

1.3 Polypeptide Block Copolymers

1.3.1 Synthetic-Polypeptide Hybrids

Synthetic-polypeptide block copolymers are polymers in which one of the blocks is a synthetic polymer, usually a long hydrocarbon chain. Di- and tri-block copolymers have been used to create micelles for either gene therapy or other medical treatments[10-12]. Kataoka et al. show some success in creating micelles in solution that have the ability to assembly into approximated 100 nm structures.

Other groups[8, 9, 13, 14] have focused on block copolymers that make vesicles instead of micelles. Deming[14] shows how to make functionalized peptides that will also form secondary structures in solution. The idea of having the block copolymer possess the ability to form a secondary structure is interesting, as it could provides a pathway to force the polymer into or out of solution. Lecommandoux[8, 9, 13] has created several polymers that are pH responsive, causing the secondary structure to change from a random coil at pH 7 to an alpha helix at pH 11. Their polymer is a synthetic-

polypeptide hybrid, with the polypeptide being the block that changes its conformation. The novel polypeptide block copolymer developed by Dr. Dan Shantz is completely amino acid based, but retains the same characteristics as Lecommandoux.

1.3.2 Polypeptide-Polypeptide Copolymers

The third variation of block copolymers are those made completely of amino acids. These polymers have similar issues as the synthetic-polypeptide polymers, but their chemical, physical and solution behaviors are more complicated since peptide chains may fold. If one block is capable of forming a secondary structure in aqueous solutions, that block might alter the delicate balance of forces controlling self-assembly and cause the polymer to precipitate out of solution. Multi-peptide block copolymers have different sections of peptides that could potentially fold at different solution conditions thus yielding multiple triggers for precipitation.

Table 1-1: List of available polypeptide block copolymers. These polypeptide block copolymers are from Dr. Dan Shantz laboratory, TAMU.

2:1 K:G ratio	4:1 K:G ratio	Triblocks
$K_{110}G_{55}$	$K_{120}G_{30}$	$K_{48}G_{12}\ K_{48}$
$K_{320}G_{160}$	$K_{200}G_{50}$	$K_{120}G_{30}\ K_{120}$
$K_{400}G_{200}$	$K_{345}G_{85}$	$K_{160}G_{40}\ K_{160}$
		$K_{110}G_{55}\ K_{110}$

Peptide block copolymer synthesis is a complicated multi-step procedure during which failure can occur before the final polymerization step. Deming[66] outlines the

steps needed to create high molecular weight block copolymers. Dr. Dan Shantz and Dr. Jan Jeng Shiung have provided access to the polypeptide block copolymers listed in Table 1-1.

There have been a few attempts to determine the assembly behavior of these types of polymers in solution, as well as polymer behavior during changing solutions conditions[67, 68]. These attempts have been mostly centered on cryogenic tunneling electron microscopy (cryo-TEM) and TEM. The limitations of these approaches are in the results, it is difficult to obtain useful results from cryo-TEM, since freezing the solutions can alter the structures formed in solution if the freezing process is done incorrectly. TEM works well for imaging solid materials, but the particles of interest are solution based. By drying out the polymer, the structures that are formed during the drying process are different that those created in solution. The dried structures are that of polymer aggregation, not self-assembly.

There have been several other copolymers developed by other groups[69-71], such as poly(γ-benzyl L-glutamate), poly(L-lysine)- b-poly(L-leucine), and poly(L-lysine)-b-poly(L-leucine and L-valine). The latter polymer has two parts, a homopolymer block of lysine and a random block of leucine and valine as the other block. These polymers were investigated due to their ability to respond to solution changes, usually pH, as well as their desire to use the polymers to template superstructures or take advantage of the ordering of the blocks in solution. One problem with the previous studies is that the experiments are carried out in deionized water, after dissolving the polymer in a solvent. This method is an acceptable method to create vesicles, regardless of polymer type, but

since the polypeptide polymers are polyelectrolytes, placing the polymer in a solution without screening ions can cause the polypeptide polymer to adopt a highly strained configuration. The goal is to obtain fluid bilayers, so moderation of the repulsions between the charged blocks on the polymer is needed. By including adequate amounts of salt, any issues from deionized water should be negated. Also, the total molecular weights for these copolymers in previously published experiments are lower than the copolymer used in our experiments.

1.3.3 Responsive Particles

Responsive particles have been a subject of research for many years. Some recent work has focused on having vesicles or micelles respond due to changing pH or ion concentration[4, 72, 73]. These previous studies examined how to invert a block copolymer in solution and to control the size of self assembled structures, rather than the responsiveness of an aggregation of polymer in solution. Particles can also respond to other stimuli, such as light, temperature changes and cleaving agents[4].

1.3.4 Novel Polypeptide Block Copolymers

The polymer choice for this research is a block polypeptide copolymer of lysine and glycine. Glycine was chosen because it is hydrophobic and a random coil. Lysine is

a hydrophilic amino acid that has been used in many other experiments, plus it is capable of changing shape in solutions with a pH greater than 11. For pH >11, poly(lysine) will change from a random coil at neutral pH to an alpha helix in basic conditions. This block copolymer should be pH responsive and form a self assembled, thermodynamically stable structure in solution, rather than a kinetically trapped vesicle.

There are several reports of amphiphilic block copolymers that form vesicles upon rapid dilution into water[66, 68, 71, 74-77], but the hydrophobic block is poly(styrene), poly(phenylalanine), or another block that is glassy or crystalline at the final solution conditions. These vesicles are not in dynamic equilibrium with free block copolymers in solution, and therefore cannot be viewed as thermodynamic complex fluids – the energy to remove or insert a molecule is much higher than 1 or 2 k_BT. The thermodynamic aspect of the vesicles found in these studies with polylysine-*b*-polyglycine is that the bilayer is the dynamic and thermodynamically stable phase. Any changes to the system conditions, such as pH change, extrusion, sonication, dialysis or vortexing, may cause the vesicles to rupture, forcing the polymer to spontaneously reform into a bilayer. The size may change due to experimental procedures, but the bilayer will continue to be the most thermodynamically stable point.

1.4 Silicone Based Block Copolymers

Poly(dimethyl siloxane) (PDMS) based block copolymers are a new entrant to the amphiphilic block copolymer research. Much of the original research on amphiphilic

block copolymers focuses on poly(ethylene oxide) (PEO) and either poly(propylene oxide) (PPO) or another hydrocarbon based chain, such as polybutadiene (PBd). Since PDMS has a higher hydrophobicity, higher gas permeability and higher chain flexibility than hydrocarbons, it is logical to investigate an amphiphilic block copolymer with PDMS as the hydrophobic block. Also, PDMS does not have the reactive groups inherent to PBd. Any reactions that occur around a block copolymer with PDMS will not affect the behavior of this block.

Some basic work has been done using this polymer or similar PDMS based polymers [55, 78-85]. Hill was one of the first to use siloxanes as a hydrophobic block for a surfactant. He reports some of the early phase behavior in aqueous solutions of ABA copolymers and comb-like structures. It is interesting to note that three of the four surfactants formed vesicles in solution [85]. Nardin and coworkers [55, 81, 83] uses a PDMS based ABA triblock copolymer for making sequestered reactors, which is not entirely in the scope of this research, but the idea and application is one possible avenue. A closed structure that possesses a reactive surface is a major requirement for a cell mimic. His ABA triblock copolymer possesses that trait.

Table 1-2: Interfacial energies for copolymer systems. A list of various interfacial energies for the different block copolymer systems in contact with water.

Hydrophobic Block	Surface Energy (mN/m)	Polar Component (mN/m)	Interfacial Energy (mN/m)
PDMS[86]	19.8	0.8	53.6
PBd[87]	48.6	0.0	59.0

Kickelbick and coworkers [78, 79] use a highly similar block copolymer to the one this research is based upon. In both papers, he investigates both the self-assembly of the polymers in solution as well as some of the basic thermodynamic properties. In Table 1-2, we see the reported values of interfacial tension of PDMS and water, as well as PBd and water. Kickelbick reports a surface energy of one PDMS block copolymer, 31.5 mN/m[79], that is higher than the value used to calculate the interfacial energy. Using his number for his largest PDMS copolymer, we get an interfacial energy of 54.74 mN/m, a marginal increase of 2.06%.

2. METHODS

2.1 Naming Convention

The naming conventions for the samples are as follows: polymer type, followed by the percentage, by weight, of the monomer encapsulated, and if a fluorescent dye was added. If acrylamide was added to the sample, a –XX is added, where the XX is the crosslink ratio, the number of monomer units to crosslinkers. If no number is indicated with acrylamide polymer, it is the 19:1 ratio monomer. A sample name would be $E_{20}Bd_{33}$ 10% AM-F, indicating $E_{20}Bd_{33}$ polymer with 10% acrylamide and FITC encapsulated on the inside. $E_{20}Bd_{33}$ 10% AM-38 would be $E_{20}Bd_{33}$ polymer with 10% acrylamide polymer with the 38:1 monomer to crosslink ratio.

2.2 Vesicle Formation

Table 2-1: Listing of the synthetic block copolymers used in various experiments.

Di-block copolymer	Total MW (g/mol)	Blocks of PEO	Blocks of Hydrophobic
$EO_{20}Bd_{33}$	2700	20	33
$EO_{89}Bd_{120}$	10400	89	120
$EO_{30}Bd_{46}$	3800	30	46
$EO_{46}PDMS_{12}$	3100	46	12

To make vesicles, polymers $K_{200}G_{50}$, $EO_{20}Bd_{33}$, $EO_{30}Bd_{46}$, $EO_{89}Bd_{120}$ or $EO_{46}PDMS_{12}$, shown on Table 2-1, were used. A stock solution of a polymer was made to a concentration of 5 mg/mL. The solvent for the stock solution is methanol for the

polypeptide polymer, chloroform or dichloromethane for the synthetic block copolymers. 50 μL of polymer solution were aliquoted out into a vial to form a polymer film. An additional 400 μL of solvent was added to ensure an even film layer at the bottom. The vial was then placed inside of the vacuum oven and left overnight. Once the film was dried, a rehydrating solution was prepared. This solution is primarily sucrose, 300 mOs (0.3 M). If more than one sample is made, the rehydrating solution was made in an additional vial, then aliquoted out in 2 mL quantities to the individual samples.

Once the rehydrating solution has been added, the vesicles are placed overnight in the oven at 60^{o}C. The vesicle solution is then removed and cooled, either by placing the vial in the refrigerator or placing the vial on a laboratory bench for a short while.

2.3 Alternate Vesicle Formation

Polypeptide block copolymer can be placed into a vial containing a rehydrating solution and form vesicles without having to first make a film. This procedure involves making the correct rehydrating solution, usually a 300 mOs (0.3 M) sucrose solution, and placing the same amount of polymer, around 250 μg, directly into the vial. The sample is then vigorously vortexed for several minutes to make sure the polymer is distributed throughout the vial. Vortexing will ensure the solvent is displaced, causing the polymer to rearrange in solution and form vesicles. The vesicles formed this way are

generally smaller and not as efficient, with more aggregated polymer observed in the samples as with the normal vesicle creation method.

2.4 Polymer Encapsulation

Encapsulating monomer on the inside of the vesicle requires a monomer to be placed in the rehydrating solution, from 5-40%, by weight. See Table 2-2 for the amounts of monomer in the specific type of polymer encapsulated vesicle. Along with encapsulating monomer, a fluorescent dye is usually added to the monomer, giving the particles a single color. In most cases, FITC is the fluorophore that is added to the monomer.

Table 2-2: Various polymer recipes used in the encapsulation experiments. These recipes are for 2 mL of rehydrating solution.

Type*	AM (μL)	NIPAM** (μL)	PHEMA (μL)	X-Link*** (μL)	Sucrose (μL)
AM 5%	250	0	0	1.125	1750
AM 10%	500	0	0	2.5	1500
NIPAM 5%	8.4	1000	0	0.42	1000
NIPAM 10%[1]	16.8	2000	0	0.84	0
PHEMA 5%	1.125	37.5	80	0.05625	1881
PHEMA 10%	2.25	75	160	0.1125	1763

[1] – For this solution, the NIPAM is dissolved in sucrose, instead of DI water.
* - This is solution amounts for each 2 mL vial
** - NIPAM is a 10% stock solution made in the laboratory for ease in aliquoting.
*** - The crosslinker is included in the acrylamide

2.5 Linked Fluorescent Bilayers

For dual color vesicles, the same vesicle formation procedure was followed, except for the film creation step, 10% acid polymer, by weight of initial polymer, was added to the film. Five μL of acid polymer was added, with 45 μL of EO_{89}-Bd_{120} polymer added for the film. The acid polymer was prepared beforehand and supplied by Karym Kinnibrugh, from Dr. Silas Research group. The additional 400 μL of chloroform was added to ensure the even film on the bottom of the vial. After the vesicles had been formed and polymerized, an EDC/NHS reaction would attach a coumarin-based dye to the ends of the acid polymer. This reaction was performed by Karym Kinnibrugh.

The peptide linkage reaction is well known and utilizes EDC and NHS[88-91]. The procedure involves taking a prepared sample, in this case a vesicles solution of EO_{89}-Bd_{120} 10% AM-F with 10% acid polymer, and reducing the solution to pH 6. The next step is to add in a five times molar excess solution of EDC and a three times molar excess solution of NHS. The solution is allowed to react for 15 minutes, and then the pH is raised back to 7-7.5. The coumarin-based dye is added to the reaction, and since it has a primary amine, it is linked to the acid polymer in the vesicle bilayer. Several additions of EDC and NHS are added over several hours to increase the yield of the reaction of coumarin-based dye to the acid polymer. Once the reaction has finished, the sample is placed in a dialysis cassette and cleaned out. The procedure for dialysis is explained in section 2.8.

2.6 Fluorescent Bilayers

In the case of some samples, a fluorophore, such as Nile Red or C-9 Acridine Orange, is added to the film polymer solution so that the fluorescent marker is evenly distributed into the bilayer. The stock solution for the fluorescent marker is made with the same solvent in which the polymer is dissolved. The fluorophore is added to a small centrifuge vial, along with the polymer solution and vortexed gently to ensure even distribution. The solution is then taken and placed in a sample vial and extra solvent is added, following the normal procedure to make vesicles.

A stock solution of Nile Red was made with a final concentration of 0.1 mg/mL. Nile Red was added after the polypeptide block copolymer had been aliquoted into a vial. A ratio of 4:1 polypeptide to Nile Red was added to the vial and then an additional 400 μL of MeOH was added to the whole solution to create a more uniform film. The final steps are exactly the same as the normal vesicle formation steps.

2.7 Extruding Vesicles

In order to create a more monodispersed or a specific size sample of vesicles, the solution of vesicles can be extruded. Extruding a sample is forcing the solution through a filter with a predetermined pore size, making the vesicles break open in order to pass

through the filter. The pore size of the filter will ultimately determine the size of the vesicles that are created.

The first step to extrude a sample, the extruder chamber is prepared after the vial is taken out of the oven. Preparing the chamber involves rinsing the syringes and filters in aqueous solution so that the osmotic pressure of the surfaces is equal to that of the bulk solution, then the sample is loaded and pushed through the filter the required number of times. All extrusions are done with an odd number of passes to make sure the samples stay clean. Once the sample has been extruded, dialysis and polymerization follows.

Before a sample is extruded, it might be necessary to run the sample through several freeze/thaw cycles. Putting samples through a freeze/thaw cycle causes vesicles to break apart due to the shearing forces during rapid cooling. By repeating the freeze/thaw steps several times, larger vesicles can be broken into smaller vesicles before extrusion.

A freeze/thaw cycle involves taking the vesicle sample and placing the entire vial in a bath of liquid nitrogen. After several minutes, the whole sample is frozen. With care, the sample is removed, and placed on a metal laboratory shelf for several minutes. This pause gives the glass sample vial time warm up so that the immersion into tepid water does not cause the glass to break. The sample is kept under tepid water until the sample has completely melted. Once the solution has melted, the sample is placed back into the liquid nitrogen. These steps are repeated several times, usually five times, and after the final warming up of the solution, the sample is extruded.

The extruding device consists of two gas-tight syringes, 1 mL each, a Teflon chamber and a stainless steel jacket. Each syringe inserts into half of the overall Teflon chamber. The two halves have between them four filter supports and one filter. Two supports are placed on either side of the filter and the Teflon blocks are compressed together. The Teflon and filter system is placed into a stainless steel jacket that is screwed together to hold the filter and Teflon tightly. The syringes are then inserted into holes on opposite sides of the stainless steel jacket.

The filter system needs to be wetted and brought up to the correct osmotic pressure to make sure that the vesicles are not destroyed during extrusion. Several passes are made with a syringe full of DI water, followed by several sets of several passes of iso-osmotic phosphate buffer solution (PBS). Once the syringe and Teflon chamber are wetted, the sample is drawn into one syringe and extruded the request number of passes.

2.8 Dialysis

Dialysis is done to remove the monomer or other chemicals that did not get encapsulated inside the vesicles. The first step in performing dialysis is done by preparing a PBS solutions that is slightly higher in osmotic pressure than the sucrose solution, usually 400 mOs (0.4 M). A dialysis cassette is prepared by soaking it in the PBS for 5-10 minutes, then injecting the sample into the cassette. The dialysis cassette is placed in the beaker of PBS and stirred gently for 3-4 hours.

Once the time has passed, the samples are removed and placed into a new vial. Before the samples are removed, a small amount of higher osmotic pressure PBS is added to the sample inside the cassette. This causes a flux of solution into the cassette and improves the recovery yield of vesicles.

2.9 Dilution Approach to Cleaning

If the block copolymer cannot contain the monomer inside the vesicle or dialysis would destroy the vesicles before the monomer could be polymerized, a dilution approach was used to polymerize the monomer. The sample is prepared following the normal vesicle creation technique, from section 2.2. Once the sample is removed from the oven, a larger quantity of rehydrating solution was prepared. The new solution has the same osmotic pressure as the rehydrating solution, but without the monomer. The reason for making a solution with the same osmotic pressure is that the overall osmotic pressure difference on the vesicles needs to stay as close to zero as possible. Once the new solution is prepared, the sample is added to the larger volume solution. Volume addition is usually done in ratios of 10, such as 1:9 sample to bulk volume. By adding the sample to the large volume of aqueous solution, the bulk exterior monomer concentration will fall below the minimum gelling value so that when polymerization occurs, the sample stays liquid.

The sample is now polymerized using the ammonium persulfate/TEMED (APS/TEMED) solution. The sample is then centrifuged, excess solution is drawn off, and the vials are consolidated to bring the sample back to its original volume.

2.10 Polymerization of Monomer

Once the sample is removed from the oven and cleaned using the dialysis or the dilution approach, it is polymerized immediately. 120 μL of APS and 30 μL of TEMED are added to initiate the reaction. The solution is usually vortexed to ensure even distribution of the initiators and the reaction takes about 1-3 hours. The reaction method is a free radical initiation; the TEMED breaks apart the APS and forms a single radical for each chemical pair.

If the vesicles are to have just a polymerized shell, the same amount of APS and TEMED are added and allowed to react once the sample is removed from the oven. The reaction takes about the same amount of time, 1-3 hours.

If the APS/TEMED system will not polymerize the solution fast enough, a light induced initiator is used. This solution is composed of N-vinyl pyrrolidone (NVP), 1 mL, and 2-Dimethoxy 2 phenylacetophenone (acetophenone), 300 mg. The acetophenone is a radical producer and initiates reactions in the same manner as the APS/TEMED system. The photoinitiator is added to the sample and then the sample is placed under a UV lamp (250 nm). After a few minutes the sample is fully polymerized.

A final initiator system for the polymerization of monomer is that of VA-44 (2,2'-Azobis[2-(2-imidazolin-2-yl)propane] Dihydrochloride). This initiator is also a free radical initiator, but relies on the temperature to activate the compound; once the sample temperature rises above 44^{o}C, the initiator is activated.

2.11 Lipid Labeling

For some fluorescent vesicles, a fluorescently labeled lipid is added after the vesicles have been formed. For this, a small part of the sample is placed in a centrifuge vial, along with the lipid labeler. The solution is then vortexed vigorously for several minutes to get the lipid labeler evenly distributed in the vesicle's hydrophobic region.

In making fluorescently labeled vesicles with Acridine Orange (AO), 3,3′-Dioctadecyloxacarbocyanine perchlorate (DiO), or 1,1'-dioctadecyl-3,3,3'3'-tetramethylindocarbocyanine perchlorate (DiL), vesicles are first made using the normal vesicle formation procedure (section 2.2). Since the fluorophore does not dissolve into aqueous solutions, methanol is added to dissolve the fluorophore so in order to be added to the sample, in a ratio of 500:1, block copolymer to dye. This ratio was added to make sure that the amount of methanol being added to the solution did not disrupt the vesicles.

2.12 Confocal Imaging

All confocal images are taken on a Leica TCS SP5 broad band confocal microscope (Bannockburn, IL). All images are kept in a raw tiff format and analyzed with ImageJ (National Institute of Health).

A three-sixteenth inch thick square rubber gasket with a hole cut of the center is placed on top of a 22x50 mm glass cover slip. A small amount, 30-50 μL, of the sample solution is added to the center. Slightly higher osmotic solution of PBS, 300-310 mOsm/kg, is added to the rest of the cavity, 120-150 μL. The sample is then placed on the confocal microscope and imaged using the 63x oil objective lens that has an NA of 1.25. Pictures are taken at a resolution of either 512x512 or 1024x1024, at a refresh rate of 400 Hz, a pinhole size of 100 μm, and a voltage of 700 V for the photomultiplier tube (PMT). The excitation wavelength for FITC, DiO or AO was 488 nm and the emission band was 500-600 nm. The excitation wavelength for Nile Red or DiL was 543 nm and the emission band was 600-700 nm for Nile Red.

2.13 Microscope Imaging

Vesicle solutions were imaged using a temporary closed sample chamber constructed by using a microscope slide, microscope glass cover, two Teflon strips and vacuum grease. In order to provide contrast for imaging, a 320 mOsm/kg NaCl solution was placed into the temporary chamber followed by a smaller amount of the vesicle

solution under study (300 mOsm/kg). DIC images of polymersomes were taken by a Carl Zeiss Axiovert 200M inverted microscope with 100 W HBO Mercury vapor lamp coupled to a Zeiss AxioCam MRm camera and a 40X objective was used. For all the cases, the recorded images were processed and analyzed with ImageJ.

2.14 Light Scattering Measurements

For testing the samples using a laser light scattering technique, the samples are made using the same formation technique, with the exception that everything is filtered to remove contaminates. A 0.22 μm syringe-tip filter is used for all liquids, from the methanol used to ensure an even film, to the sucrose rehydrating solution, to the a final filtration if the samples have been extruded, in order to remove bacteria, dust and other small particles not of interest.

For Dynamic Light Scattering (DLS) testing, the sample is added into the cuvette, about 800-1000 μL. Clean PBS is added to fill the vial up to about 3 mL. Part of the solution is then aspirated into a clean Pasteur pipette and shot back into the cuvette. This process is repeated several times to mix the sample without introducing any air bubbles. The sample is then capped and placed in the machine for testing.

The machine, a Brookhaven Instruments ZetaPals DLS, is a self-contained light scattering machine. Testing parameters are controlled using the ZetaPals software, including time delays, solution conditions and testing time. The laser used is a HeNe, with an emission of 633 nm.

For Static Light Scattering (SLS) measurements, the sample basic idea persists. About 600-1000 μL of sample is withdrawn from the sample vial and placed in the glass test tube. Clean PBS solution is added to fill the test tube about three quarters full. The tube is either capped and vortexed gently to avoid air bubble formation or a clean Pasteur pipette is used to aspirate and shoot the solution to mix it up. The test tube is then inserted into the Goniometer for measurements.

The Goniometer is a Brookhaven Instruments Corporation machine as well. The system utilizes a Melles Griot HeNe laser that runs at 633 nm, with a maximum power output of 75 mW. For the testing trials, a sweep of 10^{o} to 155^{o} was used, at 5^{o} intervals.

2.14.1 Dynamic Light Scattering

Dynamic light scattering uses a time-correlation of the photoelectron count to obtain a size distribution of particles in solution. The general form of the equation is[11]

$$g^{(2)}(\tau) = 1 + \beta\left|g^{(1)}(\tau)\right|^2 = 1 + \beta e^{(-2\bar{\Gamma}\tau)} \qquad (2\text{-}1)$$

where

$g^{(2)}(\tau) =$ Normalized second order correlation function

$\beta =$ Parameter of the optical system, constant

$g^{(1)}(\tau) =$ Normalized first order correlation function

$\tau =$ Delay time

$\overline{\Gamma}$ = Average characteristic line width

$g^{(1)}(\tau)$ can be expressed by the following equation.

$$g^{(1)}(\tau) = \int G(\Gamma) e^{(-\Gamma\tau)} d\Gamma \qquad (2\text{-}2)$$

where

$G(\Gamma)$ = Distribution function of Γ

The analysis of the autocorrelation functions used the method of cumulants, where

$$g^{(1)}(\tau) = \exp\left[-\Gamma\tau + \left(\frac{\mu_2}{2}\right)\tau^2 - \left(\frac{\mu_3}{3!}\right)\tau^3 + \ldots \right] \qquad (2\text{-}3)$$

yields the average line $\overline{\Gamma}$ and a variance or polydispersity index of $\frac{\mu_2}{\overline{\Gamma}^2}$. This approach, the cumulant approach, gives us the z-averaged diffusion coefficient, D, based on the average line width with the follow equation.

$$\overline{\Gamma} = Dq^2 \qquad (2\text{-}4)$$

$$q = 4\pi\lambda \sin\left(\frac{\theta}{2}\right) \qquad (2\text{-}5)$$

where

q = Magnitude of the scattering vector

$\theta =$ Detection angle (90^o)

Using the Stokes-Einstein equation, we can then calculate the hydrodynamic radius, R_h, for particles in solution.

$$R_h = \frac{k_B T}{(6\pi\eta D)} \qquad (2\text{-}6)$$

where

$k_B =$ Boltzmann constant

$T =$ Temperature, absolute

$\eta =$ Solution viscosity

2.14.2 Static Light Scattering

Static light scattering differs from dynamic light scattering based on two principles. One, the technique depends on the average position of the particles, not their motion. Secondly, the scattered light collected is measured over a wide range of angles, not at a set angle. This measurement relies on a completely different system property than that of DLS, but should yield a similar particle size for the same sample[92].

From Guinier, if we have particles of any shape in a random orientation, of a dilute solution, the observed intensity is

$$I(s) = n^2 \exp\left(-4\pi^2 s^2 \overline{R_D^2}\right) \qquad (2\text{-}7)$$

where

$I(s) =$ Intensity

$s = \frac{q}{2\pi}$

$\overline{R_D^2} =$ Average of R_D^2, the radius of the shape in direction D

By taking the natural log of equation II.7, we end up with

$$\ln I(s) = \ln n^2 - \frac{1}{3} q^2 R_D^2 \qquad (2\text{-}8)$$

$$R_g = \sqrt{3\overline{R_D}} \qquad (2\text{-}9)$$

where

$R_g =$ Radius of gyration

We can plot *ln I* versus q^2 to obtain the slope. The slope of the graph is the radius of gyration. Figure 2-1 shows the region of data that is considered for the Guinier analysis. The radius of a spherical particle (referred to by Guinier radius) is related to the radius of gyration by

$$R_g = R\sqrt{\frac{3}{5}} \qquad (2\text{-}10)$$

where

$R =$ Guinier radius

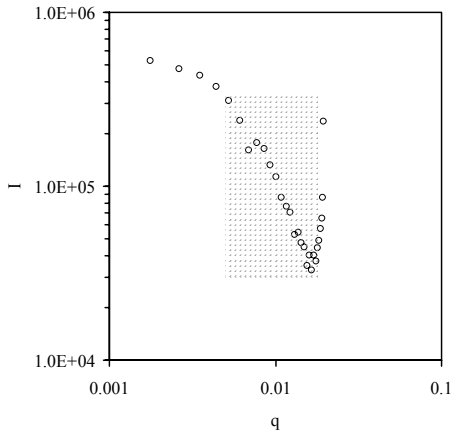

Figure 2-1: Plot of I versus q for a given sample. This graph shows the intensity as a function of angle. By looking at the data as they approach low q, we can get the size of the particle. In the analysis of this sample, the first data points are excluded. The grey box indicates shows the region of the Guinier fit. The form factor equation is overlaid onto the data and the radius is adjusted until the points correspond accordingly.

Using the same collected data, another analysis technique that can be employed is fitting the entire scattering spectra to a geometric model; in our case, we fit the scattering data to a model for spherical particles. If the solution is monodisperse and dilute, the scattered intensity is given by

$$\Sigma(s) = \int_{V,particle} \exp(2\pi i s \cdot x) dv_x \tag{2-11}$$

$$\Sigma(s) = \frac{4}{3}\pi a^3 \Phi(2\pi s a) = \frac{4}{3}\pi a^3 \left[3\frac{\sin(qR) - (qR)\cos(qR)}{(qR)^3} \right] \tag{2-12}$$

$$I_F(s) = [\Delta\rho]^2 |\Sigma(s)|^2 \qquad (2\text{-}13)$$

where

$\Delta\rho =$ Scattering intensity

$R =$ Radius, assumed

$a =$ Particle radius

Equation 2.11 is the Fourier transform of the form function, with the integral evaluated over the volume of the sphere. Once the integral is evaluated, we get the average value of the form factor over a given shape. Figure 2-2 shows a general form factor graph. From this, we can get the form factor intensity for a particle of any given radius. The most distinctive attribute of the form factor is a large minima in intensity that varies with particle radius. The radii from the Guinier analysis is input into the form factor equations to compare the location of the intensity minima with the collected data. The utility in doing this is that for a given set of data, we can look at two distinct regions of collected intensities with different sets of assumptions to arrive at a consistent particles size.

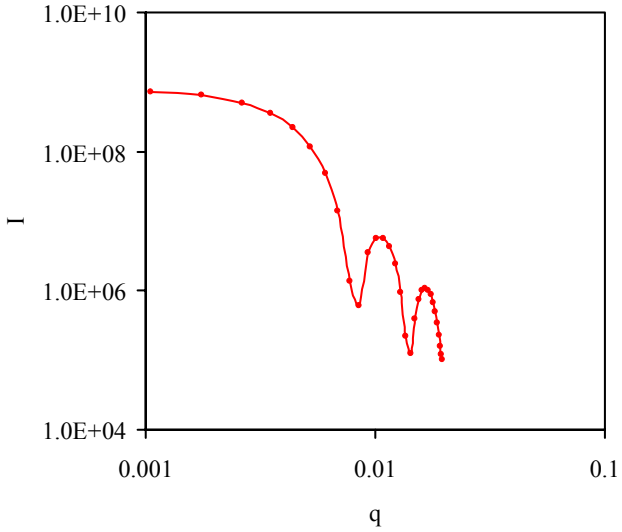

Figure 2-2: Form factor graph for a particle of a given radius. This graph shows the form factor and the local minimums.

By looking at the small angle section, we can determine a particle size from the form factor equations. By looking at the middle range of angles, we can use the Guinier analysis to pick out the particle sizes. Hopefully, the two values should be close to each other, if not identical.

We can perform this analysis based on the fact that the vesicle interior has a different refractive index then that of the solution in which the particles are suspended. When present, an encapsulated polymer network offers a defined core in which the light can be scattered efficiently. For the polypeptide block copolymer vesicles, the solution on the inside of the vesicles has a different refractive index than that of the bulk exterior solution, but there is not set defined core, so the results tend to be less efficient at scattering light than those of the small synthetic vesicles.

2.15 pH Swings

For testing the polypeptide polymer vesicles response to pH changes, two solutions of acid and base were created. The acid and base were made with NaCl to keep the solutions iso-osmotic. The acidic or basic salt solution keeps the solution from changing osmotic pressure. The acid and base were added to the DLS and SLS samples to raise or lower the pH to either 7 or 11. The acid or base was added in, mixed in the same manner as the PBS was mixed with the original sample and placed back into their respective machines to be measured again. The acid for these experiments is HCl; the base NaOH.

2.16 Pipette Measurements

Glass pipettes were prepared using standard techniques[93, 94] and placed into a custom manometer system. The pressure transducers, Validyne DP45-32 (Northridge, CA), allowed the measurement of the imposed pressure on a vesicle system and the micromanipulators, Narishige MHW-3 (East Meadows, NY), allowed the vesicles to be aspirated and moved. The Visual Basic (VB) code used in the image and pressure collection is shown in the appendix.

A custom glass chamber was created by using two Teflon strips sandwiched between a 22x50mm cover slip and a 22x22mm cover slip, sealed with vacuum grease, to give a small open ended chamber. A 1-3% bovine serum albumin (BSA) solution was

used to fill the chamber to prevent sticking of vesicles to glass surfaces. The BSA was removed and iso-osmotic solution added along with the sample. The pipette tip was coated with BSA to prevent sticking of the vesicles. The vesicle solution was allowed to settle which also allows the vesicles to deflate partially.

$$\tau = PD_p / 4\left(1 - \frac{D_p}{D_v}\right) \qquad (2\text{-}14)$$

where

$\tau =$ Tension

$P =$ Pressure difference

$D_P =$ Diameter of the pipette

$D_V =$ Diameter of the vesicle

Once a vesicle was aspirated, the pressure was recorded via the pressure transducer program to the microscope. Vesicles were allowed at least 2 minutes at each pressure to equilibrate. A picture is taken of each vesicle at each recorded pressure. From basic data collection methods, the tension is calculated from the pressure with the above equation and the surface area of the vesicle is calculated from the image. From this data set, all other reported values for each vesicle are calculated.

2.17 Material Testing

Testing the tensile properties of the bulk polymer samples requires the following equation[95]

$$E = \frac{Stress}{Strain} = \frac{FL_o}{A_o \Delta L} \qquad (2\text{-}15)$$

where

$E =$ Young's modulus, Pascals

$F =$ Force applied to the sample

$L_o =$ Original length of the sample

$A_o =$ Original area of the sample

$\Delta L =$ Change in length of the sample

For the Young's modulus and compressive modulus tests, samples were prepared by making a large vial of polymer solution. Four vials were made, 5% and 10% solutions as well as 19:1 and 38:1 ratios. Photoinitiator and monomer was added to a custom made chamber consisting of a Teflon base with several holes of decreasing size drilled successively deeper. The smallest hole had a glass rod inserted and the largest hole had a plastic drinking straw inserted. This created an annulus for the polymer solution. Approximately 2-3 mL of polymer solution was added and placed under UV (250 nm) light for 2-3 minutes. The straw/glass group was removed from the Teflon based and placed in an iso-osmotic bath to help with the removal of the glass rod and the

straw. The straw was removed first and fishing line was used to cut the polymer tube into sections. Once the small polymer rings were cut, they were placed in another tray of iso-osmotic solution to wait for testing. Once all four polymer samples were created, the rings were tested on the Instron machine.

The Instron was setup for a tensile ring test configuration. The rate of pulling was held constant at 1 mm/min. Once the ring broke, another ring was placed on the arms, after the Instron returned to the starting position. During the test, the rings were assumed to be parallel rectangular samples, with the testing beginning with the sample in an unloaded state. When the strain gauge indicated a value of 0.1 N, the recorder started to record the values for the test.

For the compressive test, the same polymer solution was utilized, once again vortexed to ensure even distribution of the photo initiator. The same custom chamber from the tensile ring test was used, except this time no glass rod was inserted. This allowed for uniform cylinders to be created. The same steps were used in creating the cylinders as the rings, except a scalpel was used to cut the cylinders and trim off excess polymer gel.

The same Instron machine was used, except with a dynamic compressive test configuration. The rate of compression was the same as the extension, 1 mm/min. The machine started the recorder when the strain gauge indicated a value of 0.1 N. The gels were compressed to a strain of 10%, and then allowed to soak in iso-osmotic solution overnight. The gels were then tested to 20%, allowed to soak again overnight and finally test to failure at 40% strain.

For compression testing of the samples, Equation 2.15 is used, with the exception that E is now a compressive modulus, not a tensile modulus.

3. POLYPEPTIDE BLOCK COPOLYMERS

3.1 Circular Dichroism

Circular Dichroism (CD) was performed by Dr. Jan Jeng Shiung of Dr. Dan Shantz's group. The results are graphed in Figure 3-1 and Figure 3-2. We can see from Figure 3-1, where the polymer concentration is below the critical micelle concentration (CMC), that as the pH is increases, two distinct peaks, one around 208 nm and the other around 222 nm, appear. These two peaks correspond to an alpha helix being formed. Since the solution contains just free polymer chains, not aggregates in solution, the polylysine block is collapsing from a random coil into an alpha helix. While we cannot determine how much of the structure is converting into an alpha helix, or how fast it is converting, the main point is that the block polypeptide polymer is converting from a random coil into a structured material due to an increasing pH.

For Figure 3-2, the polymer chains are ordered into a structure, since the solution is now above the CMC. This causes the light from 190 nm to 208-209 nm to be scattered. This makes it difficult to see the 208 nm peak, but the 222 nm peak is still visible. Once again, as the pH is increased, the definition of the peak is increased.

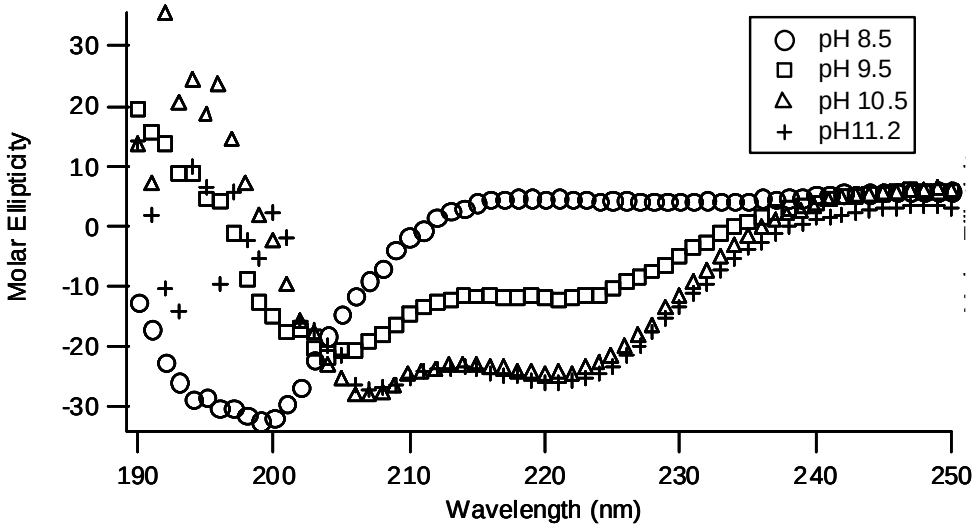

Figure 3-1: Circular dichrosim for K_{110}-*b*-G_{55} as a function of pH at 1.16 μM. This concentration is below the CMC. We have the dual peaks at both 208 and 222 nm, indicating that the block copolymer is forming an alpha helix at higher pHs.

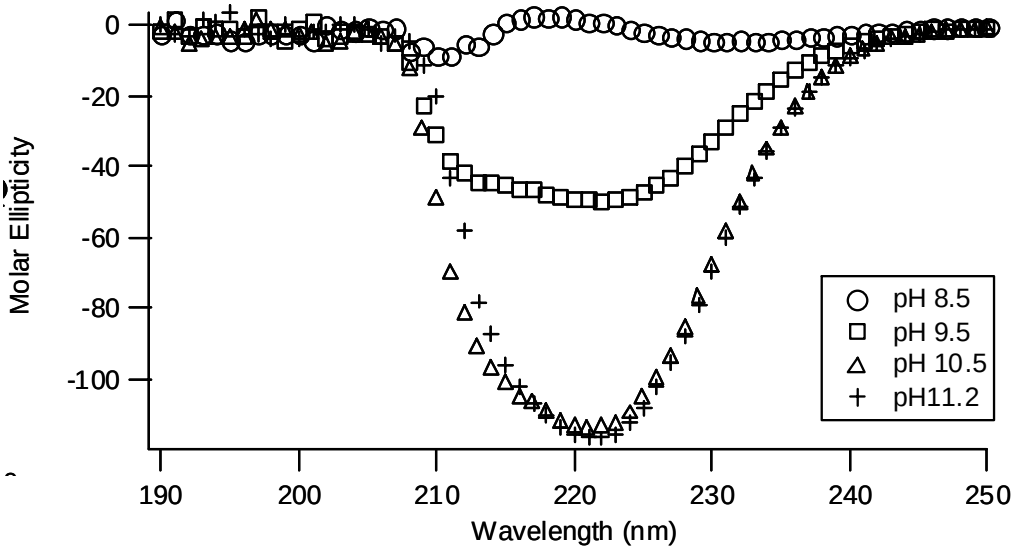

Figure 3-2: Circular dichrosim for K_{110}-*b*-G_{55} as a function of pH at 4.05 μM. This concentration is above the CMC. The peaks indicating an alpha sheet are harder to see, but the figure shows a small peak around 222 nm, with the solution scattering the 208 nm peak.

3.2 Particle Sizes in Solution

After the CD experiment was completed, larger particles were needed to see if imaging of the aggregates in solution was possible. Several methods of vesicle formation were employed, notably the standard vesicle creation technique and the alternative vesicle creation technique. Part of the drive for the various techniques was to determine and show that the vesicles being created were thermodynamically stable in solution, not a product of being kinetically trapped structures due to salt concentration or other factors. In Table 3-1, shows the hydrodynamic radius, R_h, and the Guinier radius, R as a function of salt concentration. R_h is calculated from the dynamic light scattering experiment (DLS), and R is calculated from doing a Guinier analysis on results from a static light scattering experiment (SLS). $1/\kappa$, the Debye length, is also calculated to show the effect of increasing the salt concentration[96].

Table 3-1: Radii as a function of salt concentration. This is the values used for Figure 3-3, including the Debye length for the various samples. As the salt concentration increases, the Debye length decreases, as does the difference between the hydrodynamic radius and the Guinier radius.

[NaCl], M	$1/\kappa$, nm	R_h	R	ΔR
$1x10^{-5}$	96.1	302	149	153
$1x10^{-3}$	4.3	239	138	101
0.1	0.96	179	133	46
1.0	0.3	165	146	19

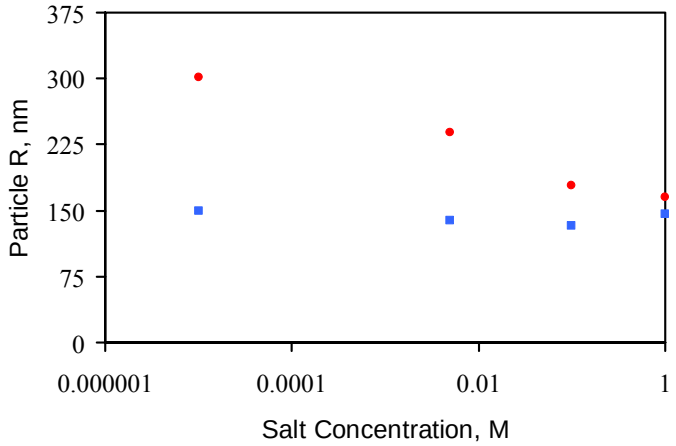

Figure 3-3: Hydrodynamic and Guinier radius as a function of salt concentration. The red circles are the hydrodynamic radius, as measured by Dr. Jan Jeng Shiung, in changing concentrations of NaCl. The blue circles are the Guinier radius, as measured by the author, with the same varying concentrations of NaCl.

As the salt concentration increases, R_h approaches the size of R, shown in Figure 3-3. This is attributed to the amount of screening charges available to the Lysine block. As the concentration of salt decreases, the Lysine chains have to elongate in order to counteract the charges from the neighboring polymer chains. As explained by others[97-101], the effect of salt can change the way the polymer chains interact with each other in solution. The one basic assumption is that of the Donnan limit: the salt added to the solution screens any long range electrostatic charges the polymer may have with neighboring chains.

For vesicles, an assumption is that the polymer is an absorbed layer with the polyelectrolyte chains acting as the polymer brush. The hydrophobic core, in this case the Glycine block, acts as a "molten film", an unresponsive block to changes in salt or pH. The Lysine brush will expand or collapse due to the decrease or increase in screening charges, in this case salt concentration.

When the salt concentration is low, the brush becomes an osmotic brush; the chains extend due the counter-ion pressure being exerted on the polymer chains. During the region of osmotic brushes, any slight variation in the salt concentration will not show any reduction in the length of the brushes.

As the salt concentration increases, the brushes cease being an osmotic brush and become a salted brush. Once in the salted brush region, the length of the brushes should scale as $L \sim c_S^{-1/3}$ *(101)*. Looking at Figure 3-4, we see the difference in radius, the hydrodynamic radius minus the Guinier radius, decrease at the power of 0.38. Due to relatively few data points, this is considered a close correlation. The difference in the two radii should give us the characteristic length of the lysine block in solution. As the lysine block collapses due to an increase in salt, the hydrodynamic radius should, and does, decrease, giving a smaller blob sphere for the lysine chains.

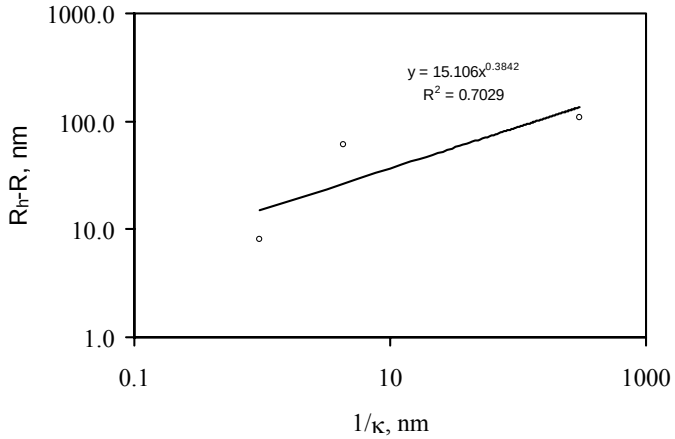

Figure 3-4: The difference between radii as a function of Debye length. Plotting the difference in hydrodynamic radius from Guinier radius as a function of the Debye length gives us a chain length reduction on the order of 1/3, which corresponds to Tirrell.

3.3 pH Swing

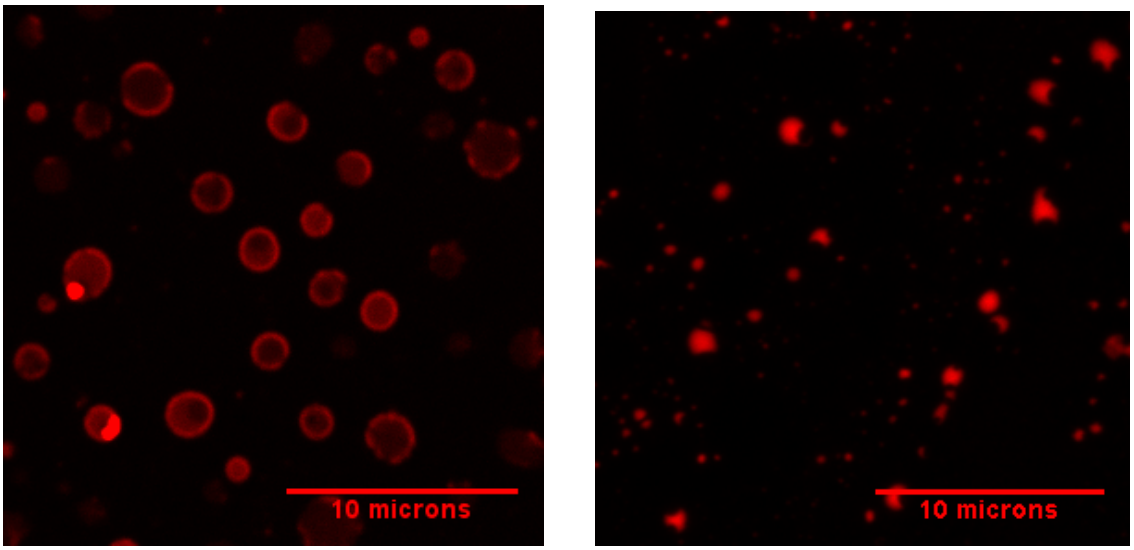

Figure 3-5: Confocal images of Lys_{200}-*b*-Gly_{50} at pH 7 and 11. The left figure is the solution at pH 7; the right image is the same solution, not the same view, at pH 11. The change in pH has caused a structural rearrangement that yields no vesicles on these size scales at pH 11.

Figure 3-5 shows the affect of increasing the pH of a sample. The vesicles in the left picture are at pH 7; they form vesicles with a clear bilayer. The right picture is of the sample after the pH has been raise up to 11. Here we see the polymer aggregating out of solution and forming large masses of polymer. The Nile Red is still incorporated into the polymer, but self-assembled bilayers are no longer visible.

To test the pH responsiveness of the polypeptide block copolymers, samples were made for both DLS and SLS. For DLS, the samples were made by the alternate vesicle formation method. For SLS, the samples were made with the standard vesicle formation technique.

The general trend for both samples is that the first cycle is higher than the other values of pH 7, and then hovers around an average value for the rest of the cycles. This trend can be seen on both Figure 3-6 and Figure 3-7. This trend can be explained as the vesicles, when first created, are of a large size distribution. When the sample is first tested, the distribution of vesicle sizes is quite extensive. Once the pH has been raised to 11, the polymer starts becoming insoluble, forcing the vesicles to collapse. Once the pH has been returned to 7, the polymer becomes soluble again, but the vesicles cannot return to their original size. An average size of vesicles is eventually reached, after several pH swings. The resulting solution is more monodispersed than the original sample, unless the original sample has had additional processing steps performed. After raising and lowering the pH several times, the vesicles approach a radius of 145 nm. The raising and then returning to the original pH is one cycle.

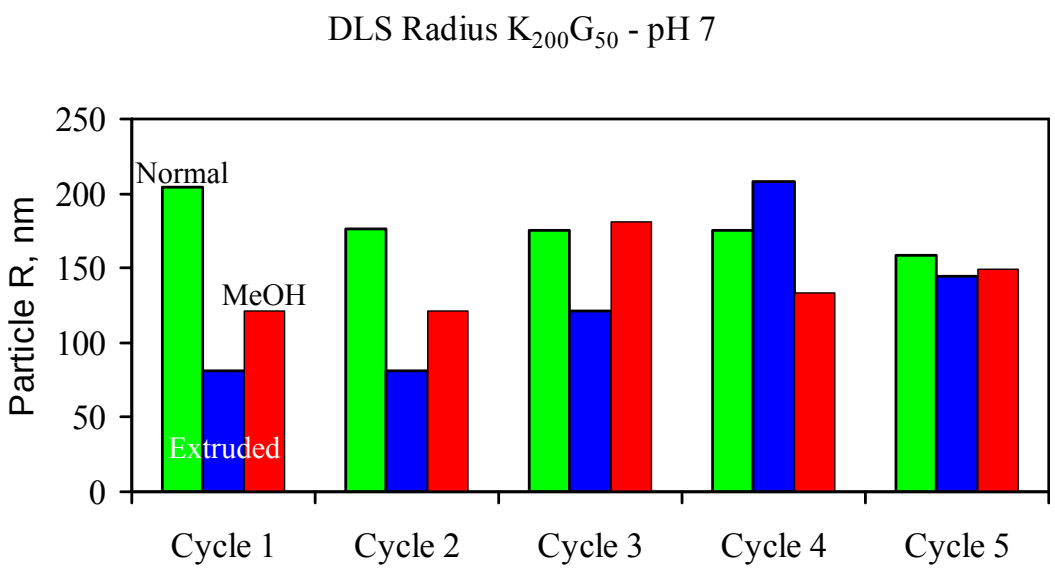

Figure 3-6: Results from a DLS pH swing. We see the changes of particle radius as we step through pH swings with DLS. We see a large particle size from normal (film rehydration) versus MeOH (dilution method) versus extruded (film rehydration followed by freeze/thaw and extrusion).

For Figure 3-7, two different, but identically made, samples were tested. The two samples were a normally made vesicle solution, utilizing the normal vesicle formation procedure. The first sample was placed in a tube and tested, allowing the pH to rise and fall for two cycles. The second sample had the pH of the solution raised and lowered for two cycles before it was placed in a tube and tested. We see the same phenomenon happen with the SLS sample as we do with the DLS sample. Although the sizes are not exactly the same, we see the same general trend of the initial particle size being high, followed by the subsequent decrease in particles sizes for the following tests at pH 7. As the pH is raised and then lowered back to 7, we see the return to an average value for the particles in solution. DLS gave a value of 145 nm for the radius; SLS gives us around 137 nm for the radius.

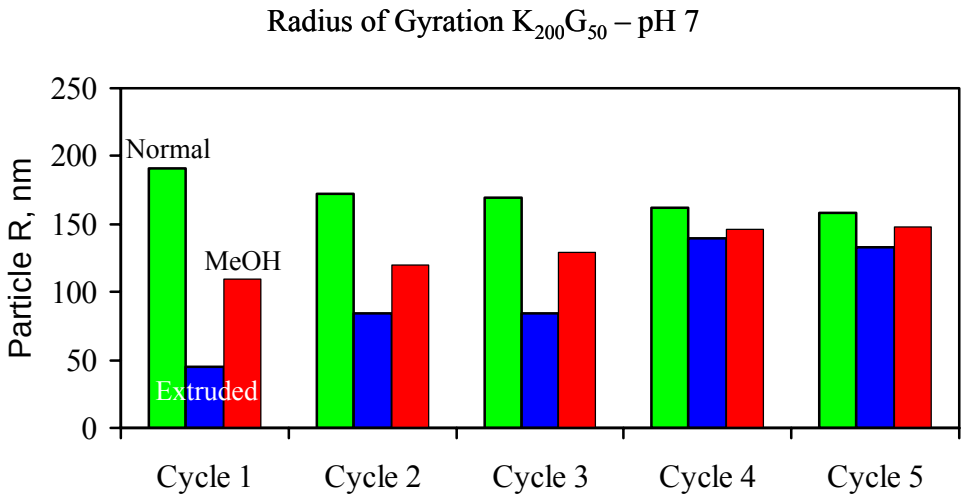

Figure 3-7: Results from a Guinier analysis on SLS data. We see the changes of particle radius as we step through pH swings with SLS. We see a large particle size from normal (film rehydration) versus MeOH (dilution method) versus extruded (film rehydration followed by freeze/thaw and extrusion).

The overall results follow the same principles as the pH swing test. As the pH of the solution is increased, the polymer starts to aggregate in solution. pH 11 will give non-reproducible numbers for the particle sizes in solution. Once the pH is returned to 7, the size returned to an average value for the samples.

For the MeOH sample, the particles start off smaller than the Normal, in part because the particles have been created nearly instantaneously. An overall increase in particle sizes is seen for the vesicles when the pH is swung up and then back down, due to the fact that the particles are smaller to begin with.

The Extruded sample offers a counterpoint to the normal vesicles. Particles in solution are about 100 nm in diameter initially, because the particles have been broken up and are more monodispersed than the other two samples. An overall increase in

particle size is seen for vesicles when the pH is swung up and then back down, due to the fact that the particles are smaller to begin. Also, the limits of curvature prevent smaller particles. When the pH increases and then is brought back to pH 7, the size increases to nearly equivalent values as the two previous samples over the course of 5 cycles.

An explanation for this phenomenon for both the MeOH and Extruded samples is that when the polymer stock solution is transferred to the aqueous solution for the MeOH sample, the polymer chains, being dissolved monomerically, are not very close to each other. The structures formed in solution are very small vesicles, in part due to the dilute nature of the stock solution. The Extruded sample is made small, so now the MeOH and Extruded samples follow the same trend. When the pH is increased, the block copolymer chains collapse and aggregate, giving the polymer chances to aggregate into larger particles with the other polymer chains in solution. Once the pH is returned to pH 7, the chains can organize into a larger structure than before, due to the fact there are now more polymer chains close enough to each other to form a larger structure.

3.4 Vesicle Creation

Figure 3-8 thru Figure 3-10 photos are the results of the experiment to see if the new polypeptide block copolymer would indeed form a self assembled bilayer. These photos were taken on the confocal microscope with Nile Red added to the film before the hydrating solution was added.

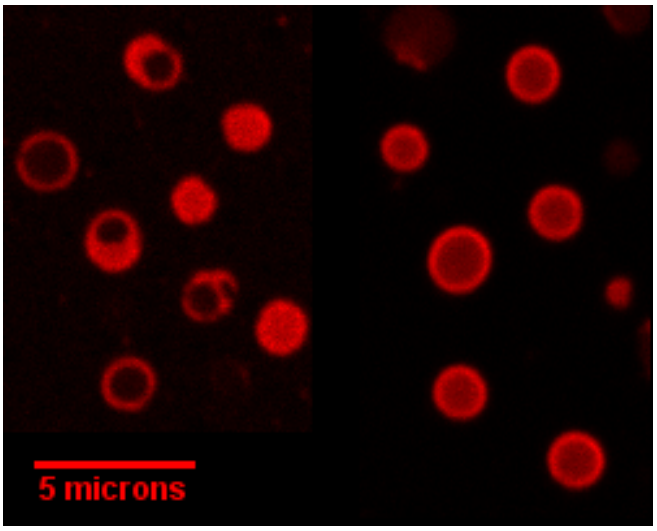

Figure 3-8: A field of view of vesicles around 2-3 microns. The vesicles show a definite bilayer region. The left and right panels are from the same sample but different areas of the sample chamber.

The first issue with the novel polymer is to determine if the polymer is indeed creating vesicles. From the DLS and SLS studies, particles are in solution; determining conclusively what the structure was, either micelles or vesicles, required microscopy. Although the sizes in solution from DLS and SLS show a much larger size than micelles, optical microscopy would shed more light on the situation and structures formed.

Using the fluorescent bilayer method, Nile Red is incorporated into the bilayer of the polypeptide polymer. These samples are then imaged on the Leica confocal microscope. Figure 3-8 thru Figure 3-10 shows the results of the vesicles. Figure 3-8, as well as Figure 3-5, shows small vesicles from the sample. We can see the halo of light indicative of a bilayer, with a small amount of light coming from the center of the ring. The photos were summed over a small range of individual photos, giving the figure.

Regardless of the intensity of the center, a small annulus of the circle should be more intense than the rest of the circle.

From Figure 3-9 and Figure 3-10, we see the top and side profiles of two individual vesicles. Figure 3-9 has two large vesicles, around 10 microns. From the profile of the vesicles, the bilayer is laying on the glass coverslip, with the top being a little out of focus, due to the Brownian motion of the vesicle top. A PBd vesicle is shown next to the polypeptide vesicle for comparison. Figure 3-10 shows the same phenomenon with a smaller vesicle, similar in size to Figure 3-9. These vesicles are only 2 microns in size, but exhibit the same characteristics of the larger vesicles. With polypeptide block copolymers, a new polymer system exists that will form closed, fluid bilayers in solution that are responsive to salt and pH changes. These polymers can be utilized as building blocks for a biomimic.

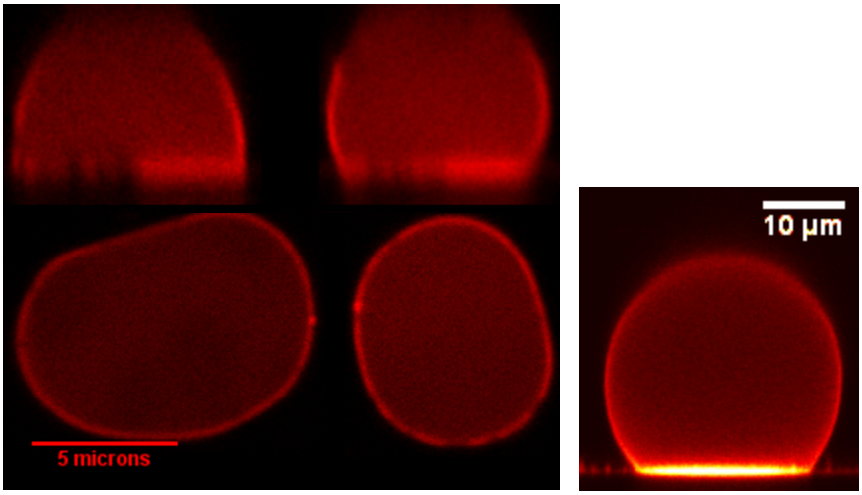

Figure 3-9: Large vesicles from the side. The left picture is of two polypeptide vesicles, the right picture a reference hydrocarbon vesicle, $EO_{20}Bd_{33}$. Notice the similar shapes and characteristics of the two vesicles. Both vesicles have Nile Red added to the bilayer for imaging purposes.

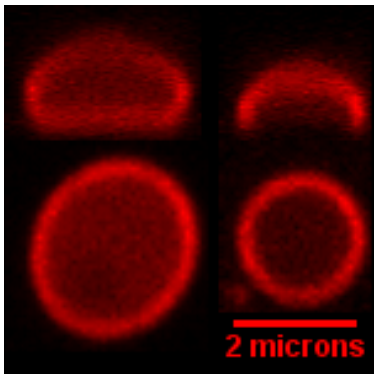

Figure 3-10: Smaller vesicles from the side. These vesicles are made the same way as Figure 3-9, just smaller in size. The vesicles imaged have Nile Red added for fluorescence.

4. POLYMER ENCAPSULATION

4.1 Compartmentalization of Monomer

In order to contain or compartmentalize the monomer, the hydrophobic region of the polymer must serve as a solubility barrier for the molecule. Acrylamide is chosen as the interior hydrogel since it is easy to work with, well understood and hydrophilic. Table 4-1 shows the enthalpic contributions, the activity coefficients and the mole fraction for all three block copolymers, butadiene, the silicone polymer and the polypeptide copolymer. Poly(propylene oxide) (PPO) is added to the table as a commercially available block copolymer comparison (Pluronics®). A group contribution method is used for solubility parameter calculations and solubility is calculated from regular solution theory. The calculated solubility of acrylamide in polyglycine and PPO reveals that the polypeptide block copolymer or PPO will not be able to contain acrylamide in the interior of a vesicle, while acrylamide has a low solubility in hydrocarbon vesicles. Experiments confirm that polyglycine cannot compartmentalize the acrylamide solution.

Table 4-1: Solubility parameters for various compounds. The reported solubility parameters for some hydrophobic blocks, an encapsulated monomer and water[21]. The reported values of enthalpic contributions, infinite dilution and mole fraction are for acrylamide inside either butadiene, glycine or poly(propylene oxide) (PPO). From this, acrylamide is too soluble in glycine or PPO to be contained inside a vesicle

Monomer	**δ (MPa$^{1/2}$)**	χ_H	γ^{∞}	$x_{solubility}$
Butadiene	11.76	2.91	18.4	0.054
Siloxane	10.80	3.658	38.7	0.026
Glycine	15.71	0.73	2.08	0.482
Propylene Oxide (PPO)	16.06	0.70	1.99	0.502
Acrylamide	21.00			
Water	48.00			

One test of encapsulation is to determine if the membrane or the bulk gel can hold onto a small molecule, such as a fluorophore. If the membrane and the gel cannot hold a small molecule, it will be impossible to image or create the vesicle or microgel. Three vesicle solutions were prepared with three types of block polymers; a short chained hydrocarbon, a long chain hydrocarbon and a silicone based block copolymer, discussed in detail in section 5, with its length in the middle of the two hydrocarbon polymers. Once the samples were dialyzed, they were placed in a pure DI vial or a Phosphate Buffered Saline (PBS) vial. They were left to dialyze for an additional 7 days. The dialyzed solution was tested; if the membrane cannot contain the small molecule the exterior solution should be equal to the interior solution at the start. The initial rehydrating solution was 116 μM, the dialysis solution was ~1.1 μM, and we would expect the interior solution to be between those two values.

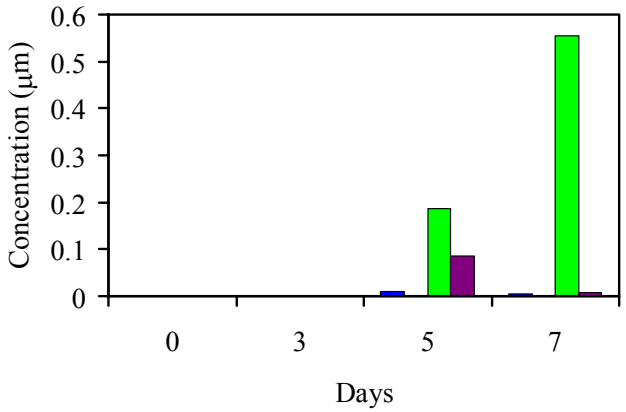

Figure 4-1: TAMRA loss from particles in PBS. Vesicles were dialyzed and then placed in a set amount of PBS and watched for TAMRA increase in the PBS. Solid blue is $EO_{20}Bd_{33}$, red is $EO_{20}Bd_{33}$-P, green is $EO_{89}Bd_{120}$ and purple is $EO_{89}Bd_{120}$-P. Polymerized particles are better at preventing leakage of small molecules, but both systems can keep small molecules below detectable limits for three days.

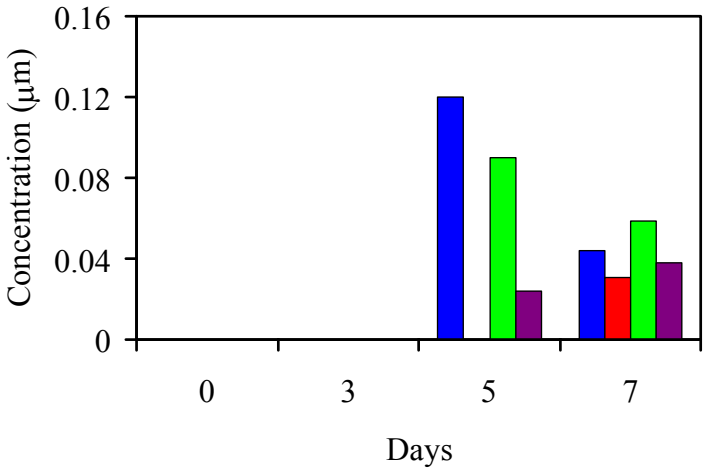

Figure 4-2: TAMRA loss from particles in DI. Vesicles were dialyzed and then placed in a set amount of DI water and watched for TAMRA increase in the DI water. Solid blue is $EO_{20}Bd_{33}$, red is $EO_{20}Bd_{33}$-P, green is $EO_{89}Bd_{120}$ and purple is $EO_{89}Bd_{120}$-P. Here polymerized particles do a much better job of keeping small molecules contained where as the unpolymerized do not. Both systems can keep the small molecules below detectable limits for at least three days, the same with the PBS case.

In Figure 4-1 and Figure 4-2, the results of the permeation test are shown. From Figure 4-2, putting the vesicles in DI, osmotically swelling the particles, eventually leads to a rise in the fluorophore concentration. Figure 4-1, shows the rise due to placing particles in an iso-osmotic solution of PBS. The rise of fluorophore, TAMRA, in either case is minimal. We see the silicone polymer has the hardest time holding in the interior solution, but only after seven days. The –P after the name indicated that the particles were polymerized prior to the DI or PBS vial placement. Polymerizing the particles severely retards the permeation of fluorophore.

The membrane is adept at keeping the interior contained for a short period of time and then a small amount of permeation after longer periods of time. The next step is to determine if a gel formed in the interior would compartmentalize a small molecule.

After three days, all the vesicle solutions maintain little or no leakage. The membrane is adept at deterring interior permeation, barring a small amount of permeation. Only by day seven does one of the vesicle samples show any significant amount of leakage, the EO_{89}-Bd_{120} vesicle solution.

Table 4-2: Loss of fluorophore in a gel. The concentration of fluorophore stays constant throughout the gel solution, indicating no impairment to permeation. All concentrations are in μM.

	19:1				**38:1**			
Marker	**1**	**3**	**4**	**Over**	**1**	**3**	**4**	**Over**
Coumarin	1.96	2.00	2.19	1.89	2.35	2.40	2.59	2.28
6AF	4.42	4.48	4.56	4.6	4.12	4.17	4.29	4.30
TAMRA	26.75	26.81	26.9	26.96	27.04	27.09	27.19	27.25

Table 4-2 shows the result of making a gel with a three different fluorophores in the monomer solution. After the gels were prepared, they were placed in a vial with DI water and the surrounding solution was tested for the fluorophore concentration after several hours. As seen in Table 4-2, the gel is not adept at keeping the fluorophore entrapped. Within three hours, the gel has completely lost all of the fluorophore initially in the gel. This is seen by the lack of change in the fluorophore concentration over time.

From these results, it is evident that the interior microgel is unable to contain any fluorophore or small molecule unless it is chemically linked to the microgel. The membrane is the limiting step in the permeation of small molecules in the system, which is a desired biomimetic trait. This offers the ability to tune desired traits independently.

4.2 DLS Analysis of Extruded Vesicles

Table 4-3: DLS results from the extruded and freeze/thaw series.

Sample Name	Passes	Mean D	Relative Skew	Span of D
$EO_{20}Bd_{33}$ Extruded a	5	200	0.048	198
$EO_{20}Bd_{33}$ Extruded b	9	190	0.054	216
$EO_{20}Bd_{33}$ Freeze/Thaw a	5	230	0.015	107
$E_{20}Bd_{33}$ Freeze/Thaw b	9	206	0.010	92
$EOO_{30}Bd_{46}$ Extruded a	5	278	0.875	624
$EO_{30}Bd_{46}$ Extruded b	9	325	-0.067	110
$EO_{30}Bd_{46}$ Freeze/Thaw a	5	332	0.287	375
$EO_{30}Bd_{46}$ Freeze/Thaw b	9	308	0.487	83

The results in Table 4-3 come from a set of experiments using both the polyethylene-b-polybutadiene ($EO_{20}Bd_{33}$) polymer and the $EO_{89}Bd_{120}$ polymer with a 10% AM-19 encapsulated inside. The recipe can be seen on Table 2-2.

The experiment set out to determine what effect a set of freeze/thaw cycles would have on a sample before the sample was extruded. This experiment also sought to see how small of vesicles could be created. The number of passes through the extruder was also changed. From the table, we see that that freezing and thawing the samples before the extrusion makes the sample diameter variability smaller. This can be seen in the span of diameters and the mean diameters of the particles. With each sample, except for one, by extruding the samples for a few more passes, the average size of the particles decreases.

When comparing the $EO_{20}Bd_{33}$ extruded vesicles versus the $EO_{20}Bd_{33}$ freeze/thaw samples, the span of diameters is reduced from 200 nm to 100 nm. The diameters seem about the same, 200 nm vs. 230 nm. Comparing sizes with each subset of samples, we see the average size of the particles is reduced.

For the $EO_{30}Bd_{46}$ samples, using the two methods as before, the span of diameters drops from 624 nm to 375 nm. The one outlier can be accounted for because of the large variance with the two samples. The $EO_{30}Bd_{46}$ extruded sample has a large variance for the first sample, putting most of the data to the left of a normal distribution. The second sample has a negative skew, placing the bulk of the data on the right of a normal distribution. Both of these factors combine to make it seem that the particles average size increased with an increase of extruder passes. The $EO_{30}Bd_{46}$ freeze/thaw sample shows a more normal distribution, as well as a smaller span.

4.3 Guinier Analysis of Vesicles

Table 4-4: Guinier analysis and results from $EO_{20}Bd_{33}$ and $EO_{89}Bd_{120}$ series. The table shows the Guinier radius, the form factor radius and the mean diameter from Guinier analysis. The particles show no statistical size difference between the various samples.

Sample Name	Guinier R	Form Factor R	Mean Diameter, Guinier
$EO_{20}Bd_{33}$ Extruded N	136	140	273
$EO_{20}Bd_{33}$ Extruded PH	129	129	257
$EO_{89}Bd_{120}$ Extruded N	131	128	262
$EO_{89}Bd_{120}$ Extruded PH	128	130	256
$EO_{20}Bd_{33}$ Freeze/Thaw N	183	186	366
$EO_{20}Bd_{33}$ Freeze/Thaw PH	138	138	276
$EO_{89}Bd_{120}$ Freeze/Thaw N	99	99	198
$EO_{89}Bd_{120}$ Freeze/Thaw PH	115	116	229

For the Guinier analysis, seen in Table 4-4, all of the samples have been extruded nine times, instead of varying the number of extrusion. The extruded samples have only been extruded, where the freeze/thaw samples went through a freeze/thaw cycle five times before being extruded, just like the steps in the DLS test. The total concentration of polymer inside the vesicles was held at a constant 5%.

For this experiment, the type of polymer encapsulated on the inside was altered, switching between N-isopropyl-acrylamide (NIPAM) and poly 1-hydroxy ethyl-methacrylate (PHEMA). The different types of polymer encapsulated on the inside did not make a major difference in the mean diameter. The experimental focus was to determine if the type of polymer encapsulated in the interior of a vesicle would change the particle distribution or particle size. The difference with these monomer systems, compared with the acrylamide monomer (AM) is that they are not heavily crosslinked.

Both monomer systems are still viscous. The AM system is heavily crosslinked, making a solid microgel in the interior of the vesicle, as compared to the NIPAM or PHEMA particles, which maintain a visco-elastic interior.

The sizes listed in Table 4-4 are the result of doing a Guinier analysis, as outlined in the light scattering measurements section under the Methods section. The following graphs are the two graphs from the Guinier analysis as well as the form factor analysis. The first set of graphs are from a plain extruded sample; the second set is from a freeze/thaw sample.

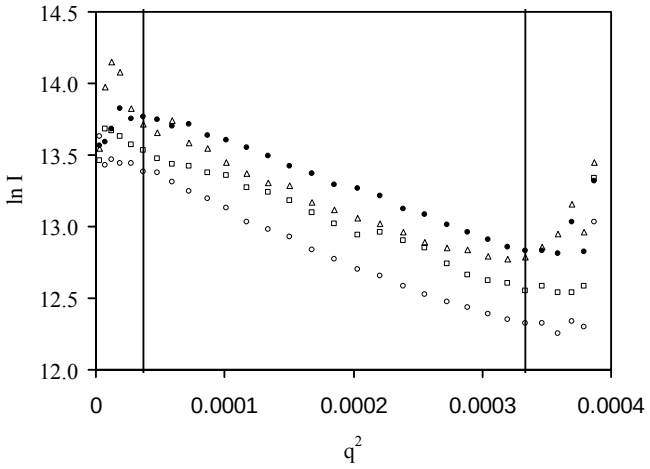

Figure 4-3: The Guinier analysis of the extruded series. The data points for the four samples are as follows: open circles (○) are $EO_{20}Bd_{33}$ Extruded N, the open squares (□) are EO_{20}-Bd_{33} Extruded PH, the open triangles (Δ) are $EO_{89}Bd_{120}$ Extruded N, and the filled circles (●) are $EO_{89}Bd_{120}$ Extruded PH. The two black lines represent the area that was considered for the Guinier analysis.

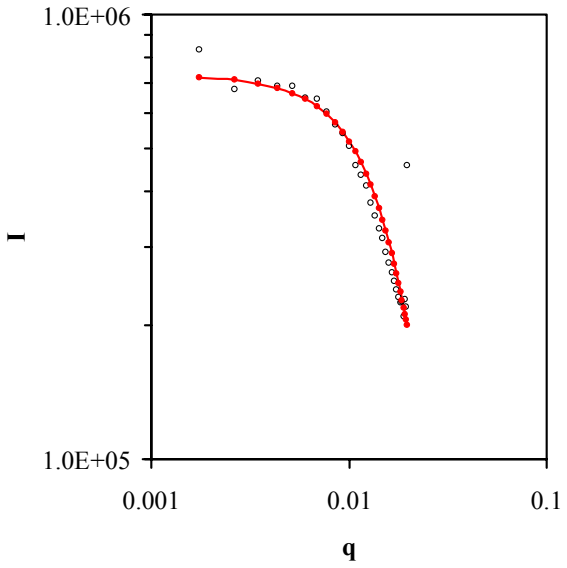

Figure 4-4: Form factor graph for $EO_{20}Bd_{33}$. Here one of the samples is compared to a form factor equation. This is the $EO_{20}Bd_{33}$ Extruded NIPAM sample. The form factor fits the data almost completely. The minimum of the form factor here corresponds to a radius of 140 nm. The red line corresponds to the form factor equation fit.

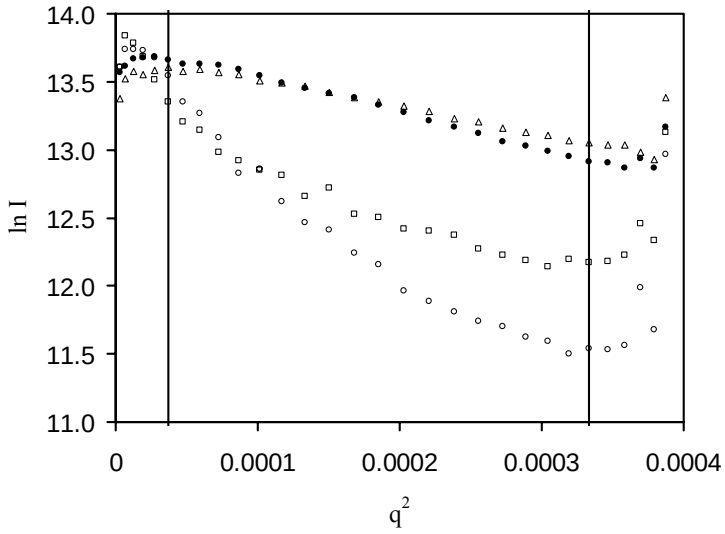

Figure 4-5: The Guinier analysis of the freeze/thaw series. The data points for the four samples are as follows: open circles (○) are $EO_{20}Bd_{33}$ freeze/thaw N, the open squares (□) are $EO_{20}Bd_{33}$ freeze/thaw PH, the open triangles (Δ) are $EO_{89}Bd_{120}$ freeze/thaw N, and the filled circles (●) are $EO_{89}Bd_{120}$ freeze/thaw PH. The two black lines represent the area that was considered for the Guinier analysis, 55^{o} to 135^{o}.

Figure 4-3 and Figure 4-5 shows the *ln I* versus q^2. From Figure 4-3, illustrates that the extruded samples inside of the black lines are fairly linear. The linear trend gives a good linear region in which the Guinier analysis will give reasonable values for the size of the particles in solution. For both the N and PH cases on the extruded series, the only difference between the two systems is the bilayer polymer. All four radii are within limits of each other, indicating that an average size is achieved regardless of the polymer outside or the monomer inside of the vesicle. In the form factor graph, Figure 4-4, the sample matches fairly well.

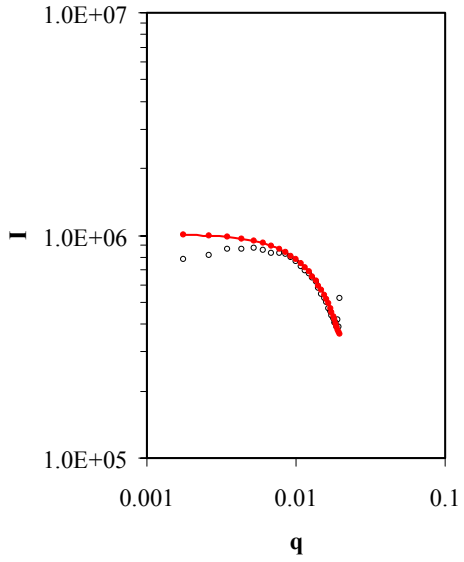

Figure 4-6: Form factor graph for $EO_{30}Bd_{46}$. Here one of the samples is compared to a form factor equation. This is the $EO_{30}Bd_{46}$ freeze/thaw PHEMA sample. The form factor fits the data almost completely. The minimum of the form factor here corresponds to a radius of 116 nm. The red line corresponds to the form factor equation fir.

For Figure 4-5, the freeze/thaw series was not as linear as the extruded series. As seen on Table 4-4, the values are strikingly different from each other. The $EO_{20}Bd_{33}$ freeze/thaw samples did not behave as the extruded series. It is unclear if the $EO_{20}Bd_{33}$ samples were contaminated or if the vesicle structures failed before testing, giving scattered results. Since the $EO_{30}Bd_{46}$ polymer was able to perform similar to the extruded trial, the $EO_{20}Bd_{33}$ runs were probably contaminated. The $EO_{30}Bd_{46}$ freeze/thaw samples performed almost identical, with the N sample having a smaller slope than the PH sample. The $EO_{30}Bd_{46}$ solutions produced similar sizes in radii, with the freeze/thaw producing smaller average vesicles. Once again, the form factor graph, Figure 4-6, shows a good correlation.

For both experiments, DLS and SLS report back similar values, indicating the ability to control the size of particles, as well as a possible early success of encapsulation. This claim of success is due to the fact that the particles scattered quite efficiently, as compared to the polypeptide block copolymer vesicles, explained in section 3. By looking at the intensity of the scattered light from the synthetic block copolymer vesicles, the interior of the vesicle has a sequestered volume that has a markedly different refractive index than that of the bulk solution. When looking at the polypeptide block copolymers, the scattered light is not as intense, giving rise to the idea that the interior refractive index is not as different from the bulk solution. These results are indicative that the interior of the synthetic block copolymer vesicles have successfully contained and polymerized the encapsulated monomer in their interior.

4.4 SEM Photo of Freeze/Thaw Series

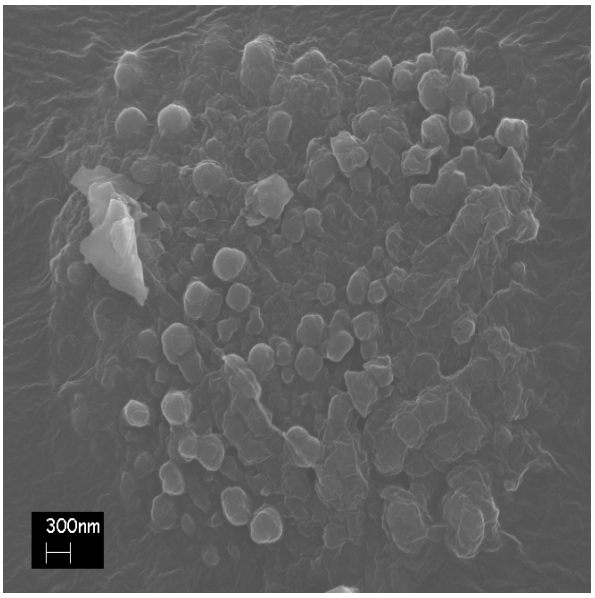

Figure 4-7: A SEM photo of 200-400 nm particles. The small spheres are the remains of the acrylamide inside the vesicles.

A sample of the $EO_{89}Bd_{120}$ freeze/thaw 10% AM particles were dialyzed against DI water for five days to remove as much of the sucrose and salt solutions present in the sample to be sent off for imaging. As stated before, SEM or TEM does not provide a good example of what structures are formed in solution, since the drying out process necessary for imaging destroys any self-assembly, and the resulting image is that of aggregation of the polymer. In this case, acrylamide encapsulated in the interior of the vesicles is fully polymerized to produce solid samples. The internal polymer network is not changed nor destroyed due to those processing steps; the image from Figure 4-7 is that of our final polymerized particles.

When the sample is dialyzed against DI and the sucrose or salt is removed from the sample, the vesicles will start to aggregate when the solution is dried. This is why the image has an island of polymer with the individual remains of a vesicle protruding from the surface. According to the scale, most of the acrylamide microgels are around 300 nm.

4.5 Dual Color Encapsulation

For dual color encapsulation, acrylamide was encapsulated with a fluorescent marker inside an $EO_{89}Bd_{120}$ vesicle. There was success with encapsulating fluorescent monomer into the interior of a vesicle, as seen with the next section, interior polymer networks. From that success, an attempt to see if acrylamide could be encapsulated with the addition of a small amount of modified synthetic block copolymer in the bilayer. The modified block copolymer would be available to undergo chemical reaction to link a fluorophore to the copolymer. The interior network was a 10% AM-F network with 10% of the $EO_{89}Bd_{120}$ polymer being acid polymer. Once the vesicles were created, dialyzed, and then polymerized, a coumarin-based dye was attached to the acid polymer. The resulting two-toned images, Figure 4-8, are from the vesicle sample.

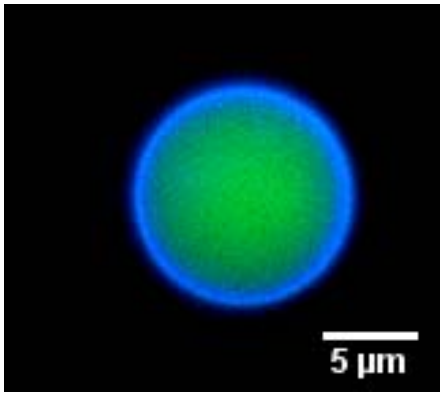

Figure 4-8: $EO_{89}Bd_{120}$ with 10% $EO_{89}Bd_{120}$-COO^- and 10% AM-19-F. Karym Kinnibrugh did the reaction to link a coumarin based dye with the acid polymer inside the vesicle bilayer. The reaction details are discussed in section 2.5. The coumarin dye, left, is linked to the acid polymer in the bilayer of the vesicle. The FITC, right, is integrated into an internal polymer network inside the vesicle. This is the same vesicle pictured for both images.

Upon doing a control experiment with identically created polymerized microgel vesicles, the coumarin dye was unable to offer the same results as the chemically linked vesicles. One explanation for this is that once the bilayer of a vesicle is polymerized, it is difficult to get hydrophobic dye to solubilize inside of the bilayer. Some residual coumarin was found in the bilayer, but not the same amount or intensity as the chemically linked vesicles.

With this the synthetic block copolymer system, a vesicle with an adjustable surface chemistry is achieved. Simply by changing the amount of acid polymer that is added to the normal synthetic block copolymer, a vesicle is made that possesses both a hollow membrane structure as well as a structure that possesses adjustable surface chemistry. The next section discusses the steps to create an internal polymer network that offers the ability to tailor a specific mechanical property. The only drawback to

using the synthetic system is that in polymerizing the internal network, the fluid bilayer attribute is lost. The butadiene block in the copolymer polymerizes with itself and causes the hydrophobic region to become rigid. This is an advantage, as it makes the sample more robust so that it can undergo the linkage chemistry, but it sacrifices the fluid nature of the bilayer interface.

4.6 Interior Polymer Networks

One of the main goals of this research was to encapsulate monomer in the interior of a vesicle and polymerize it, giving the vesicle an interior polymer network. The internal polymer network offers the capability to tailor specific mechanical properties desired for the biomimic. Mechanical properties are changed by changing the monomer encapsulated, the concentration of the monomer and the crosslink density of the monomer. With these widely adjustable parameters, a polymer network can be created that can be either elastic or viscous, depending on the desired mechanical properties.

For this experiment, four sets of vesicles were created. All vesicles were created following the normal vesicle creation procedure, but two of the samples had acrylamide encapsulated into the interior of the vesicle. The crosslink density was varied, both 19:1 and 38:1 ratio, monomer to crosslink, with a set concentration of acrylamide. A fluorescent dye was incorporated into the internal polymer network to make imaging possible. The remaining two samples are controls with the fluorophore Nile Red

incorporated into the bilayer. One of the samples underwent polymerization of the bilayer, while the other remains fluid. All four samples were imaged and later, the values of each vesicle's height, width and contact length with a glass coverslip were measured. These data points are used for image analysis as well as mechanical analysis, as discussed in the next section.

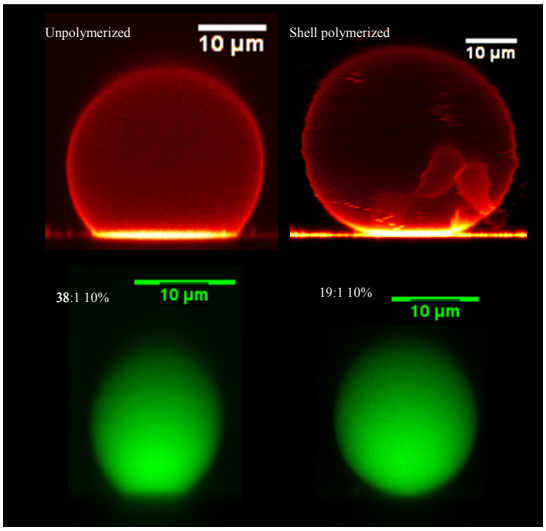

Figure 4-9: The progression of polymerization on vesicles. The upper left picture is a vesicle with Nile Red embedded into the bilayer but unpolymerized. The upper right picture is a vesicle, made from the same technique as the previous picture, but has the bilayer polymerized. The lower left picture is a vesicle with 10% AM-F that has a 38:1 crosslink density. The lower right picture is of a 10% AM-F vesicle with a 19:1 crosslink density. Notice how the vesicle becomes more laid out on the surface as the amount of polymerization done to the vesicle decreases.

For the various profiles of the vesicles in this experiment, there is an interesting trend. The amount that the vesicle lays down on the surface changes due to various levels of polymerization and encapsulation. In Figure 4-9, shows this progression. The upper left picture is a vesicle without polymerization. The upper right picture is a

vesicle that has only the butadiene on the block copolymer polymerized; in effect, polymerizing the vesicle bilayer into a solid shell. The lower left picture is of an encapsulated vesicle, with at 10% solution of AM-F and a 38:1 crosslink density. Finally the last picture, lower right, is of a 10% solution AM-F, but with a 19:1 crosslink density. The amount of deformation changes with the degree of polymerization.

With the acrylamide encapsulated vesicles, a monomer has indeed been encapsulated polymer on the interior of the vesicle. This proves the mechanical properties of the internal polymer network can be changed, since the concentration, crosslink density and the type of monomer are all adjustable. The next step in determining the various moduli for the different monomer systems is with the mechanical testing of the monomer systems is discussed in section 4.9.

Looking at just the profiles of the four cases, a trend emerges. Since the particles are not uniform in size, normalizing the vesicles will allow the deformation to be determined on an equal level.

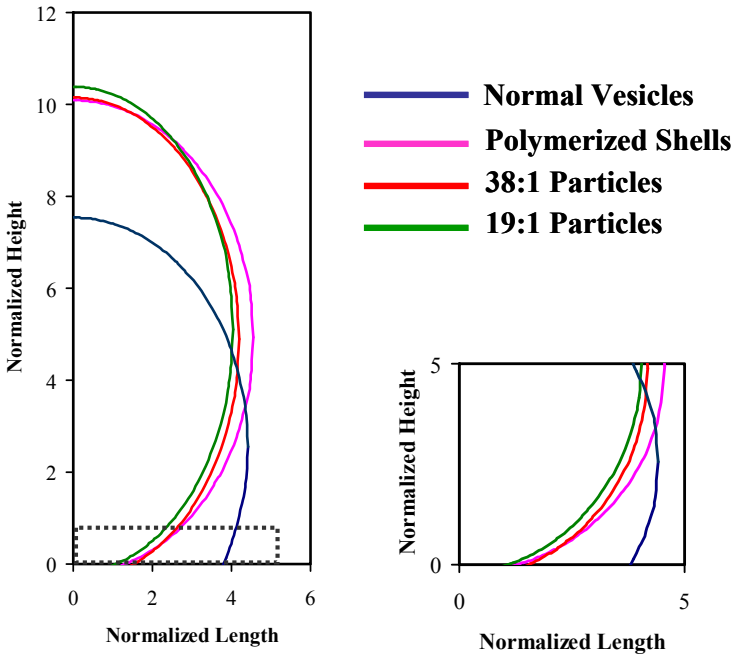

Figure 4-10: Normalized profiles of particles. Here we have the normalized profiles of the four cases of polymerization: the blue line (●) is the unpolymerized particles, the pink line (●) is the polymerized shell particles, the green line (●) is the 38:1 acrylamide particles and the red line (●) is the 19:1 acrylamide particles.

Figure 4-10 illustrates that profiles of the four cases of polymerized particles are distinct. The particles are normalized to surface area, since the polymerized (solid) particles cannot change surface area. This plot indicates that as the material on the interior of the vesicle increases in rigidity the particle stands taller on the glass. The polymerized particles surface contact area is much less than the unpolymerized membrane. This indicates that the modulus of the interior network affects the overall shape of the particle when it is in contact and adhering with a surface.

Under the conditions tested here, small forces and deformations, quantitative differences in the deformation of the two crosslink densities and the shell polymerized

particles are difficult to discern. However, it is expected that there will be significant differences in the deformation at higher forces due to the varying structure of the particles. This approach is a way to design the mechanical behavior of compartmentalized particles independent of the polymer bilayer structure. The surface of the particle is the self-assembled membrane, which will control aspects of initial approach and adhesion while the mechanical properties of the hydrogel control the ultimate deformation of the particle. Having a particle that is initially deformable and then resists any additional deformation is trait representative of a cellular adhesion and is beneficial in selective or chemically controlled adhesion systems[102]. This allows the particle to have some adhesion contact area, but maintain it shape in response to forces applied to the vesicle in solution.

4.7 Image Analysis

Once the pictures were taken of the various polymer encapsulation tests, three variables were collected from the images: the height of the particle, the width of the particle and the length of contact to the surface of the particle. Using geometric equations, we can calculate the volume of the particle, as well as the depressed volume. The follow equations were used in order to calculate the various parameters.

$$d = a\left(1-\left(1-\frac{y^2}{b^2}\right)^{0.5}\right) \qquad (4\text{-}1)$$

where

d = Depression depth of particle

y = Contact length, divided by two

a = Radius of major axis

b = Radius of minor axis

$$V = \frac{4}{3}\pi b^2 a \tag{4-2}$$

where

V = Total volume of particle

$$V_d = \frac{\pi}{3}\left(\frac{b^2}{a^2}\right)\left(2a^3 - 3a^2(a-d) + (a-d)^3\right) \tag{4-3}$$

where

V_d = Depressed volume

$$y_{Normalized} = (a-d) + a\sqrt{\left(1 - \frac{x}{b^2}\right)} \tag{4-4}$$

where

$y_{Normalized}$ = Normalized contact length, divided by two

To understand the role of adhesion and particle structure, it is helpful to characterize the deformation of the particles and estimate the forces and energies experienced by the particles. Some common attributes are seen in the classes of particles: unpolymerized, shell polymerized, 38:1 and 19:1 particles. In the unpolymerized cases, the contact length to the particle radius, is less than 1/2, giving us a moderate amount of deformation. The contact angle on these particles is approximately 60^{o}, with an overall size of around 20 microns.

For polymerized particles, the shell polymerized, 38:1 and 19:1, the contact angle is less, around 40^{o} and the ratio of contact length to particle radius is lower, approximately 1/4-1/6. The only common feature between the two cases, internal support versus no internal support, is the particle size distribution. This is to be expected, since the polymerization locks in the size distribution of the original vesicle solution.

The particle adhesion comes from the interaction of PEO with the glass coverslide and can be reduced if the cover glass is coated with another layer, such as bovine serum albumin (BSA). However, it is interesting to note the type and force of this adhesion on the structure of the particle in contact. To find the adhesion energy of the PEO layer of the particles to glass, the interfacial tensions for glass-water, water-PEO and PEO-glass must be determined. Reported values for the surface energies of water and PEO are 72.8 and 43.5 mN/m[(103)]. Using these reported values, coupled with goniometer experiments, we measure 73.3 mN/m for PEO-water and 244 mN/m for the water-glass interfaces. The interfacial energy of PEO-glass is determined from[(103)]

$$\gamma_{sl} = \gamma_s + \gamma_l(\cos\theta) \tag{4-5}$$

where

γ_i = Interfacial energy of the solid or liquid

PEO-glass has an interfacial tension of 175 mN/m. This yields a driving force for adhesion of -142 mJ/m^2.

It is useful to gauge the order of the forces on the vesicle; gravity, adhesion, bending, membrane stretching and osmotic pressure. For particles in the size range of 10-20 microns, the gravitational potential for a micron change in height is the smallest of these forces, with an energy of 10^{-19} to 10^{-15} mJ. Bending does play a role, but it too is too small to make much of a difference; bending of a fluid membrane with a bending constant on the order of k_BT over a curvature of 1/10 μm is on the order of 10^{-14} mJ. Adhesion energies for 5 μm radius contact areas are on the order of 10^{-8} mJ. Membrane stretching on unpolymerized particles takes about 10^{-8} - 10^{-7} mJ of energy. With a small osmotic pressure difference of about 10-20 mOs (~10-20 mM) and a deformation of the particles of 5% of its initial volume yield energies of 10^{-11} to 10^{-10} mJ. This indicates the dominant energies will be from adhesion, membrane stretching and osmotic pressure. While the deformation of the particle against an osmotic pressure is smaller than the other two, it is useful to keep this term as it is the main difference between fluid and polymerized systems.

Several theories of spherical particle deformation already contain these considerations and were investigated including those based on Hertz[(96, 104)], JKR[(96, 105)], and Shanahan's[(106)] modification to elastic membranes. Hertz theory assumes that the

sphere is perfectly elastic and that there are no interactions, either adhesion or friction, between the sphere and a contacting plate or two spheres in contact. JKR theory includes a surface energy based interaction between the sphere and flat surface instead of the impinging force used in Hertz. Shanahan switched the particles in JKR theory from solid spheres with adhesion to elastic membranes with deformations and small internal pressures.

Following the analysis for JKR theory, an estimate for the apparent Young's modulus from the contact area observed in the images and the estimated values of PEO glass adhesion energy can be obtained:

$$K = \frac{6\pi W_{12} r^2}{a^3} \tag{4-6}$$

where

a = contact length with the glass

W_{12} = Adhesion energy of two materials

r = Radius of the particle

K = Compression modulus

This yields a modulus of 300, 800, 1000, 3000 kPa for unpolymerized, shell polymerized, 38:1 and 19:1 particles. The stiffening of the particles with the change in internal structure is evident under this analysis, but the magnitude of the moduli is larger than expected (10-100 times the modulus of the hydrogel). While the presence of a high concentration of sucrose in the particles could lead to a large osmotic restoring force, there are assumptions inherent in JKR theory which do not apply to this system. The

hydrogel particles are not perfectly elastic spheres and the unpolymerized particles are not solid at all. However, a more detailed description of the mechanical properties of the hydrogel-membrane particles requires experiments over a larger range of particle deformations.

4.8 Adhesion of Fluid Vesicles

The adhesion of fluid vesicles to surfaces has received a great deal of interest in recent years[107-111] and has clarified the role of the mechanical properties of the membrane to the shape of the vesicle after adhesion. We wish to clarify the role of osmotic pressure and membrane tension in the particle deformations observed in this system. The following model is a minimization of the free energy of an adhering spherical vesicle at constant surface area. The particle is assumed to have the shape of a spherical cap during deformation. While this is a simplification of more complicated models, it explicitly couples the osmotic pressure in the interior of the vesicle to the membrane tension. During deformation, the compression of an immobile solute, sucrose, in the interior of the vesicle causes an osmotic pressure that stabilizes the vesicle shape when in contact. The vesicles are imaged with 300 mOs of sucrose encapsulated in the interior of the vesicle while being suspended in ~312 mOs PBS solution. This means that there is some amount of NaCl that has migrated to the interior of the vesicle that can be ejected during adhesion without any change in membrane tension or osmotic pressure. This initial deformation of the vesicle requires no energy to

deform the vesicle beyond the change in bending near the region of contact, which is neglected. This initial contact corresponds to a change in volume of the vesicle of about V_f/V_i = 300/312 or 0.96, where V_f is the imaged volume of the particle and V_i is the volume of a particle with the same surface area as the imaged (deformed) particle. The osmotic pressure is zero up to this point and then increases as

$$\Delta P_{osmotic} = RT\left(C - C_i\right) = C_i RT\left(\frac{C_i V_i}{C_o V} - 1\right) \tag{4-7}$$

where

ΔP = Pressure difference across the membrane

R = Gas constant, 8.314

C, C_i, C_o = Concentration of solute, initial, outside

V, V_i = Volume of particle, initial

From our analysis from before, we will use three terms in the free energy; adhesion, osmotic energy, and membrane stretching. The adhesion energy is simply

$$\Delta E_{adhesion} = -W_{12} \cdot Area \tag{4-8}$$

where

ΔE = Energy of adhesion

Where W_{12} is measured to be 140 mJ/m^2. The contact area is modeled as the bottom of a truncated sphere, with a corresponding particle volume of the interior of the sphere minus the truncated part. The set of geometries is held to those with constant surface area, for simplicity. Opposing the energy of adhesion will be the work done on

the particle to deform it against its osmotic pressure and stretch the membrane. The work of deformation is:

$$\begin{aligned}\Delta E_{osmotic} &= -\int_{V_i}^{V_f} P_{osmotic} \cdot dV \\ &= -C_i RT \int_{V_i \cdot \frac{C_{in}}{C_{out}}}^{V_f} \left\{ \frac{C_i V_i}{C_o V} - 1 \right\} dV \\ &= -C_i RT \left(\frac{V_i C_i}{C_o} \right) \left\{ \ln \frac{V_f}{\frac{V_i C_{in}}{C_{out}}} - \frac{C_o V_f}{C_i V_i} + 1 \right\}\end{aligned} \tag{4-9}$$

where

$\Delta E_{osmotic}$ = Osmotic energy

The relationship between the osmotic pressure and membrane tension is given by

$$\tau = \frac{\Delta P R}{2} \tag{4-10}$$

where

ΔP = Pressure difference across the membrane

R = Radius of the particle

τ = Membrane tension

And the response of the membrane to an increase in tension, for lipid and polybutadiene membranes only, is[112]

$$\alpha = \left(\frac{k_B T}{8\pi k_c} \right) \ln\left(1 + c S_0 \tau\right) + \frac{\tau}{K} \tag{4-11}$$

where

α = Change in surface area, $\alpha = \frac{A - A_o}{A_o}$

k_B = Boltzmann's constant

S_o = Surface area of the particle

c = constant, $1/24\pi$ (quasi-spherical approximation)

The work of membrane stretching is

$$\begin{aligned}\Delta E_{stretch} &= S_0 \int \tau d\alpha = S_0 \left(\tau\alpha - \int \alpha d\tau\right) \\ &= \frac{S_0 \tau^2}{2K} + \left(\frac{k_B T}{8\pi k_c}\right)\left[S_0 \tau - \frac{1}{c}\ln\left(1 + cS_0\tau\right)\right]\end{aligned} \quad (4\text{-}12)$$

where $c = 1/24\pi$ (quasi-spherical approximation), $k_c \sim k_B T$, and K = 50,120, or 200 mJ/m^2. The polymer used is these experiments has a modulus K = 120 mN/m[18]. The total free energy is approximated as

$$G \approx \Delta E_{adhesion} + \Delta E_{osmotic} + \Delta E_{stretch} \quad (4\text{-}13)$$

where

G = Gibbs' free energy

and minimized with respect to the amount of deformation of the particle. The value of V_f/V_i that minimizes this equation for vesicles of different sizes is shown in Figure 4-11.

Figure 4-11 shows the deformation of unpolymerized vesicles after coming into contact with the glass slide. V_f/V_i is the ratio of the volume of the vesicle after contact as measured by confocal microscopy to its initial volume as calculated by a sphere of equal surface area. The deformation of unpolymerized vesicles comes from the adhesion of

the PEO block to the glass surface which deforms and reduces the volume of the interior of the vesicle. Since the vesicles encapsulate sucrose, which cannot pass the membrane, the deformation raises the osmotic pressure inside the vesicles and induces a tension in the vesicle membrane. The line is the calculated deformation for a spherical vesicle. The tension induced is calculated and shown.

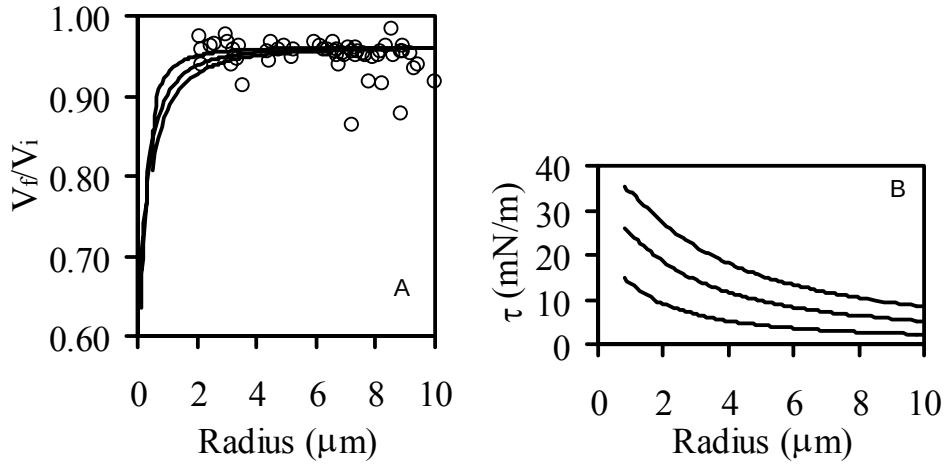

Figure 4-11: Modeled deformation versus observed. Comparison of the observed deformation of unpolymerized vesicles to the model deformation of a spherical particle with osmotic and stretching energies. A) Circles represent the observed final volume divided by the volume of a sphere with equivalent surface area. The lines are the deformation of a model vesicle that balances the energy of adhesion (W_{12} = 140 mJ/m^2) with the energy of membrane stretching with modulus K = 50,120, and 200 mJ/m^2 (top to bottom). B) The tensions calculated for the particles in part A with modulus K = 50,120, and 200 mJ/m2 (bottom to top). The ultimate tension for these vesicles is reported to be ~15 mN/m.

Notice how it is nearly constant at 0.96 for most of the size range investigated. The expected deformation is mostly from the osmotic pressure difference between the vesicle and outside solution with minimal additional deformation coming from the

adhesion energy, until the particle size approaches 1 μm. The deformation and tension increase as the size of the particle decreases. For a K = 120 mN/m at 2 μm radius, the membrane tension is calculated to be 16 mJ/m^2, which is close to the ultimate tension of these vesicles as measured by pipette techniques. The observed minimum size of around 2 μm is consistent with the know values of K and k_c, and the measured value of W_{12} = 140 mN/m. The calculated membrane tensions for vesicles 8 μm and larger is 5 mJ/m^2 or less. Even with several assumptions about the geometry of adhering particles, the relative importance of the adhesion energy and membrane modulus is apparent, along with the role of the initial osmotic pressure of the solution. These results are consistent with the values of W_{12}, K and k_C for this system.

4.9 Material Tests of Acrylamide

Table 4-5: Material moduli for acrylamide gels. All values are in units of kilopascals.

Crosslink Density	Young's Modulus	Compressive Modulus
19:1 – 5% AM	3.1±0.6	8.4 ± 0.9
38:1 – 5% AM	2.6±0.3	4.8 ± 1.2
19:1 – 10% AM	22.0±1.0	38.6 ± 6.1
38:1 – 10% AM	14.9±2.0	15.8 ± 4.0

The final aspect of encapsulation of a monomer, in this case acrylamide, is to look at the material characteristics. From this, the individual properties can be independently determined, then incorporated into the biomimic. Looking at the bulk Young's moduli for the two cases in Table 4-5, the moduli do not scale by a simple

factor. In the Young's moduli for the 5% concentration samples, the two values are nearly identical. This can be explained by the low concentration of polymer and the large concentration of water. Under extension, the polymer chains are less likely to encounter other polymer chains, making it hard to build up a completely continuous polymer network. The minimum gelling concentration for acrylamide has been experimentally determined to be between 1 and 4%.

For the 5% concentration, the compressive modulus is about twice as much for the 19:1 compared to the 38:1. This sample shows that as the crosslink density is doubled, the compressive modulus follows a similar trend.

In the 10% concentration case, the values are quite different from each other. For the compressive modulus, the 19:1 is about two and a half times the modulus for the 38:1. Doubling the crosslink density once again gives almost a similar doubling in the compressive modulus. Since the standard deviation of the 19:1 sample is quite large, the effect of doubling the crosslink density may be close to just two times the compressive modulus, and not two and half times.

For the Young's modulus, the value for 19:1 differs by only 66%. The difference in the two sets of numbers and how they are not linearly related can be explained by the large amount of water in each sample. These samples still have large percentage of water making up the sample volume. For the 10% polymer concentration case, the polymer should be able to make a single, continuous polymer network. Having the continuous network will allow the sample to undergo larger strains.

Looking at the same crosslink density samples, but changing the polymer concentration, an interesting trend emerges. For the 19:1 ratio, as the polymer concentration is increased from 5% to 10%, the values for the Young's modulus increase seven-fold. The values for the compressive modulus increase almost three-fold. What is interesting is that both sets increase at the same rate.

At the small strains that were investigated, the polymer network was not strained past the reversible, elastic point. As the strains were increased, the polymer network was stressed, as well as the gel expunging the water from the network. Because the crosslink density can affect the way the polymer network retains water, when the strain is applied, the water can leave the sample at a varying rate. This gives an uncontrolled variable to this system that cannot be accounted for.

The reported values are of all the tests conducted on the cylinders. Three overall tests were performed: a 10% compression, a 20% compression, and a 40% failure test. Figure A-1 thru Figure A-4 in Appendix A show the results from each of the individual tests.

5. SILICONE BLOCK COPOLYMERS

5.1 New Silicone Polymer

Part of the future research goals from the initial master's work was to look at new block copolymers. One of the new polymers investigated was a silicone based block copolymer. This polymer is similar to the hydrocarbon based block copolymers used earlier, but has a poly(dimethyl siloxane) (PDMS) backbone as the hydrophobic block. This new block copolymer will also spontaneously form self assembled structures inside of aqueous solutions. For a comparison between the two polymer systems, several criteria will be used. The first criterion is interfacial energies, as shown on Table 1-2. There is no major difference in the interfacial energy; interfacial energy of the hydrophobic blocks and water. The second criteria will be imaging the structures formed in solution. This is determined by use of confocal imaging. The third criteria will be mechanical testing. This can be achieved through pipette testing. The final criteria will be phase mixture behavior. This can be realized through a combination of imaging techniques and mechanical testing.

Since this polymer has not been characterized by conventional testing methods and most of the images of the polymer are from cryo-TEM[78, 79, 84, 85], one of the first experiments is to see what structures are formed in solution. Figure 5-1 shows the PDMS block copolymer structures in solution. On the right image, a pair of PDMS vesicles, with a small amount of Nile Red in the hydrophobic section for imaging

purposes, is shown. The image on the left, for comparison, is a PBd vesicle. The PBd vesicle also has a small amount of Nile Red added to the hydrophobic section of the polymer for imaging purposes. As the images show, the structures are indeed fluid vesicles: the large contact area on the glass by the vesicles, indicated by the brighter contrast, the continuous, circular structure and the "fuzzy" top. Since the vesicle is fluid and moving inside the solution, the top is difficult to resolve due to the Brownian motion.

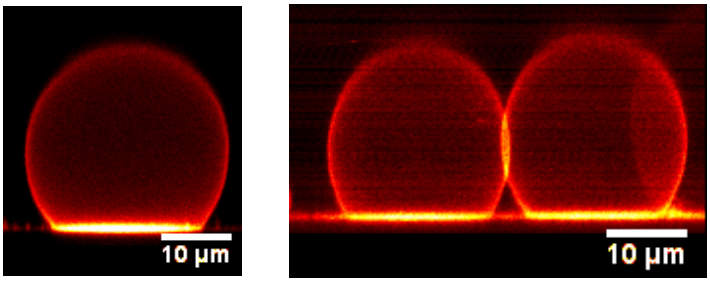

Figure 5-1: Silicone vesicles from initial tests. A comparison of Butadiene vesicles to PDMS vesicles, both with Nile Red in the membrane. The left image is a PBd vesicle, with a small amount of Nile Red added. The right image is a pair of PDMS vesicles, also with Nile Red. Both images show fluid bilayer structures: the large contact area with the glass coverslip, the continuous circular structure and undulating top, made apparent by the lack of definition.

5.2 Mechanical Properties of Silicone Polymer

To determine some basic mechanical values for the new silicone polymer, a pipette study was needed to obtain stress versus strain curves. Pipette work has been used extensively in both lipid and hydrocarbon vesicle measurements [7, 28, 112-124]. From

stress-strain curves, values can be determined for the bending modulus, the area expansion modulus as well as getting estimates for other mechanical properties, such as ultimate tension, ultimate extension and the amount of energy absorbed by the bilayer before breaking. This work can be derived from Figure 5-2. The left figure shows a tension versus area expansion or in other terms, stress versus strain. The right figure shows the same data sets, but with *ln* τ. From here, a clear distinction between the two piecewise functions can be made. For the tensed point, we chose any value above 0.05α. From the slope of the various lines past the tensed point, the area expansion modulus is obtained. Since most lipid vesicles cannot undergo an area expansion greater than 5% and hydrocarbon vesicles withstanding up to 20% area expansion, 5% is an adequate starting point.

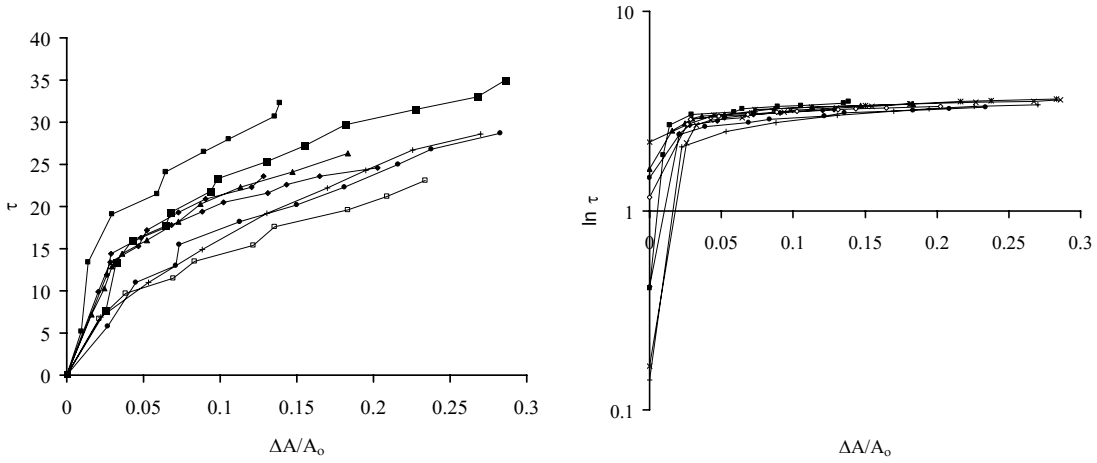

Figure 5-2: A stress-strain curve for our PDMS based block copolymer. The left figure is the normal stress-strain curve for the polymer. The right figure is the logarithm of the left data. The area dominated by bending is more apparent. The sharp transition from bending to areal expansion can be seen. The bending modulus is derived from the initial slope and the area expansion is obtained from the second slope region.

Following the equation put forth by Evans and Rawicz[112], fitting the left image in Figure 5-3, the values of interest can be found. The equation, $\alpha = (k_BT/8\pi k_c)ln(1+ c\tau_m A/k_c) + \tau_m/K_A$, where k_c and K_A are the moduli, bending and area expansion respectively, can be used piece-wise once it has been rearranged. The new form of the equation $ln[\tau_m/\tau_m(0)] \approx (8\pi k_c/k_BT)\alpha$, c being an unimportant constant equaling ~ 0.1 (c depends on the type of modes, either spherical harmonics or plane waves), will allow k_c, the bending modulus to be found from Figure 5-3; to determine K_A, $\tau_m \approx K_A\alpha$ in the region of high tension.

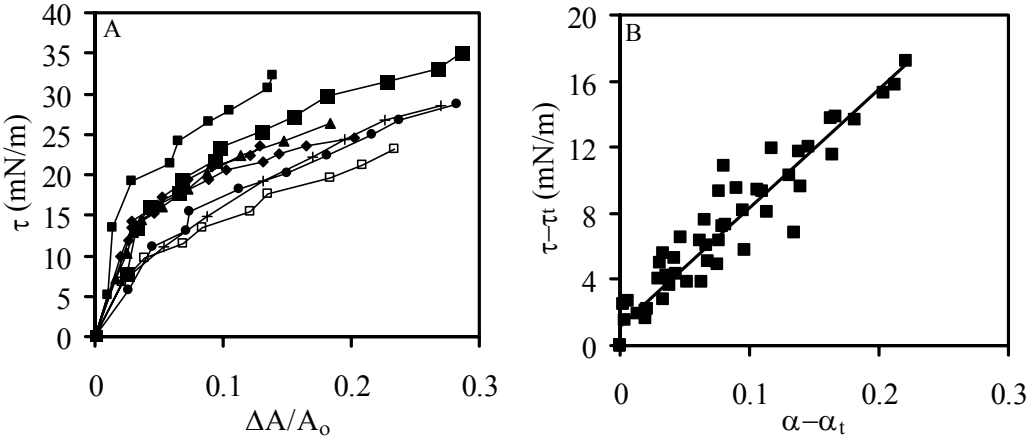

Figure 5-3: Comparison of the average energy absorbed. A) A stress-strain curve for the $PDMS_{12}$-PEO_{46} based block copolymer. This graph shows the individual vesicle samples. B) A tensed stress-strain curve for the $PDMS_{12}$-PEO_{46} based block copolymer. The upper graph shows each individual sample's data above the tensed point. The lower graph shows all of the data above the tensed point and showing the overall fit. This fit is the reported measured value. From this graph, and the subsequent graphs for the other vesicle solutions used in this study, the $\tau_{ultimate}$ and $\alpha_{ultimate}$ were derived.

The area expansion modulus can be determined by taking the slope of the points after the tensed point, as seen in Figure 5-3. After this point the vesicle should have no excess slack in the membrane and the pipette study is testing the mechanical properties of the membrane. The area expansion modulus is 55.8 ± 2.1 mN/m.

From Figure 5-3, right image, we see that we have a y-intercept of 1.11, indicating that our initial tensed value of 5% is adequate. Due to the fact that the data is not at regular intervals, it is difficult to get the data, $\tau-\tau_c$ versus $\alpha-\alpha_c$, to go through the origin.

From the replotted data, Figure 5-3, we can get an estimate of the ultimate tension and the ultimate extension of the silicone based block copolymer. Looking at Table 5-1 in the mixture section, we see that $\tau_{ultimate}$ is 17.24 mN/m and $\alpha_{ultimate}$ is 0.2213 or 22.13% expansion before failure.

From Figure 5-4, the difference in the stress-strain curve between the two pure systems is apparent. The open circles show the PDMS membranes and the close circles show the PBd membranes. With the PDMS, the general shape of the curve is a trapezium, where the PBd curve is a triangle. With the PDMS, the K_A value changes around the 0.05α point, whereas the PBd system has a relatively constant K_A value throughout the entire curve. This change in K_A can be attributed to PDMS' chemical structure and characteristics. This is observed with the 75/25 PDMS/PBd mixture vesicle. Here, the reduction of the initial slope K_A is noted and starts to adopt a uniform K_A over the entire range of α.

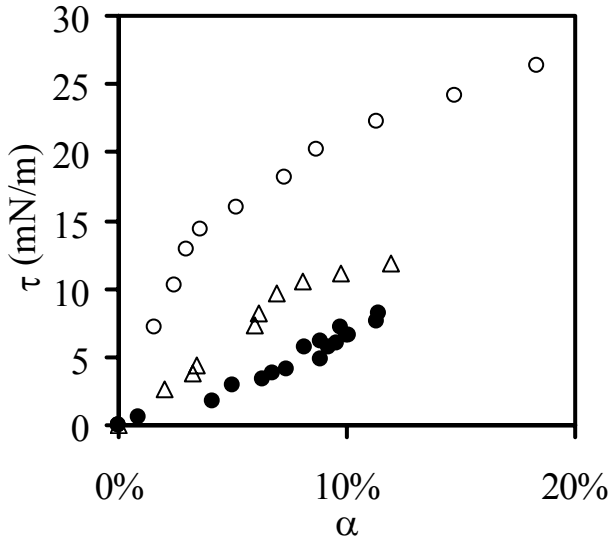

Figure 5-4: Comparison of the three vesicle deformations. Here are three mixtures of the $PDMS_{12}$-PEO_{46} vesicles and the PBd_{33}-PEO_{20} vesicles. The open circles are pure PDMS vesicles, the closed circles are pure PBd vesicles and the open triangles are a 75/25 mixture of PDMS/PBd. As the concentration of PDMS is decreased, the reduction of the initial K_A slope is apparent.

Studies of PDMS at high concentrations show that PDMS forms ordered structures[125, 126]. These structures are initially resistant to motion and deformation, but eventually move; this phenomena is called shear thinning. With PDMS in the bilayer, there is a high concentrated system although overall, the concentration is quite dilute. There is an increased energy to initially deform the PDMS polymer. This is due to some initial packing of the PDMS polymer chains. With the PDMS/PBd systems, discussed in detail in the mixtures section, a linear trend corresponding to the decrease in PDMS and the decrease in the shear thinning phenomena is observed. It is this dual K_A feature that gives the PDMS polymer the increased ability to absorb energy. Since the slope towards

the end of the curves are similar, the phenomena should only be limited to the PDMS system.

Since energy absorbed is the integrated area under the curve, from Figure 5-4, the energy absorbed of the pure PDMS system is much higher than the pure PBd system. A more detailed explanation of the PDMS/PBd system is in the mixture section. The difference in absorbed energy can be attributed to the chain flexibility of PDMS over PBd.

From previous studies[17], the length of the hydrophobic block does not change the area expansion, just the bending modulus. The reasoning is that the surface energy does not change as you increase the chain length. Since the surface energy of PDMS and PBd are similar, the K_A should be similar as well. The same idea can be applied to the comparison of silicone and hydrocarbon; somewhat similar surface tensions drive the area expansion, but chain flexibility drives the energy absorbed by the bilayer. Since the K_A are different, but only by a factor of 0.67 or 67%, surface energy cannot be the sole reason for the vastly different energy absorbed. Energy absorbed can be a factor of chemical and physical properties inherent to the hydrophobic blocks. One physical aspect is the hydrophobic block length.

For the statistical segmental length of the polymer chains, the PDMS block copolymer has a length of 0.41 nm, whereas the PBd possesses a length of 0.36 nm. The overall total stretched lengths of the hydrophobic blocks are 8.1 nm for the PBd block and 3.4 nm for the PDMS block for the two copolymers systems in question. For the either the freely rotating length or symmetric restricted rotational length, the total PDMS

block is about 65% shorter than the total PBd block. As seen with the study by Bermudez et al[17], the length of the hydrophobic section should not affect the area expansion modulus or the total amount of areal strain. If the areal strain is not affected, the amount of energy absorbed by the bilayer should not change as well.

Since the difference in energy absorbed by the bilayer cannot be explained by the overall length, the next values that offer some insight are both the T_g and the C_∞. The C_∞ value, a measurement of the chain stiffness, is 6.25 and 5.4 for both PDMS and PBd, respectively[87]. For C_∞, the lower the value, the more stiff the chain. C_∞ is a function of bond angle as well. With the C_∞ value, PBd shows signs of being stiffer and more resistant to elongation or areal expansion.

Although the C_∞ offers some difference in chain stiffness, the largest contributor to the ability of the bilayer to absorb the energy has to lie with the T_g. Since the experiments were performed at or around 25°C, butadiene is near its T_g. Since PDMS T_g is -120°C[87], the polymer chains are well above their glass transition temperature. This offers the best explanation of why $PDMS_{12}$-PEO_{46} absorbed roughly seven times the energy than the PBd_{33}-PEO_{20} system.

Another part of the reason for the variable K_A is due to the highly flexible nature of the siloxane backbone of the silicone polymer. The Si-O bond angle is 142° or 110°, depending on the measurement, either from Si to Si or O to O, respectively. With the hydrocarbon chain backbone, there is only 109.5° bond angle. This increased bond angle allows the siloxane to undertake more conformations and extended structures to remove stress in the polymer chains. Since the chain is much more flexible, the siloxane

polymer can cover a larger area compared to a similar molecular weight hydrocarbon polymer, giving the silicone polymer the ability to stretch more, as seen by the increase in ultimate extension.

As seen from the studies on the silicone based block copolymer, PDMS is another system in which to base the cell mimic; a robust, durable block copolymer that forms vesicles and can withstand more solution changes than our previous hydrocarbon based block copolymers. The obvious next step is to look at mixtures of the two systems.

5.3 Silicone Mixtures

After analyzing the pure silicone block copolymer system, mixtures of the two block copolymers systems can be investigated. Since both classes of block copolymers are soluble in organic solvents, making a film for the film rehydration technique, the polymer is randomly distributed in solution. The film will form vesicles with an average distribution of both polymers, based on the initial amounts of polymer placed in solution. A total of seven solutions were created: 100%, 95%, 75%, 50%, 25%, 10% and 0% silicone polymer, all weight percent. The remaining amount is the hydrocarbon block copolymer. All of the experimental values are shown in Table 5-1.

Table 5-1: Various moduli for PDMS/PBd mixtures. Here are the reported values for bending modulus, area expansion modulus, estimates for ultimate tension and extension.

% PDMS	kc (k_BT)	K_A (mN/m)	Energy Abs. (mJ/m^2)	$\tau_{ultimate}$ (mN/m)	$\alpha_{ultimate}$
100%	2.34 ± 1.01	55.8 ± 2.1	4.12 ± 1.5	17.24	0.2213
95%	1.76 ± 0.67	76.6 ± 5.6	3.43 ± 2.9	13.90	0.1398
75%	1.32 ± 0.23	76.3 ± 2.3	1.93 ± 0.4	15.62	0.2189
50%	1.12 ± 0.38	68.7 ± 2.3	0.79 ± 0.4	11.25	0.1200
25%	1.41 ± 0.50	97.9 ± 2.7	0.73 ± 0.4	10.86	0.0957
10%	1.42 ± 0.15	86.9 ± 3.5	0.35 ± 0.1	6.614	0.1404
0%	1.51 ± 0.46	92.3 ± 2.1	0.51 ± 0.3	8.364	0.1091

After making the various mixtures of silicone and hydrocarbon block copolymer, the same pipette aspiration study was used to determine the same parameters as the pure system. Using the same testing procedures and critical values, the bending and the area expansion modulus, as well as estimates for the ultimate tension, ultimate extension and energy absorbed by the bilayer were found for the polymer vesicles. Figure 5-5 shows graphically four out of the five calculated values: the ultimate tension and area expansion, the area expansion modulus and the bending modulus. These are all functions of silicone block copolymer concentrations.

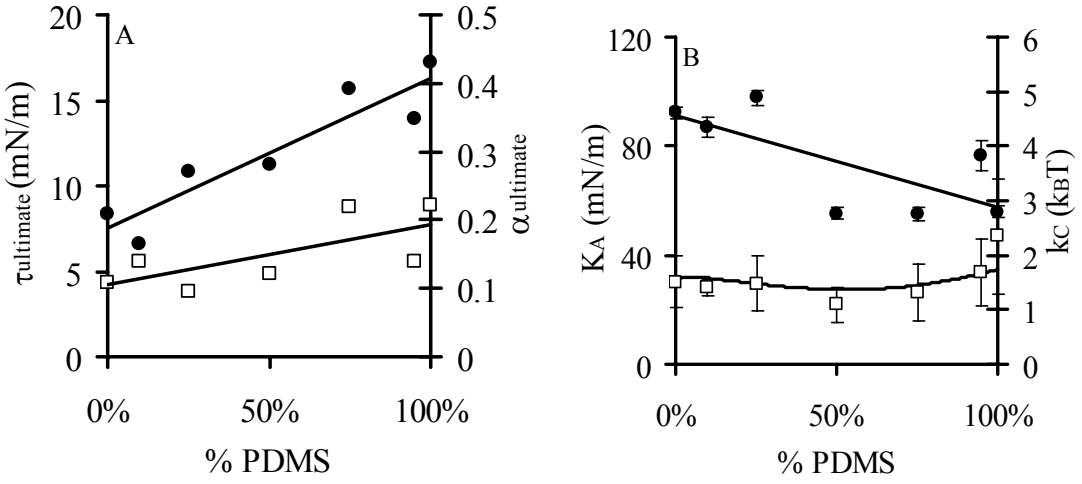

Figure 5-5: Comparison of values as a function of composition. A) The black dots are the ultimate tension, in mJ/m^2 and the white squares are ultimate area expansion. Both trends are linear with respect to silicone polymer concentration. B) Here the black dots are the area expansion modulus, K_A, in mN/m. The white squares are the bending modulus, k_C, in terms of k_BT. With the area expansion modulus, again a linear trend emerges. With the bending modulus, a slight quadratic is observed. This is similar to the model put forth by Safran[80].

Looking at Figure 5-5, in the left figure, the solid circles are the ultimate tension and the open squares is the ultimate area expansion, α. As the concentration of silicone polymer in the vesicle increases, both ultimate values increase. The increase for the mixtures is linear, which is to be expected. Since there is no phase separation between the two systems, and their interfacial energies are similar, most trends are expected to be linear functions of silicone polymer concentration. The equations for the linear fits are

$$\begin{aligned} K_A(\varphi) &= -33.39\varphi + 91.22 \\ \alpha_{ultimate}(\varphi) &= 0.087\varphi + 0.105 \\ \tau_{ultimate}(\varphi) &= 8.75\varphi + 7.54 \end{aligned} \tag{5-1}$$

where

φ = weight percentage of polymer

For Figure 5-5 right, the closed circles are the area expansion moduli, K_A. Once again, the linear trend as a function of silicone polymer concentration is apparent. The open squares are the bending modulus, k_C, in units of k_BT. Here, the linear trend is not continued. The best fit for this data is using the model put forth by Safran[80, 117]. The Safran model for our system is

$$\frac{K(\varphi)}{K(\varphi=0)} = \frac{f_2^A(\alpha,\varphi_A) + \frac{B}{A} f_S^B(\alpha,\varphi_B)}{f_2^A(\alpha,\varphi_A=0) + \frac{B}{A} f_S^B(\alpha,\varphi_B=0)}$$

$$f_2^{A,B}(\alpha,\Phi) = 1 + 3\alpha\varphi_{A,B}{}^{(1+2\upsilon)/2\upsilon} + 3\alpha\varphi_{A,B}{}^{(2+\upsilon)/2\upsilon} + \alpha^3\varphi_{A,B}{}^{3/2\upsilon} \qquad (5\text{-}2)$$

$$\frac{B}{A} = \left(\frac{N_S^A}{N_S^B}\right)^3$$

where

α = Ratio of molar volumes, $\alpha = \dfrac{\left(\frac{MW}{\rho}\right)_L - \left(\frac{MW}{\rho}\right)_s}{\left(\frac{MW}{\rho}\right)_L}$

φ = Chain fraction of A or B

υ = Either 3/5 or 1/2, based upon solvent quality

N_S^A, N_S^B = Molecular volume of block A or B

One drawback to the Safran model is that it does not account for differing types of blocks on the copolymer. A slight modification to the Safran model corrects for that. Instead of using molecular weights, molar volume is used. The results of the experiments show that the bending modulus is relatively unchanged over the range of compositions. There is a general trend of a quadratic with a minimum, around 50% silicone polymer, which would make sense, due to the idea of mixing. This is to be expected; in order to have fluid structures, the bending modulus cannot be higher than 1-2 k_BT. The results show that the bending for the pure PBd system is 1.51 ± 0.46 k_BT and the bending modulus for the PDMS system is 2.34 ± 1.01 k_BT. Given the larger 95% confidence range on the PDMS system, the two values are not statistically different.

One explanation about the apparent minimum at 50% PDMS/50% PBd is that the PDMS acts like inelastic spheres. Until sufficient strain has been placed on the system, the silicone polymer will resist deformation. Once the strain has reached sufficient levels, the PDMS will deform along with the PBd. Since the silicone polymer concentration is low, the polymer acts more like a weak point in a system that is largely hydrocarbon polymer. Once the silicone gets above the minority level, the silicone chains can start acting more like a pure silicone system, rather than a diluted silicone system. As noted by Komura[80], a small addition of shorter chain polymers, in this case the silicone, has more of an effect on a long chain rich system, than a small addition of long chain polymers to a short chain polymer mixture (PBd into a PDMS rich system). This notion ties back with the phase behavior of the mixture. If there was a phase separation, there would be a sharp minimum in the bending modulus of the various

mixtures of polymer. Since there is not a sharp minimum, the assumption that the two block copolymers are miscible is valid. Figure 5-6 shows a comparison image of a non-phase separated system and a phase separated system.

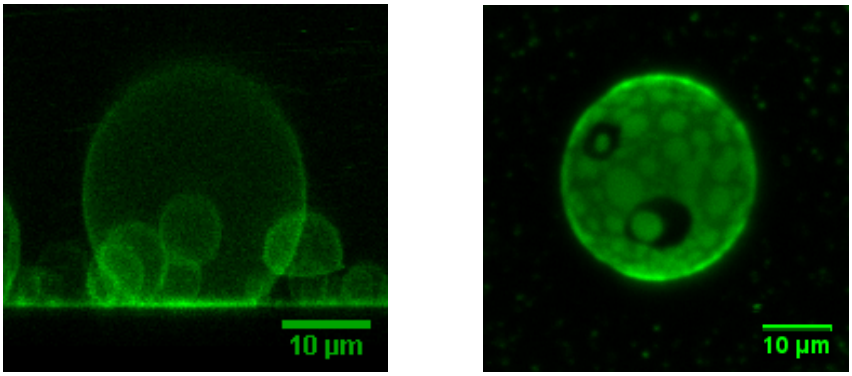

Figure 5-6: Phase behavior of PDMS and PBd mixtures. The image on the left is a mixture of 25% PBd polymer ($EO_{20}Bd_{33}$) and 75% PDMS polymer. From this, there is no apparent phase separation between the PDMS and the PBd chains. The image on the right is a phase separated polymer/lipid vesicle. The polymer is a polypeptide block copolymer, $K_{200}G_{50}$, unlabelled, with a lipid added for imaging. The lipid is a long chain hydrocarbon with a fluorophore attached.

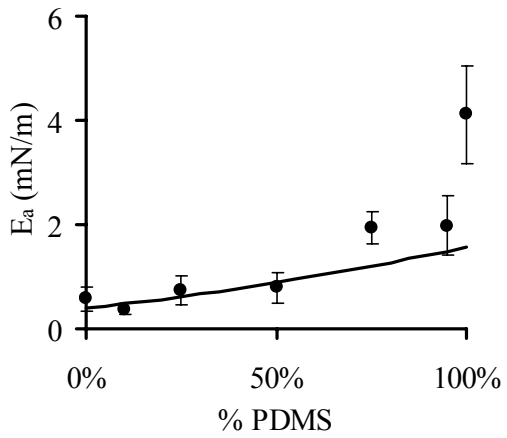

Figure 5-7: Energy absorbed by the bilayer according the composition. As the concentration of silicone increases, we see an increased departure from the model (line). This departure is due to the increased amount of energy required to initial deform the membrane. The PDMS membrane is able to absorb about eight times the energy as a PBd membrane.

Following the idea of non-linear trends in the mixture behavior extends to the energy absorbed by the bilayer, as seen in Figure 5-7. Here, another quadratic function appears. If the idea that K_A is constant over the range of α, integrating $\tau\, d\alpha$, from 0 to α_{max} should return $\frac{1}{2}K_A(\phi)\alpha_{max}(\phi)^2$, using the values from Equation 5.1. This will allow a prediction of the amount of energy absorbed as a function of composition, since the values of K_A and α are also function of polymer concentration. This model works well for low concentrations of silicone polymer in the bilayer. As the concentration of silicone gets above 50%, the model begins to fail. This is due to the assumption that the K_A value is constant over the range of α. As noted on Figure 5-4, the initial curve has a vastly different slope than the latter part for PDMS. Because the two slopes differ, the assumption fails. As PDMS concentration is decreased, the initial slope of the stress-strain curve does diminish until about 50% PDMS, at which K_A is constant throughout α.

From concentrated PDMS studies[125, 126], PDMS structures can be broken up; in this system, it is, by PBd. Since PDMS cannot form structures due to both concentration and entropic constraints, PDMS behaves more like inelastic spheres mention before.

There is some interesting apparent binning of Figure 5-7 as well as experimental values from Table 5-1. Here roughly three groupings of polymer solutions: the pure silicone, the high concentration of silicone, and the low silicone/high hydrocarbon zones. The first zone, the pure, shows how far the silicone polymer can stretch before rupture. The second zone has both the 95% and the 75%. Both samples have a similar values for the area expansion modulus and the energy absorbed by the bilayer. In the third zone, the 50% PDMS and below, the bilayers all have similar area expansion moduli and energy absorbed. Since the pure silicone vesicles have already been discussed, the region of 95/75% is of some note.

In the 95/75% region, the silicone is dominating the molecular interactions. Since there are more siloxane-siloxane interfaces than siloxane-hydrocarbon interfaces, the silicone values should be preserved, but at a lower total value than the pure system. This is apparent with the energy absorbed. The area expansion modulus is almost identical to the pure system, but the energy absorbed is only about 75% of the pure. Following this trend, the 75% silicone would be expected to have about 75% of the energy absorbed; the 95% silicone polymer having about 95% of the pure system. Instead, the 95% and the 75% have nearly identical values for area expansion modulus and energy absorbed.

The idea is that as the concentration of hydrocarbon chains increases, the stress a vesicle can undergo before rupture is diminished. The silicone chains can swell or flex to cover a larger area, essentially "covering" for the hydrocarbon chain weakness. At a certain limit, the siloxane-hydrocarbon interfaces are to few compared to the hydrocarbon-hydrocarbon interfaces (concentrations below 50%) and the hydrocarbon chain modulus take a more major role. Although the data does begin to suggest there are discrete levels, 0% and 10%, 25% and 50%, 75% and 95% and 100%, that would indicate a level of phase separation, none was seen in any of the experiments. The more probable explanation is that the flexible nature of the silicone polymer can swell to absorb more of the stress in the vesicle, preventing some of the hydrocarbon chains from forming a rupture point in the vesicle. Since the changes are likely to be small in nature at the lower concentrations, the limits of the instrumentation are what give the data the discrete leveled nature.

5.4 Silicone Encapsulation

The final experiment was to see if the silicone polymer could encapsulate a monomer system as well as the butadiene block copolymer did. For this, acrylamide was chosen again, since the previous work was successful. Similar conditions were used in the formation, dialysis and imaging of the encapsulated vesicles. The only experimental condition changed was the polymer used. From previous calculations,

Table 4-1, the silicone should be able to contain the monomer acrylamide with ease. Figure 5-8 shows the results of the encapsulation experiment.

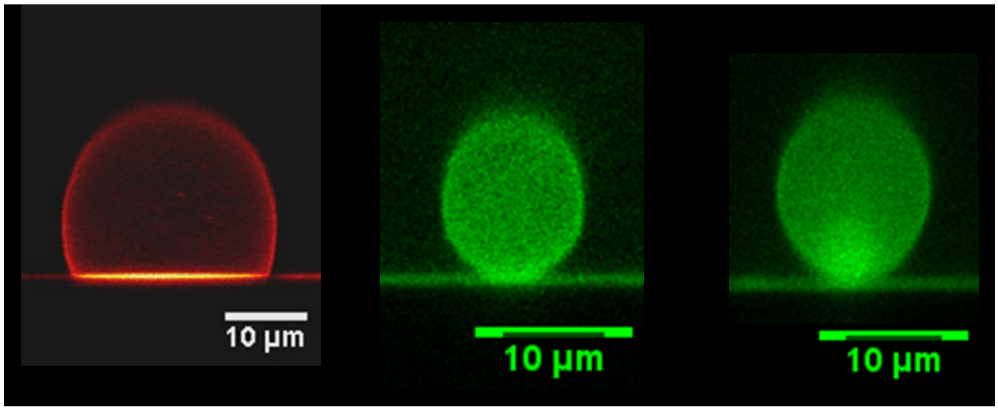

Figure 5-8: Silicone vesicles from AM tests. Several silicone based vesicles; the red vesicle is an unpolymerized, unencapsulated silicone vesicles with Nile Red incorporated into the bilayer. The green particles are acrylamide encapsulated microgels; the left particle is a 38:1 ratio monomer to crosslinker, the right particle a 19:1.

From Figure 5-8, the left-most image is that of a PDMS vesicle with Nile Red added to the bilayer during rehydration. The tell tale signs of a fluid vesicle are present. Since the PDMS polymer has no reactive species in the hydrophobic section like the butadiene, there is not polymerized shell vesicle. The middle image shows a vesicle with the 38:1 acrylamide to crosslink ratio monomer. Once again, the tell tale sign that the interior has been stiffened appears. The vesicle is markedly off the surface of the glass and shows no real sign of deformation. The far right picture shows a PDMS vesicle with the 19:1 monomer solution. Here, the particle is deformed very little; it appears almost to be an undeformed solid. Indeed, the PDMS polymer is capable of

sufficiently holding back a hydrophilic monomer solution long enough to polymerize it inside a vesicle.

An experiment that was never able to come to fruition was making an acid PDMS polymer. The end result of this experiment would have been a working, blank biomimic. With the acid PDMS polymer, the end structure would have possessed all of the characteristics needed to fulfill the requirements for our biomimic. The PDMS polymer allows the vesicle to maintain a fluid structure through the processing steps. The acid polymer gives the biomimic an active surface chemistry in which to attach molecules of interest to, as well as being able to control the surface density of the active sites by varying the concentration. The interior of the vesicle possesses the inherent characteristics of a controllable solid; varying the concentration of the monomer or crosslink ratio would give the biomimic the needed resistance to deformation. In order to have a responsive particle to solution conditions, a responsive unit would need to be attached to the end of the acid polymer. One option would be to attach cystine; this would offer a di-sulfide linkage, an acid group and a primary amine to the surface.

With the acid polymer, an added feature would have been inherent to the system. Since acrylamide presents a primary amine and the acid polymer possesses a carboxylic acid, the two free ends would have reacted in the interior of the vesicle. Once they reacted, a peptide linkage would have been formed. This peptide linkage would then link the bilayer structure to the interior core; essentially creating a transmembrane element. This would not have been a true transmembrane element, since the element

does not cross the entirety of the membrane, from the interior aqueous volume to the bulk aqueous volume.

Overall, the silicone shows increased robustness compared to both the polypeptide block copolymer and the butadiene polymer. The PDMS is also an easily drop-in replacement for the PBd polymer. The PDMS also offers advantages over the PBd polymer, mostly in respect with FDA approval.

6. FUTURE WORK AND CONCLUSIONS

6.1 Future Work with Encapsulation

The investigation of a new encapsulant is always warranted. Since every situation and need is different, a "catch all" monomer would not be sufficient to fill the needs of all future biomimics. One idea is to have a new encapsulant monomer that is degradable by acid or bases. One possible system is a monomer that possesses an ether linkage, with one of the side groups being methyl or ethyl, is hydrophilic and is polymerizable by free radical reactions. The ether linkage could be cleaved by a change in the pH; the cleaved group then would be either methanol or ethanol. This would offer a mechanism that would allow the bilayer structure to be swollen after the vesicle is created. By swelling the membrane after the vesicle is formed, if a specific macromolecule of interest is contained inside the vesicle, this would offer a pathway out for the macromolecule. If the compound or macromolecule of interest in sequestered in the hydrophobic core of the membrane, the flux of the solvent would still carry out the compound or macromolecule. Since ethanol, in dilute quantities, is non-toxic to humans, this could offer a pathway to get less hydrophilic macromolecules into the bloodstream.

Another aspect of a degradable internal network is that it would allow for a greater covering or adhesion to a specific site by degrading the internal support structure. By degrading the internal structure, the bilayer would regain its flexible, allowing the

membrane to experience osmotic pressure differences. One possible use would be to block or cover certain areas, either of specific cells or a damaged area. The solid vesicle could adhere to a contact point of interest. Once adhered, the vesicle's internal structure would undergo degradation and the vesicle would now be responsive to osmotic pressure differences. Since the particle is not osmotically balanced when it was created, the bilayer structure should deflate. As the particle deflates, the amount of surface area on the vesicle in contact increases. This would effectively block or seal off the area of contact.

A third aspect of a degradable internal structure would be the ability to measure the permeation of the bilayer. By knowing what the limits of permeability are, the internal structure can be tailored to achieve a desired permeation rate by incorporating a percentage of degradable polymer to non-degradable polymer. This would also allow specific control of the degradation rates as well as the permeation rates.

6.2 New Block Copolymer Systems

Since polypeptide block copolymers are difficult to maintain, due to their semi-reactive nature, one possible alteration to the structure would be to change out the hydrophobic block. Since most of the previous work has changed the hydrophobic block with other more hydrophobic peptides or glassy, synthetic blocks, replacing the hydrophobic block with PDMS would offer a unique solution. The polymer would have a high hydrophobicity, as compared to the glycine and other synthetic blocks, as well as

being a barrier to acrylamide or other hydrophilic monomers used as an internal support. PDMS is also not an electrolyte.

Another feature of note is that PDMS is already FDA approved. If the end result would be a therapeutic drug delivery device or a therapeutic biomimic, having the main structural components approved by the FDA already would be an added benefit. Since lysine is a natural component of the human body, no additional approval is needed.

PDMS has a high affinity for gases; one possible therapeutic application is to use vesicles with a fluorophore encapsulated inside as a gas detector *in situ*. Since PDMS has a high diffusivity of oxygen compounds, such as reactive oxygen species and nitric oxide (NO), these molecules of interest could permeate into the interior of the vesicle. With the detecting fluorophore contained in the interior of the vesicle, the concentration of dissolved gases could be easily determined. If the vesicle is given the ability to adhere to a spot along a wall or surface, by measuring the fluorescent emission from various vesicles, a concentration map can be determined. In the case of NO, which controls vasodilation, detail studies could be performed on how the concentration varies as position *in situ*.

Although this setup could be performed with the current PEO-*b*-PDMS polymer, the PDMS-*b*-K polymer would offer some distinct advantages. Lysine has a terminal amine group, which would allow the addition of various end groups; any compound with a primary acid could be linked. Secondly, since lysine is salt and pH sensitive, the apparent size can be controlled. One drawback is that lysine is a polyelectrolyte. This

may cause an autoimmune response from the host. This is a drawback the PDMS-*b*-PEO polymer does not have.

6.3 Phase Separation

Early work with the polypeptide block copolymer system showed that it was not miscible with hydrocarbon chains, as shown in Figure 6-1. Before this work could be further explored, the polymer deteriorated. Part of the idea would be to investigate further the limitation and phase separation boundaries in a polypeptide-hydrocarbon system. This would involve looking at chain lengths in both components, the polypeptide and the hydrocarbon.

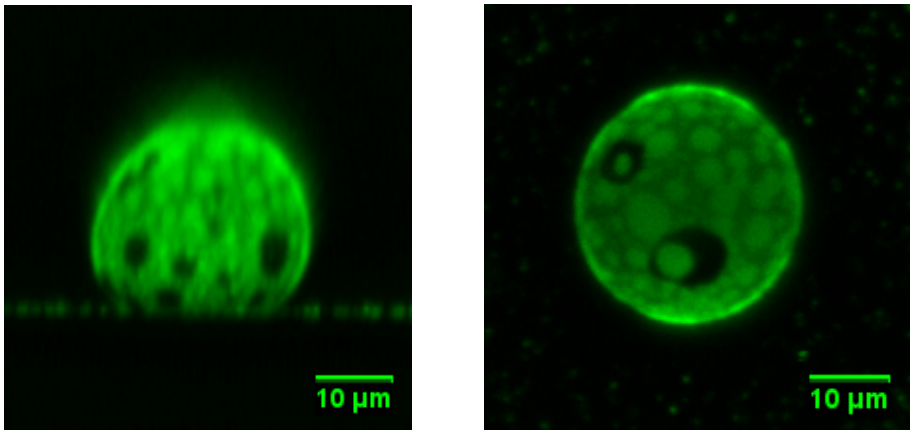

Figure 6-1: Phase separation in vesicles. Phase separation of a short chain hydrocarbon and a polypeptide block copolymer, $K_{200}G_{50}$. The left image is a side view; the right image is a top down view of the same vesicle.

Since it is known that polypeptides phase separate from hydrocarbons, insight can be gained from also looking at the PDMS-hydrocarbon interface. From the mixed system study, there was no apparent phase separation between these two polymers. Both polymers in that system were short chained block copolymers. Another avenue for investigation would be to look at the effects of PDMS with a long chained hydrocarbon. The reason for this investigation would be to see if there was a specific chain length or a ratio between the chain lengths that would offer a phase transition point. This can set up either an operational limit to mixtures or a chain length limit.

If the length of the hydrophobic block is key to phase separation, then by having an interior polymer network that has a solvent eluting capability, the bilayer structure could undergo a phase transition, from a single phase to a phase separated system. Under these conditions, the bilayer could either mechanically fail, offer a release mechanism or offer an increased diffusion or transport effect. This would allow a macromolecule of interest to be solubilized into the internal structure, carried to the destination and allowed to permeate through the membrane at a set rate, once phase separation was induced.

This approach allows the use of a non-conformational changing hydrophilic block to change the structure of a bilayer. This could continue the use of PEO as the hydrophobic block, which is not a polyelectrolyte and more understood than lysine.

Another approach is to see and investigate undiscovered, novel block copolymers for phase separation with either the PBd or PDMS system. These untested polymers

could possess a trait similar to a lysine block, conformational changes under pH changes, which would trigger phase separation.

6.4 Exterior Crosslinking

Exterior crosslinking would be an effort to put reactive ends on the hydrophilic block of the block copolymer. This would only be for cases in which the hydrophobic blocks do not have reactive groups, such as the case of PDMS. This would give the PDMS system under study or future PDMS systems the ability to increase the mechanical strength of the bilayer without use of an internal support structure. The external crosslinks can be connected to the block copolymer through acid chemistry linkage. From an reactive acid end group, using peptide linkage, one possibility for crosslinking would be a di-sulfide linkage.

Using a di-sulfide linkage would allow the end groups to link and delink with the use of a cleaving agent. Also, di-sulfide linkages are susceptible to decreases in pH, which would allow the vesicle to be weakened through a drop in the pH. If the exterior crosslinkers are in place with a phase separating system, the crosslinkers can hold the system in place until the desired place or time even thought the bilayer system is attempting to phase separate.

6.5 Conclusions

The results of these experiments show that we are able to create a cellular biomimic. We can create hollow vesicles with fluid membranes ranging in size from 250 nm to 25 μm. The size is confirmed by multiple experimental results: DLS, SLS, SEM and confocal imaging.

The second goal of creating a cellular mimic was the controllable surface chemistry and surface density. We have been able to develop a process to modify the current synthetic block copolymers ends to include a reactive end, as well as being able to modify the polypeptide block copolymers with the already present reactive ends. We can attach a wide range of compounds, either before or after vesicle formation.

The third goal in creating a biomimic is being able to control the characteristic mechanical properties of the vesicle. We have shown that the interior of the vesicle can be made to offer similar mechanical abilities to natural systems. By mixing both butadiene and silicone block copolymers, we can achieve specific membrane mechanical requirements.

The fourth goal is having a modifiable surface chemistry. The polypeptide block copolymer offers both goals inherent to the system, but the semi-reactive nature of the polymer prevents long term stability. PDMS polymer offers a more stable solution, with a minor modification to the PEO end. Once the acid form of the PDMS is created, the silicone block copolymer has both the fluid bilayer characteristic as well as the ability to tailor the surface chemistry.

Combining these elements together, a useful biomimic can be created that can be tailored for specific needs and research goals. This system offers flexibility, ease of use and robustness not offered by other polymers or polymer systems.

REFERENCES AND NOTES

1. D. E. Discher, Eisenberg, A, *Science* **297**, 967 (2002).
2. H.-A. Klok, S. Lecommandoux, *Advanced Polymer Science* **202**, 75 (2006).
3. G. M. Whitesides, J. P. Mathias, C. T. Seto, *Science* **254**, 1312 (Nov, 1991).
4. M. H. Li, P. Keller, *Soft Matter* **5**, 927 (2009).
5. K. Kita-Tokarczyk, W. Meier, *Chimia* **62**, 820 (2008).
6. K. Kita-Tokarczyk, J. Grumelard, T. Haefele, W. Meier, *Polymer* **46**, 3540 (May, 2005).
7. B. M. Discher, D.A. Hammer, D. E. Discher, *Science* **284**, 1143 (1999).
8. J. Babin, J. Rodriguez-Hernandez, S. Lecommandoux, H.-A. Klok, M.-F. Achard, *Faraday Discussions* **128**, 179 (2005).
9. F. Checot, S. Lecommandoux, H.-A. Klok, Y. Gnanou, *European Physical Journal E* **10**, 25 (2003).
10. S. Fukushima K. Miyata, N. Nishiyama, N. Kanayama, Y. Yamasaki, K. Kataoka, *, J. Am. Chem. Soc.* **127**, 2810 (2005).
11. A. Harada, K. Kataoka, *Macromolecules* **28**, 5294 (1995).
12. A. Harada, K. Kataoka, *Science* **283**, 65 (1999).
13. J. Rodrıguez-Hernandez, J. Babin, B. Zappone, S. Lecommandoux, *Biomacromolecules* **6**, 2213 (2005).

14. M. Yu, A. P. Nowak, T. J. Deming, D. J. Pochan, *J. Am. Chem. Soc.* **121**, 12210 (1999).

15. A. Chilkoti, M. R. Dreher, D. E. Meyer, D. Raucher, *Advanced Drug Delivery Reviews* **54**, 613 (Sep, 2002).

16. Y. Bae, K. Kataoka, *Advanced Drug Delivery Reviews* **61**, 768 (Aug, 2009).

17. H. Bermudez, A. K. Brannan, D. A. Hammer, F. S. Bates, D. E. Discher, *Macromolecules* **35**, 8203 (2002).

18. H. Bermudez, D. A. Hammer, D. E. Discher, *Langmuir* **20**, 540 (2004).

19. B. M. Discher, D. A. Hammer, F. S. Bates, D. E. Discher, *Current Opinion in Colloid & Interface Science* **5**, 125 (2000).

20. B. M. Discher, A. Eisenberg, *Science* **284**, 1143 (May, 1999).

21. D. A. Hammer, D. E. Discher, *Annu. Rev. Mater. Res.* **31**, 387 (2001).

22. B. M. Discher, H. Bermudez, D.A. Hammer, D.E. Discher, Y. Won, F.S. Bates, *J. Phys. Chem. B* **106**, 2848 (2002).

23. J. J. Lin, J.A. Silas, H. Bermudez, V.T. Milam, F.S. Bates, D.A. Hammer, *Langmuir* **20**, 5493 (2004).

24. J. N. Israelachvili, D. J. Mitchell, B. W. Ninham, *Biochim. Biophys. Acta* **470**, 185 (1977).

25. P. Attard, D. J. Mitchell, B. W. Ninham, *Biophysical Journal* **53**, 457 (1988).

26. M. Bostrom, V. Deniz, B. W. Ninham, *J. Phys. Chem. B* **110**, 9645 (2006).

27. J. J. Lin, P. P. Ghoroghchian, Y. Zhang, D. A. Hammer, *Langmuir* **22**, 3975 (2006).

28. J. J. Lin, F. S. Bates, D. A. Hammer, J. A. Silas, *Physical Review Letters* **95**, 026101 (2005).

29. S. K. Bhatia, D. A. Hammer, *Langmuir* **18**, 5881 (2002).

30. C. E. Orsello, D. A. Lauffenburger, D. A. Hammer, *Trends in Biotechnology* **19**, 310 (2001).

31. S. Mann, *Nature* **365**, 499 (Oct, 1993).

32. I. A. Aksay, M. Trau, S. Manne, I. Honma, N. Yao, *et al.*, *Science* **273**, 892 (Aug, 1996).

33. H.-P. Hentze, E. W. Kaler, *Current Opinion in Colloid and Interface Science* **8**, 164 (2003).

34. M. Antonietti, C. Goltner, H.-P. Hentze, *Langmuir* **14**, 2670 (1998).

35. H. P. Hentze. E. Kramer, B. Berton, S. Forster, M. Antonietti, M. Dreja, *Macromolecules* **32**, 5803 (1999).

36. M. Jung, D.H.W. Hubert, P.H.H. Bomans, P.M. Frederik, J. Meuldijk, *et al.*, *Langmuir* **13**, 6877 (1997).

37. J. Hotz, W. Meier, *Advanced Materials* **10**, 1387 (1998).

38. S. Mann, S. Burkett, S.A. Davis, C.E. Fowler, N.H. Mendelson, *et al.*, *Chem. Mater.* **9**, 2300 (1997).

39. M. Jung, D.H.W. Hubert, P.H.H. Bomans, P. M. Frederik, A. van Herk, A.L. German, *Advanced Materials* **12**, 210 (2000).

40. D. H. W. Hubert, M. Jung, A. L. German, *Advanced Materials* **12**, 1291 (2000).

41. S. Forster, B. Berton, H.P. Hentze, E. Kramer, M. Antonietti, P. Linder, *Macromolecules* **34**, 4610 (2001).

42. M. Muthukumar, C. K. Ober, E. L. Thomas, *Science* **277**, 1225 (1997).

43. G. M. Whitesides, J. P. Mathias, C. T. Seto, *Science* **254**, 1312 (1991).

44. S. C. Glotzer, M. J. Soloman, N. A. Kotov, *AIChE Journal* **50**, 2978 (2004).

45. B. P. Binks, S. O. Lumsdun, *Phys. Chem. Chem. Phys.* **1**, 3007 (1999).

46. D. B. Lawrence, T. Cai, Z. Hu, M. Marquez, A. D. Dinsmore, *Langmuir* **23**, 395 (2007).

47. H. Deng, D. L. Gin, R. C. Smith, *J. Am. Chem. Soc.* **120**, 3522 (1998).

48. O. Lade, C. C. Co, P. Cotts, R. Strey, E. W. Kaler, *Colloid Polym. Sci.* **283**, 905 (2005).

49. M. Jung, I. Ouden, A. Montoya-Goni, D.H.W. Hubert, P.M. Frederik, *et al.*, *Langmuir* **16**, 4185 (2000).

50. W. Meier, J. Hotz, *Langmuir* **14**, 1031 (1998).

51. C. A. McKelvey, E. W. Kaler, *Journal of Colloid and Interface Science* **245**, 68 (2002).

52. C. A. McKelvey, E. W. Kaler, J. A. Zasadzinski, B. Coldren, H.-T. Jung, *Langmuir* **16**, 8285 (2000).

53. A. Graff, M. Winterhalter, W. Meier, *Langmuir* **17**, 919 (2001).

54. C. Nardin, S. Thoeni, J. Widmer, M. Winterhalter, W. Meier, *Chemical Communications*, 1433 (2000).

55. C. Nardin, J. Widmer, M. Winterhalter, W. Meier, *European Physical Journal E* **4**, 403 (2001).

56. R. B. Khomane, B. D. Kulkarni, *International Journal of Chemical Reactor Engineering* **6**, 94 (2008).

57. A. Jesorka, M. Markstrom, O. Orwar, *Langmuir* **21**, 1230 (2005).

58. N. A. Peppas, C. T. Reinhart, *Journal of Membrane Science* **15**, 275 (1983).

59. R. W. Korsmeyer, R. Gurny, E. Doelker, P. Buri, N. A. Peppas, *International Journal of Pharmaceutics* **15**, 25 (1983).

60. C. C. Lin, A. T. Metters, *Advanced Drug Delivery Reviews* **58**, 1379 (Nov, 2006).

61. Y. H. Bae, S. W. Kim, *Advanced Drug Delivery Reviews* **11**, 109 (Jul-Aug, 1993).

62. Y. Qiu, K. Park, *Advanced Drug Delivery Reviews* **53**, 321 (Dec, 2001).

63. O. Wichterle, D. Lim, *Nature* **185**, 117 (1960).

64. R. Langer, N. Peppas, *Journal of Macromolecular Science-Reviews in Macromolecular Chemistry and Physics* **C23**, 61 (1983).

65. R. S. Langer, N. A. Peppas, *Biomaterials* **2**, 201 (1981).

66. T. J. Deming, *Nature* **390**, 386 (1997).

67. A. P. Nowak, V. Breedveld, L. Pakstis, B. Ozbas, D.J. Pine, *et al.*, *Nature* **417**, 424 (2002).

68. E. G. Bellomo, M. D. Wyrsta, L. Pakstis, D. J. Pochan, T. J. Deming, *Nature Materials* **3**, 244 (2004).

69. E. P. Holowka, D. J. Pochan, T. J. Deming, *J. Am. Chem. Soc.* **127**, 12423 (2005).

70. E. A. Minich, A. P. Nowak, T. J. Deming, D. J. Pochan, *Polymer* **45**, 1951 (2004).

71. D. J. Pochan, L. Pakstis, B. Ozbas, A. P. Nowak, T. J. Deming, *Macromolecules* **35**, 5358 (2002).

72. F. Checot, J. Rodrıguez-Hernandez, Y. Gnanou, S. Lecommandoux, *Biomolecular Engineering* **24**, 81 (2007).

73. F. Checot, A. Brulet, J. Oberdisse, Y. Gnanou, O. Mondain-Monval, S. Lecommandoux, *Langmuir* **21**, 4308 (2005).

74. V. Breedveld, A. P. Nowak, J. Sato, T. J. Deming, D. J. Pine, *Macromolecules* **37**, 3943 (2004).

75. T. J. Deming, *J. Am. Chem. Soc.* **120**, 4240 (1998).

76. T. J. Deming, S. A. Curtin, *J. Am. Chem. Soc.* **122**, 5710 (2000).

77. L. Pakstis, B, Ozbas, K.D. Hales, A.P. Nowak, T.J. Deming, D. Pochan, *Biomacromolecules* **5**, 312 (2004).

78. G. Kickelbick, J. Bauer, N. Huesing, M. Andersson, K. Holmberg, *Langmuir* **19**, 10073 (2003).

79. G. Kickelbick, J. Bauer, N. Husing, M. Andersson, A. Palmqvist, *Langmuir* **19**, 3198 (2003).

80. S. Komura, S. A. Safran, *European Physical Journal E* **5**, 337 (Jun, 2001).

81. C. Nardin, T. Hirt, J. Leukel, W. Meier, *Langmuir* **16**, 1035 (2000).

82. O. Rheingans, N. Hugenberg, J. R. Harris, K. Fischer, M. Maskos, *Macromolecules* **33**, 4780 (2000).

83. C. Nardin, W. Meier, *Chimia* **55**, 142 (2001).

84. M. He, R. M. Hill, Z. Lin, L. E. Scriven, H. T. Davis, *Journal of Physical Chemistry* **97**, 8820 (Aug, 1993).

85. R. M. Hill, M. T. He, Z. Lin, H. T. Davis, L. E. Scriven, *Langmuir* **9**, 2789 (Nov, 1993).

86. J. Jasper, *J. Phys. Chem. Ref. Data* **1**, 841 (1972).

87. J. Brandrup, E. H. Immergut, E. A. Grulke, Eds. *Polymer Handbook*. (J. Wiley & Sons, Inc., Hobeken, NJ, ed. 4th, 1999), pp.

88. D. F. DeTar, R. Silversteid, *J. Am. Chem. Soc.* **88**, 1013 (1966).

89. D. F. DeTar, R. Silverstein, *J. Am. Chem. Soc.* **88**, 1020 (1966).

90. D. R. Halpin, J. A. Lee, S. J. Wrenn, P. B. Harbury, *PLoS Biology* **2**, 1031 (2004).

91. M. M. Rozenman, D. R. Liu, *ChemBioChem* **7**, 253 (2006).

92. A. Guinier, G. Fournet, *Small-Angle Scattering of X-Rays* (John Wiley and Sons, New York, 1955).

93. K. Olbrich, W. Rawicz, D. Needham, E. Evans, *Biophysical Journal* **79**, 321 (Jul, 2000).

94. W. Rawicz, K. C. Olbrich, T. McIntosh, D. Needham, E. Evans, *Biophysical Journal* **79**, 328 (Jul, 2000).

95. J. William D. Callister, *Material Science and Engineering* (John Wiley & Sons, New York, 2003).

96. J. N. Israelachvili, *Intermolecular & Surface Forces* (Academic Press, New York, 1992).

97. A. V. Kyrylyuk, J. G. E. M. Fraaije, *Journal of Chemical Physics* **121**, 2806 (2004).

98. N. Dan, M. Tirrell, *Macromolecules* **26**, 4310 (1993).

99. A. V. Kyrylyuk, J. G. E. M. Fraaije, *Journal of Chemical Physics* **121**, 9166 (2004).

100. A. S. Lee, V. Butun, M. Vamvakaki, S. Armes, J. Pople, A. Gast, *Macromolecules* **35**, 8540 (2002).

101. S. Forster, N. Hermsdorf, C. Bottcher, P. Lindner, *Macromolecules* **35**, 4096 (2002).

102. K. K. Liu, *Journal of Physics D-Applied Physics* **39**, R189 (2006).

103. E. Chibowski, A. Ontiveros-Ortega, R. Perea-Carpio, *J. Adhesion Science Technology* **16**, 1367 (2002).

104. H. Hertz, *J. Reine Angew. Math.* **92**, 156 (1881).

105. K. L. Johnson, K. Kendall, A. D. Roberts, *Proceedings of the Royal Society of London Series A-Mathematical, Physical and Engineering Sciences Series,* **324**, 301 (1971).

106. M. E. R. Shanahan, *J. Adhesion* **63**, 15 (1997).

107. G. T. Linke, R. Lipowsky, T. Gruhn, *European Physical Journal E* **24**, 217 (2007).

108. U. Seifert, K. Berndl, R. Lipowsky, *Physical Review A* **44**, 1182 (1991).

109. A. S. Smith, U. Seifert, *Physical Review E* **71**, 11 (2005).

110. A. S. Smith, E. Sackmann, *Chemphyschem* **10**, 66 (2009).

111. R. Lipowsky, *Physical Review Letters* **77**, 1652 (1996).

112. E. Evans, W. Rawicz, *Physical Review Letters* **64**, 2094 (1990).

113. D. Marsh, *Biophysical Journal* **73**, 865 (1997).

114. O. Holderer, H. Frielinghaus, D. Byelov, M. Monkenbusch, J. Allgaier, D. Richter, *J. Chem. Phys.* **122**, 094908 (2005).

115. E. Evans, D. Needham, *Macromolecules* **21**, 1822 (1988).

116. D. Needham, E. Evans, *Biochemistry* **27**, 8261 (1988).

117. S. T. Milner, S. A. Safran, *Physical Review A* **36**, 4371 (1987).

118. E. A. Evans, *Biophysical Journal* **48**, 175 (1985).

119. E. A. Evans, *Biophysical Journal* **48**, 185 (1985).

120. S. Leibler, R. R. P. Singh, M. E. Fisher, *Physical Review A* **59**, 1989 (1987).

121. P. Gutjahr, R. Lipowsky, J. Kierfeld, *Europhysics Letters* **76**, 994 (2006).

122. F. A. M. Leermakers, C. M. Wijmans, G. J. Fleer, *Macromolecules* **28**, 3434 (1995).

123. V. A. Baulin, E. B. Zhulina, A. Halperin, *Journal of Chemical Physics* **119**, 10977 (2003).

124. N. Dan, M. Tirrell, *Macromolecules* **26**, 6467 (1993).

125. A. J. Lovinger, D. Davis, F. Schilling, F. Padden, F. Bovey, J. Zeigler, *Macromolecules* **24**, 132 (Jan, 1991).

126. A. Habenschuss, M. Tsige, J. G. Curro, G. S. Grest, S. K. Nath, *Macromolecules* **40**, 7036 (Sep, 2007).

APPENDIX

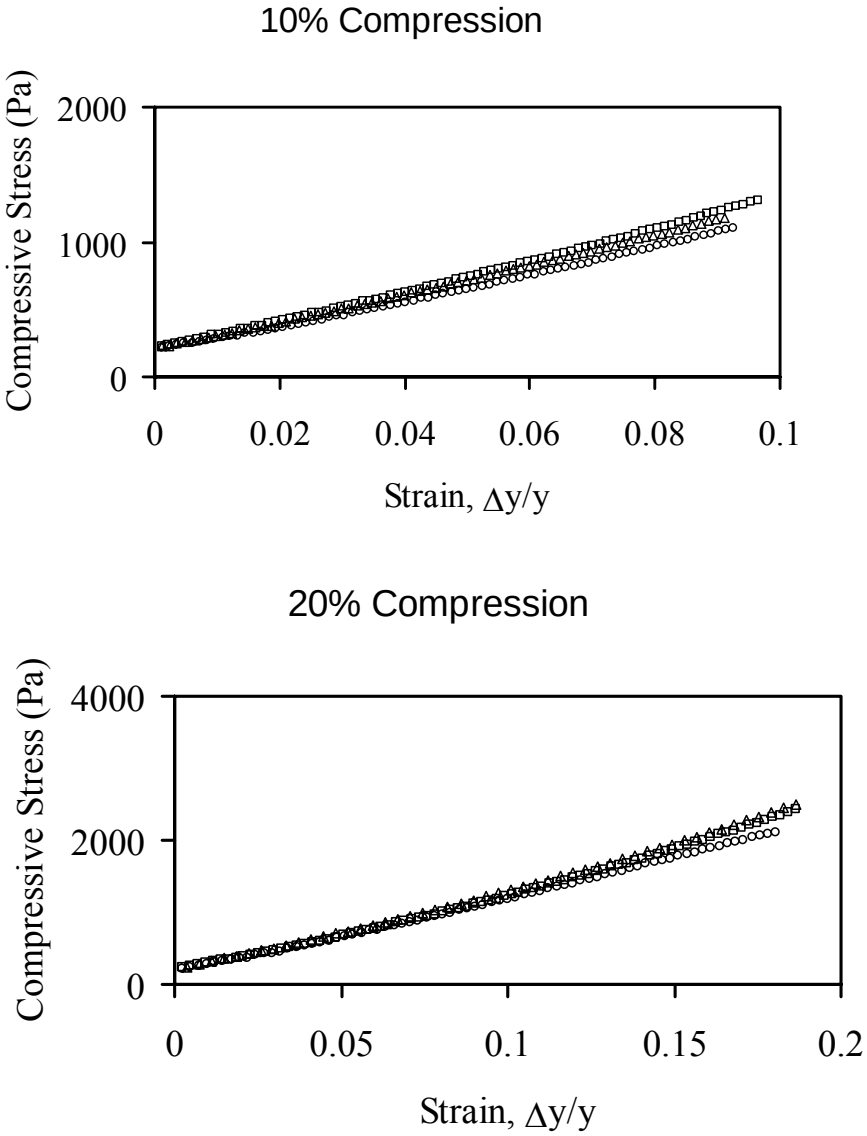

Figure A-1: The 19:1 5% AM compression test. The first graph is the 10% compression test. The middle graph is the 20% compression test, and the bottom graph is the 40% failure compression test. The values from the graphs are tabulated in Table III-3. The open circle (○) is the first cylinder, the open square (□) is the second cylinder and the open triangle (Δ) is the third cylinder.

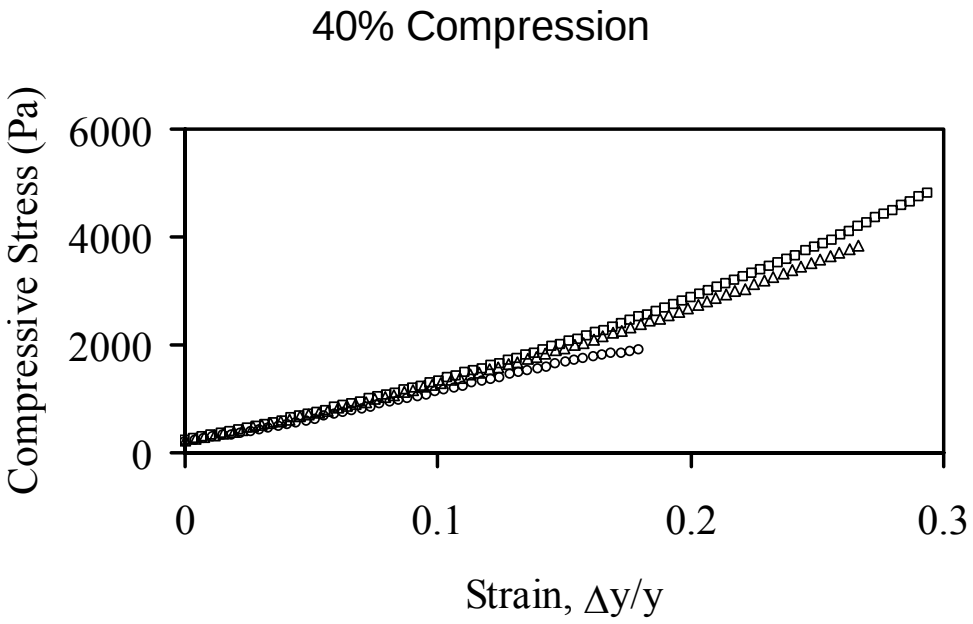

Figure A-1 continued

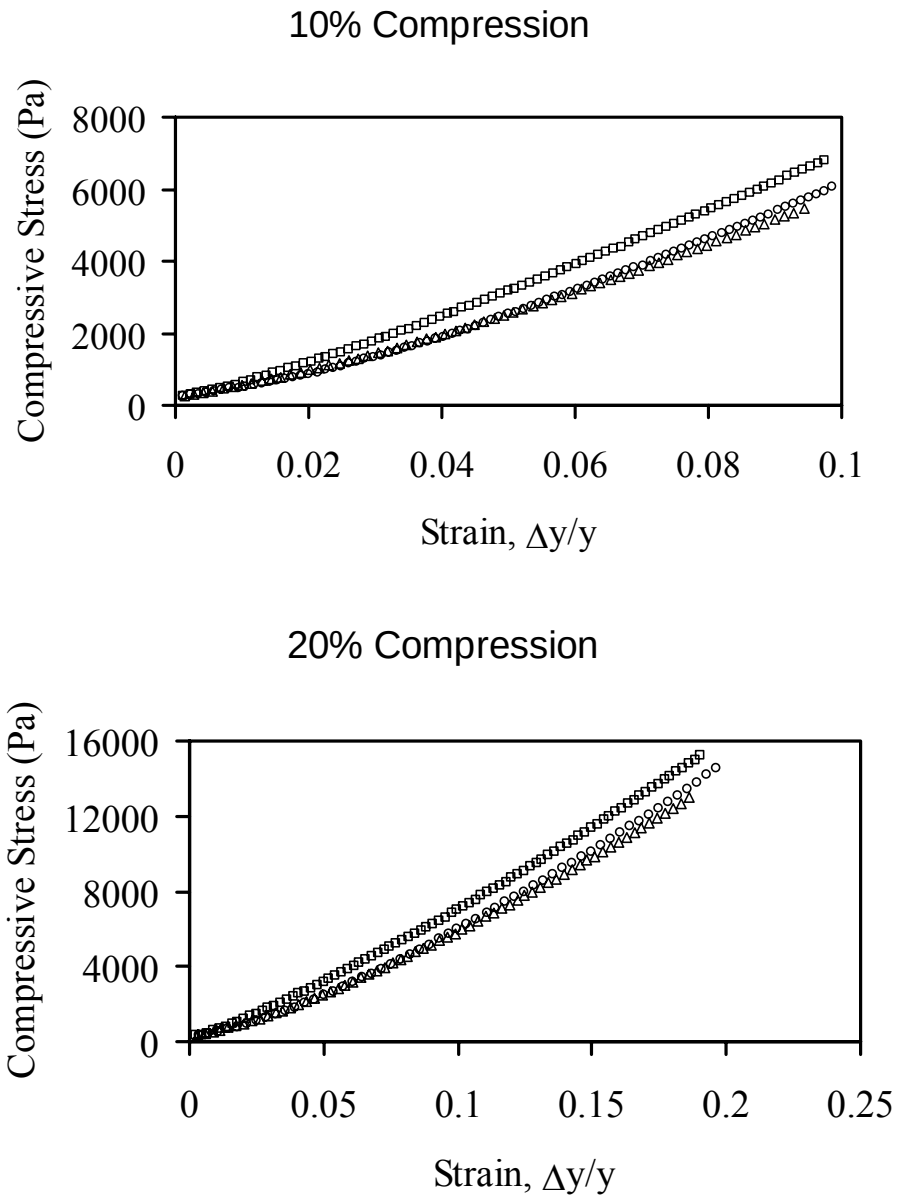

Figure A-2: The 19:1 10% AM compression test. The first graph is the 10% compression test. The middle graph is the 20% compression test, and the bottom graph is the 40% failure compression test. The values from the graphs are tabulated in Table III-3. The open circle (○) is the first cylinder, the open square (□) is the second cylinder and the open triangle (Δ) is the third cylinder.

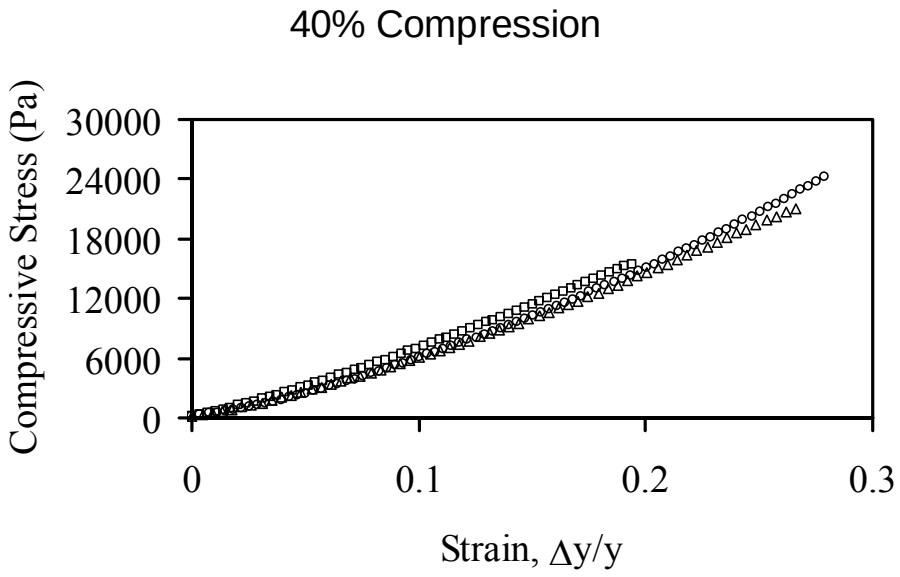

Figure A-2 continued.

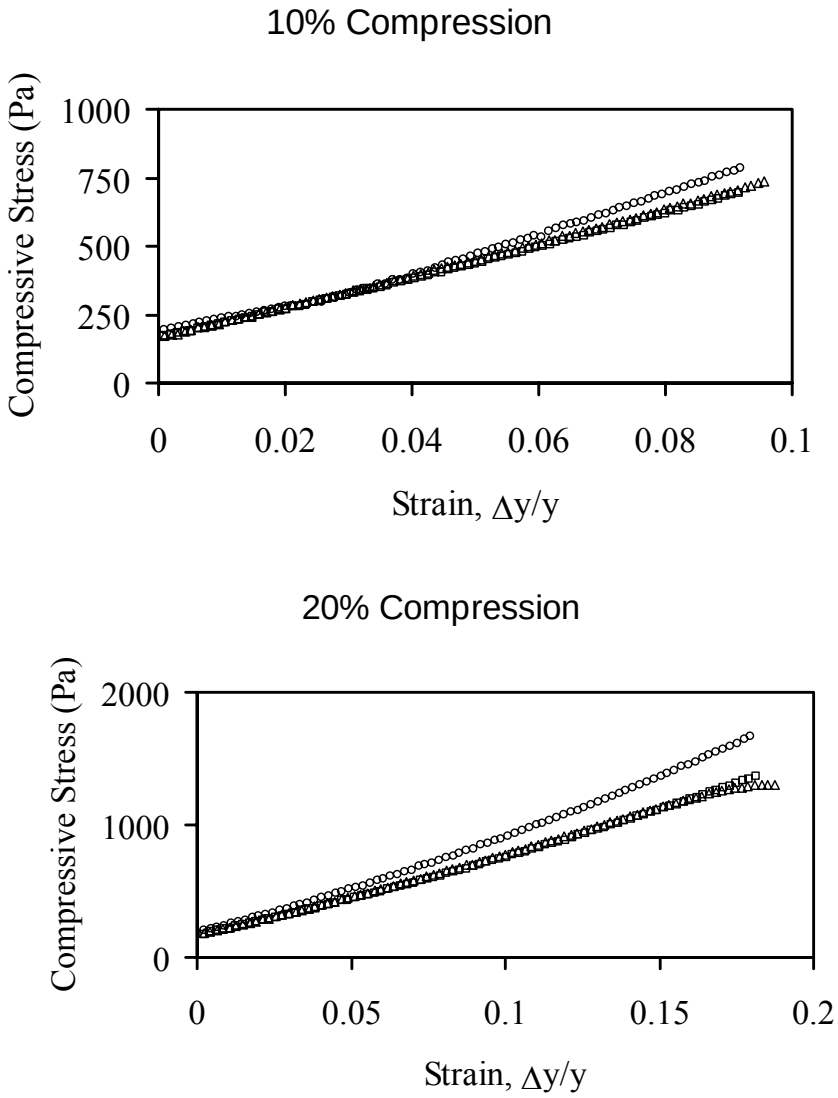

Figure A-3: The 38:1 5% AM compression test. The first graph is the 10% compression test. The middle graph is the 20% compression test, and the bottom graph is the 40% failure compression test. The values from the graphs are tabulated in Table III-4. The open circle (○) is the first cylinder, the open square (□) is the second cylinder and the open triangle (Δ) is the third cylinder.

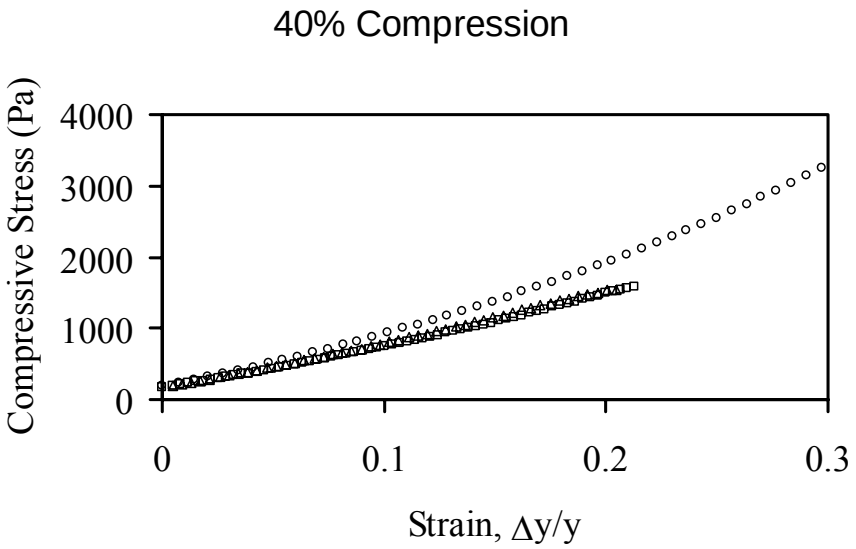

Figure A-3 continued.

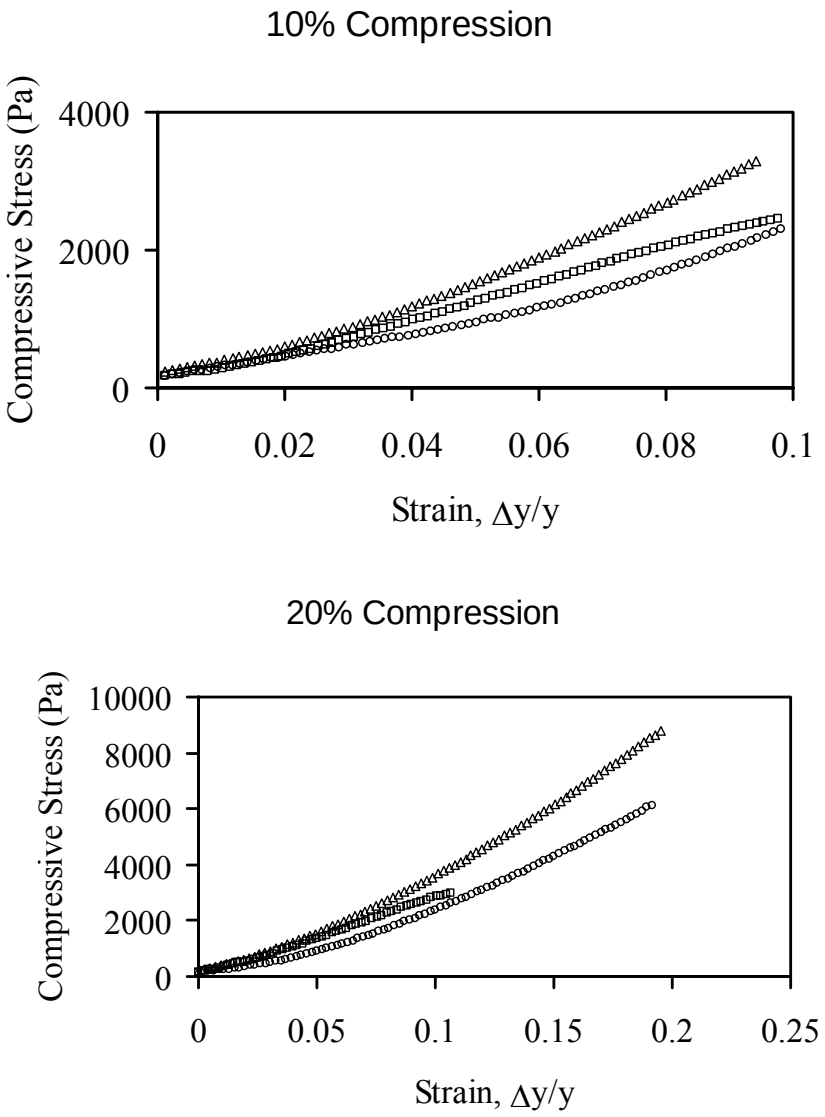

Figure A-4: The 38:1 10% AM compression test. The first graph is the 10% compression test. The middle graph is the 20% compression test, and the bottom graph is the 40% failure compression test. The values from the graphs are tabulated in Table III-4. The open circle (○) is the first cylinder, the open square (□) is the second cylinder and the open triangle (Δ) is the third cylinder.

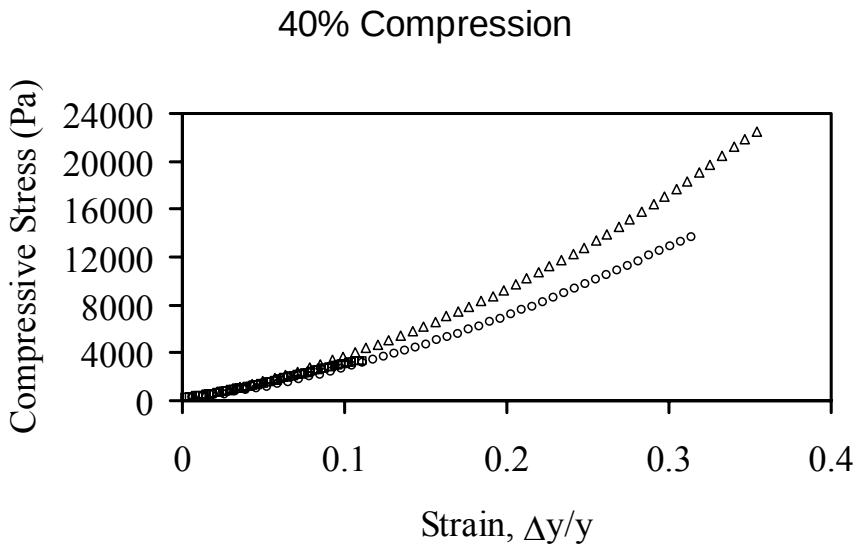

Figure A-4 continued.

The following Visual Basic (VB) code for use in the pipette image capture program. The code allows images to be taken and the corresponding pressure recorded directly onto the image for recordkeeping. This was written for use with excel and the microscope imaging software.

```
Attribute VB_Name = "Module1"
Private Declare Function UPC2_PCI_Connect Lib "upc2_pci.dll" Alias
"_UPC2_PCI_Connect@4" (ByVal card_ndx As Long) As Long
Private Declare Function UPC2_PCI_Disconnect Lib "upc2_pci.dll" Alias
"_UPC2_PCI_Disconnect@4" (ByVal card_ndx As Long) As Long
Private Declare Function UPC2_PCI_GetData Lib "upc2_pci.dll" Alias
"_UPC2_PCI_GetData@16" (ByVal card_ndx As Long, ByVal access_type As Long,
ByVal nframes As Long, pFrame As Frame_t) As Long
Private Declare Function UPC2_PCI_Start Lib "upc2_pci.dll" Alias
"_UPC2_PCI_StartDataCollection@4" (ByVal card_ndx As Long) As Long
Private Declare Function UPC2_PCI_Stop Lib "upc2_pci.dll" Alias
"_UPC2_PCI_StopDataCollection@4" (ByVal card_ndx As Long) As Long

Private Type Frame_t
status As Long
timestamp As Long
data(0 To 23) As Single
```

```
End Type

Public Sub Form_Load()
' initialize UPC variables and error handling
Dim Mode As Long
Dim CardID As Long
Dim retval As Long

Mode = 4 ' UPC mode to get latest item readings
CardID = 0

retval = UPC2_PCI_Connect(CardID)  'Connect to card with CardID=0

If retval < 0 Then
MsgBox ("Failed to Connect to UPC2100 Card")
Else
MsgBox ("Connected to UPC2100 Card")
End If

retval = UPC2_PCI_Start(CardID) 'Start data collection on card
If retval < 0 Then
MsgBox ("Failed to Start UPC2100 Card")
Else
MsgBox ("UPC2100 Card Started")
End If

End Sub

Public Sub Form_Unload()
'This disconnects the card on exit
Dim retval As Long
Dim CardID As Long

CardID = 0

retval = UPC2_PCI_Stop(CardID) 'Stop data collection on card
If retval < 0 Then
MsgBox ("Failed to Stop UPC2100 Card")
Else
MsgBox ("UPC2100 Card Stopped")
End If

retval = UPC2_PCI_Disconnect(0)
```

```
If retval < 0 Then
MsgBox ("Failed to Disconnect from UPC2100 Card")
Else
MsgBox ("Disconnected from UPC2100 Card")
End If
'On Error Resume Next
'retval = UPC2_PCI_Disconnect(0)

End Sub

Public Sub SnapAndPressure()
Dim CardID As Long
Dim Mode As Long
Dim MaxItems As Long
Dim retval As Long
Dim DataFrame As Frame_t
   Dim Image As ZiImage
   Dim Layer As ZiLayer
   Dim Layers As ZiLayers
   Dim Shape As ZiShape
   Dim Shape2 As ZiShape
   Dim Parameter As ZiParameter
   Dim Device As ZiDevice

CardID = 0
Mode = 4
MaxItems = 1

retval = UPC2_PCI_GetData(CardID, Mode, MaxItems, DataFrame)

If retval < 0 Then
MsgBox ("Get Data Failed")
End If

ZiApplication.ExecuteCommand ("Snap_ActiveAcq")

   Set Image = ZiApplication.ActiveDocument
   Set Layers = Image.Layers
   Set Layer = Layers.Open("Annotations")

   Set Shape = Layer.Shapes.Add("LeftPressure", ziShapeText)

   With Shape
      .SetRectangle 25, 1000, 825, 1050
```

```
        .CanGrow = True
        .Text = "Left Pressure (in. H2O) = " & CStr(DataFrame.data(1))
        .FONTSIZE = 18
        .DrawStyle = ziDrawStyleNone
        .Visible = True
      End With


    Set Shape2 = Layer.Shapes.Add("RightPressure", ziShapeText)

    With Shape2
        .SetRectangle 750, 1000, 1382, 1050
        .CanGrow = True
        .Text = "Right Pressure (in. H2O) = " & CStr(DataFrame.data(0))
        .FONTSIZE = 18
        .DrawStyle = ziDrawStyleNone
        .Visible = True
    End With
    Image.SendDataChanged 1

End Sub

Public Sub PrintAllFunctions()
Dim AVFunctions As ZiFunctions
Dim AVFunction As ZiFunction

Set AVFunctions = ZiApplication.Functions

For Each AVFunction In AVFunctions

    Debug.Print AVFunction.Key

Next AVFunction

End Sub


Sub LowerLeftBox()
Attribute LowerLeftBox.VB_Description = "Make Annotation in lower left corner of
image"
    Dim Image As ZiImage
    Dim Layer As ZiLayer
    Dim Layers As ZiLayers
    Dim Shape As ZiShape
```

```
    Set Image = ZiApplication.ActiveDocument


    Set Layers = Image.Layers
    Set Layer = Layers.Open("myLayer")

    Set Shape = Layer.Shapes.Add("myText", ziShapeText)

    With Shape
        .SetRectangle 25, 1000, 525, 1030
        .Text = "Pipette Pressure (units) = "
        .FONTSIZE = 18
        .DrawStyle = ziDrawStyleNone
        .Visible = True
        .Selected = True
    End With

    Image.SendDataChanged 1
End Sub
```

VITA

Name:	Jeffery Simon Gaspard
Address:	Texas A&M University – Chemical Engineering Department
	Jack E. Brown Engineering Building 3122 TAMU 200
	College Station, TX 77843-3122
Email address:	jsg@tamu.edu
Education:	B.S., Chemical Engineering, Texas A&M University, 2005
	M.S., Chemical Engineering, Texas A&M University, 2007
	Ph.D., Chemical Engineering, Texas A&M University, 2009